Title
KINETICS OF NITROGEN DIOXIDE FLUORESCENCE

Author
Schwartz, Stephen E.

Publication Date
1968-09-01

UCRL-18431

cy. 2

University of California

Ernest O. Lawrence Radiation Laboratory

KINETICS OF NITROGEN DIOXIDE FLUORESCENCE

Stephen E. Schwartz

(Ph. D. Thesis)

September 1968

UCRL-18431

UNIVERSITY OF CALIFORNIA

Lawrence Radiation Laboratory
University of California

AEC Contract W-7405-eng-48

KINETICS OF NITROGEN DIOXIDE FLUORESCENCE

Stephen E. Schwartz

(Ph.D. Thesis)

September 1968

KINETICS OF NITROGEN DIOXIDE FLUORESCENCE

Stephen E. Schwartz

Inorganic Materials Research Division, Lawrence Radiation Laboratory,
Department of Chemistry, University of California,
Berkeley, California

ABSTRACT

The fluorescence lifetime and intensity of gas phase nitrogen dioxide ($^2B_1$) have been measured as a function of excitation wavelength, fluorescence wavelength, and pressure. The phase-shift method was used; this technique allows lifetime measurements to be obtained with signal intensities of 100 counts per second and lower. The excitation source, tunable throughout the visible region, had a half width bandpass as low as 15 A. Fluorescence wavelength separation was accomplished with interference filters. The radiative lifetimes range from 55 to 90 μsec for excitation from 3980 to 6000 A, and tend to increase with excitation wavelength; however, the lifetimes exhibit considerable variation within a narrow excitation region.

The fluorescence sample was contained in a 33 cm diameter spherical bulb; apparent fluorescence lifetimes in smaller cells were reduced because of migration of excited molecules (under collision free conditions) and wall quenching. In order that the measured lifetime exhibit no more than 5% error, observation must be extended beyond the excitation region to a distance 5 times the product of the lifetime by the most probable velocity.

The Stern-Volmer analysis of fluorescence kinetics has been generalized to a multi-level system under conditions of modulated excitation

and phase-sensitive detection. Analysis of fluorescence data in terms of this mechanism yields average values for energy transfer rate constants and efficiencies (amount of energy lost by the excited polyatomic molecule per effective collision). Energy transfer rate constants for excited NO_2 ($^2B_1$) with a ground state collision partner are approximately gas kinetic; efficiencies are approximately 2300 cm^{-1}.

TABLE OF CONTENTS

LIST OF FIGURES

LIST OF TABLES

INTRODUCTION

The study of relaxation processes is of major importance in coming to an understanding of the chemistry of gas phase reactions. The activation of reactant molecules in unimolecular reactions and the stabilization of products in bimolecular recombination reactions take place by the mechanism of collisional energy transfer.[1,2] Further, there is an increasing body of experimental work that indicates that a major fraction of the enthalpy in certain exothermic bimolecular atom transfer reactions is localized in the newly formed bond immediately after the reactive encounter.[3-5] The excited molecules are subsequently relaxed by collisional processes.

The use of fluorescence techniques to study the energy transfer processes of molecules dates to the early part of this century.[6] In recent years a wide number of additional experimental approaches, direct and indirect, have been applied to the study of these processes: ultrasonics,[7a,8] unimolecular reactions,[9] chemical activation,[10] shock wave studies,[11] chemiluminescence,[12] and kinetic absorption spectroscopy.[13] Of these, the techniques that make use of spectral observation of the quantum states participating in the energy transfer processes provide the most detailed information, and fluorescence continues to be a valuable technique for these studies.[14] In particular, time resolved fluorescence studies allow a direct measurement of energy transfer rates of energetic molecules.[15] Recent reviews of relaxation processes in gases and the techniques of their study have been given by Flygare,[16] and Stevens.[17]

The present study is an investigation of the kinetics of nitrogen dioxide fluorescence excited by visible radiation and the associated energy transfer processes of the excited molecules. Nitrogen dioxide

is of interest as the subject of such a study for a number of reasons, which are listed here:

1) There exists very little direct quantitative information about the rates and efficiencies of energy transfer processes in highly excited small polyatomic molecules and no direct evidence concerning these processes in tri-atomic molecules. Previous experiments have indicated that energy transfer processes involving NO_2 take place with high probability[18] and that such processes may take place by a stepwise mechanism.[19] Hence this molecule is well suited to such a study.

2) There have been recent doubts concerning the existing value of the radiative lifetime of NO_2 fluorescence.[20-22] The existing value (44μsec)[18,20] is anomalously long for an allowed electronic transition, as inferred from the magnitude of the absorption coefficient. No dependence of the radiative lifetime upon the energy of the excited molecule has been reported previously, although such a dependence is expected on the basis of radiation theory from the frequency factor in the A coefficient for spontaneous radiation.[20, 23-24] It has been anticipated on spectroscopic grounds that the fluorescence lifetime might exhibit fluctuations because of severe perturbations in the upper electronic state.[20] Theoretical interpretations of the causes of long fluorescence lifetimes in molecules have recently been given by several authors.[5, 25-28]

3) The fluorescence of NO_2 is of interest as an elementary process in the NO + O[29-36] and NO + O_3[21, 22, 37, 38] chemiluminescence reactions, which have received considerable study in the laboratory and, in the former case, as an upper atmosphere reaction.[39, 40] Any understanding of the rates of radiative and non-radiative processes that is obtained

from fluorescence studies can be used to increase our understanding of the chemical processes responsible for the population and depopulation of the excited electronic state in these specific reactions.

4) Nitrogen dioxide is advantageous from an experimental point of view. The molecule has an electronic transition in a spectral region that is well suited to experimental investigation. The upper state is presumed to be the lowest excited electronic state of the molecule on the basis of theoretical considerations[41] and of a partial rotational analysis of the absorption spectrum.[42] Consequently, studies of the relaxation processes are probably not complicated by the presence of other electronic states. The lowest electronic transition of NO_2 has the additional property of a pre-dissociation limit in the absorption region.[42] By use of excitation close to this limit the behavior of molecules in the neighborhood of a dissociation continuum may be examined.

In a fluorescence study such as the present one, the system is disturbed from equilibrium optically; fluorescence is used analytically to observe the relaxation of the system back to equilibrium. Optical excitation is an advantageous way to study the luminescence and associated processes, as compared to electrical or chemical means of excitation, as one is able to achieve highly mono-energetic excitation and good time resolution. Under conditions of continuous, or dc, excitation such a system establishes steady concentrations in all quantum states. For ac excitation the system acts as a set of linear circuit elements that follow the excitation at the modulation frequency, but with phase lag and amplitude characteristics that depend on the transition probabilities connecting the various states. In the limit of zero pressure the

only mechanism of relaxation will be optical, that is, fluorescence. For this to be true we also require that other processes, such as predissociation, or diffusion to the walls, are negligible. Non-radiative (collisional) energy transfer processes begin to compete with radiative processes at finite pressures and at sufficiently high pressure become the dominant mechanism for restoring the system to equilibrium. Thus pressure is the significant independent variable available to play off one relaxation mechanism against the other.

The remainder of this introduction is divided into four sections. In the first a discussion will be given concerning the relation between the absorption coefficient and the lifetime in electronic transitions with specific reference to NO_2. In the second and third sections will be given the theory of measurements by the phase shift technique and a resume' of Stern-Volmer (quenching) kinetics. Finally, the previous studies of NO_2 fluorescence will be summarized.

A. Relation Between Absorption Coefficient and Radiative Rate Constant

The original relation between the absorption coefficient and the radiative rate constant for an optical transition was developed by Einstein.[43] The basis of the relation is that absorption and spontaneous emission are inverse processes and must satisfy detailed balancing. The precise mathematical statement of the relation depends on the choice of units for light intensity and absorption coefficient. A useful and self-consistent set of units has been given by Brewer.[44,45] Here light intensity I is measured in units of quanta/(cm^2×sec×unit frequency interval sec^{-1}). The Einstein B coefficient is used directly in the rate equation:

$$\frac{dN'}{dt}\ [\text{molecules}/(\text{cm}^3 \times \text{sec})] = IN''B \qquad (1)$$

With these conventions the electronic transition moment (squared) of a single atomic line for electric dipole radiation is given by

$$|R_e|^2 = \frac{3h}{8\pi^3 \nu} \frac{1}{g'} B \qquad (2)$$

The A coefficient (radiative rate constant) is related to the electronic transition moment by

$$A = \frac{64\pi^4}{3h} \tilde{\nu}^3 g'' |R_e|^2 \qquad (3)$$

In these expressions g' and g'' are the degeneracies of the upper and lower states respectively; $\tilde{\nu}$ is the optical frequency between the two states in wave numbers (cm^{-1}).

At this point we wish to relate I and B to the usual (for kineticists) laboratory quantities I_o (quanta/cm^2 sec) and $k_a \equiv \sigma$, the absorption coefficient in cm^2. These relations are given by

$$B = \int \sigma \, d\nu \qquad (4a)$$

$$I_o = \int I \, d\nu \qquad (4b)$$

The requirement to satisfy (1) that $I_o \sigma = I B$ is fulfilled.

We wish now to consider molecular transitions. Under the assumptions:

1) that the total wave function of the molecule is separable into the product of electronic and nuclear wave functions, and

2) that the configuration of the nuclei changes slightly between the two vibronic states and that the transition moment varies slowly with the nuclear configuration,

then the radiation relations may be carried over to molecular spectroscopy.[46] In molecular transitions the electronic moment, rather than being concentrated in a single line, is spread over transitions to a number of final states. Thus in the evaluation of the electronic transition moment from the absorption spectrum the contribution to the absorption intensity must be summed over the electronic transition.[24]

$$|R_e|^2 = \frac{3h}{8\pi^3} \frac{1}{G'} \sum_{v'} \frac{B_{v'v''}}{\tilde{\nu}_{v'v''}}$$

From (4a)

$$|R_e|^2 = \frac{3h}{8\pi^3} \frac{1}{G'} \sum_{v'} \frac{\int \sigma_{v'v''} \, d\nu}{\tilde{\nu}_{v'v''}}$$

$$= \frac{3hc}{8\pi^3} \frac{1}{G'} \int \frac{\sigma_{v''}}{\tilde{\nu}} \, d\tilde{\nu} \qquad (5)$$

The integration indicated in (5) is now to be taken over the entire electronic band. We may designate

$$\underset{\sim}{\sigma} \equiv \int \frac{\sigma_{v'}}{\tilde{\nu}} \, d\tilde{\nu}$$

as the integrated absorption coefficient having units cm^2. G' and G" are the numbers of suitable orbitals to which molecular transitions can take place. The ratio G"/G' is equal to the ratio g"/g' of the electronic degeneracies.[24]

We now consider the rate of emission from the level v'. This discussion parallels that of Strickler and Berg.[23] The rate constant for fluorescence into a particular v" level of the lower electronic state is given by

$$A_{v'v''} = \frac{64\pi^4}{3h} G'' |R_e|^2 q_{v'v''} \tilde{\nu}^3_{v'v''} \qquad (6)$$

where

$$q_{v'v''} \equiv |\langle \psi_{v'} | \psi_{v''} \rangle|^2$$

is the Franck-Condon factor between the two vibrational wave functions. By normalization and completeness, (i.e., by the assumption that the Franck-Condon region of the transition to the lower electronic state is concentrated entirely in the bound vibrational levels of the lower state) we obtain the sum rule for Franck-Condon factors:

$$\sum_{v''} q_{v'v''} = 1. \qquad (7)$$

The total fluorescence rate constant from level v' is given by the sum of rate constants to all v'':

$$\begin{aligned} A_{v'} &= \sum_{v''} A_{v'v''} \\ &= \frac{64\pi^4}{3h} G'' |R_e|^2 \sum_{v''} \tilde{\nu}^3_{v'v''} \\ &= 8\pi c \frac{G''}{G'} \underset{\sim}{\sigma} \langle \tilde{\nu}^3_{v'} \rangle_{F\text{-}C} \end{aligned} \qquad (8)$$

where

$$\langle \tilde{\nu}^3_{v'} \rangle_{F\text{-}C} \equiv \sum_{v''} \tilde{\nu}^3_{v'v''} q_{v'v''} \qquad (9)$$

is the average of the fluorescence frequency cubed, taken over Franck-Condon factors. This average may readily be obtained experimentally as developed by the following arguments. The Franck-Condon factor is proportional to the intensity of a given band divided by the frequency

cubed:

$$q_{v'v''} \propto \frac{I_{v'v''}}{\tilde{\nu}^3_{v'v''}} \tag{10}$$

If we define

$$E \equiv \sum_{v''} \frac{I_{v'v''}}{\tilde{\nu}^3_{v'v''}} \tag{11}$$

then

$$q_{v'v''} = \frac{I_{v'v''}}{\tilde{\nu}^3_{v'v''} E}$$

satisfies (7) and (10). Consequently, we may write

$$\langle \tilde{\nu}^3_{v'} \rangle_{F-C} = \frac{\sum_{v''} I_{v'v''}}{\sum_{v''} I_{v'v''}/\tilde{\nu}^3_{v'v''}} = \frac{\int I_{v'} \, d\tilde{\nu}}{\int (I_{v'}/\tilde{\nu}^3) \, d\tilde{\nu}} \tag{12}$$

where the integrals are to be taken over the entire fluorescence spectrum.

The relation between the (measured) absorption coefficient and the (predicted) radiative rate constant is now given by

$$A_{v'} = 8\pi c \frac{G''}{G'} \underset{\sim}{\sigma} \langle \tilde{\nu}^3_{v'} \rangle_{F-C} \tag{13}$$

It should be stressed that in order to apply this relation both $\underset{\sim}{\sigma}$ and $\langle \tilde{\nu}^3_{v'} \rangle_{F-C}$ must be measured in independent experiments. Further $\langle \tilde{\nu}^3_{v'} \rangle_{F-C}$ will be different for different v'. Consequently any comparison between radiative rate constants for different v' must take into account the emission spectra of the two vibrational levels. This point has been stressed by Radford and Broida.[47] Without knowledge of the emission spectra, the comparison of measured lifetimes of two v' levels must be somewhat qualitative. However, a general conclusion that may be inferred

is that the more energetic levels will tend to fluoresce at higher energies and consequently will tend to have greater fluorescence rate constants (shorter lifetimes).

We wish to turn now to the application of these expressions to the $\tilde{A} \longrightarrow \tilde{X}$ transition in nitrogen dioxide. The red-brown color of gas phase NO_2 is due to a strong very broad electronic absorption which extends from 2500 A in the near ultraviolet to at least 10000 A in the near infrared. The gas is in equilibrium with its dimer, which is transparent at wavelengths greater than 4000 A.[48] At the pressures of the present fluorescence experiments this equilibrium is entirely to the side of the monomer;[49] however, at the pressures required for obtaining absorption spectra the proportion of N_2O_4 is quite significant. The problem was overcome by Hall and Blacet[48] who used spectra obtained at two pressures and the equilibrium data[49] to obtain absorption spectra of the two species (Fig. 1). A continuation of the absorption spectrum to 7000 A has been given by Dixon.[50] From the two spectra, which are in good agreement in the region of overlap, the integrated absorption coefficient $\underset{\sim}{\sigma}$ was obtained by numerical integration (Table I).

The entire resonance fluorescence spectrum of any vibrational level of NO_2 has never been measured. Consequently the average quantity $\langle \tilde{\nu}^3_{v'} \rangle_{F-C}$ which is needed for application of Eq. (13) is not available. However, this quantity may be estimated by various means. First, from the absorption spectrum, the average frequency of absorption may be determined[18] (Table I) and used as an estimate of the fluorescence frequency. However, this quantity might be expected to be too large for two reasons:

1) The absorption continues well beyond the dissociation limit

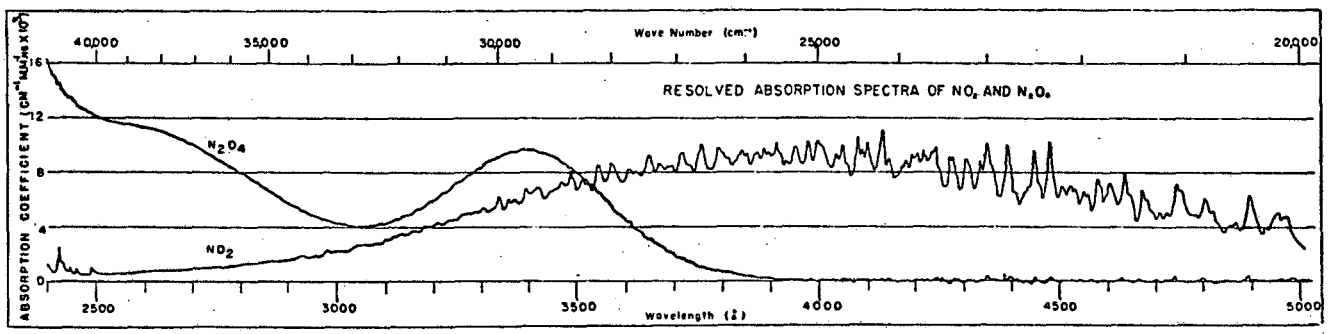

XBL 688-5748

Fig. 1 Absorption spectrum of NO_2 as determined by Hall and Blacet (Ref. 48). From spectra at equilibrium mixtures of NO_2 and N_2O_4 at 33 and 306 torr the spectra of the two species were resolved by use of the equilbrium data. (Figure reproduced by permission of the authors and the copyright holder, the American Institute of Physics).

Table I. Fluorescence lifetime of NO_2 calculated from radiation relations

Integrated Quantity	Value	Calc. Lifetime, μsec	Source of Data	Ref.
$\underset{\sim}{\sigma}$	2.99×10^{-19} cm^2		absorption	a, b
$\int\sigma d\tilde{\nu}/\int(\sigma/\tilde{\nu})\ d\tilde{\nu}$	25880 cm^{-1}	0.256	absorption	a, b
$[\langle\tilde{\nu}^3\rangle_{F-C}]^{1/3}$	12300 cm^{-1}	2.38	NO + O	c
$[\langle\tilde{\nu}^3\rangle_{F-C}]^{1/3}$	6233 cm^{-1}	18.3	NO + O_3	d

Results of numerical integrations of absorption and fluorescence spectra. Fluorescence lifetimes were calculated from integrated absorption coefficient, $\underset{\sim}{\sigma}$, using three estimates of the mean frequency of fluorescence.

a. Ref. 48

b. Ref. 50

c. Ref. 31

d. Refs. 21, 22

3975A, while fluorescence is obtained only from molecules with energies below that limit.

2) Fluorescence can take place to high levels of the ground state. The second approach to the values of $\langle\tilde{\nu}^3\rangle_{F-C}$ can be obtained from chemical reactions that yield excited NO_2.[21,22, 31] If it may be assumed that the electronic state here is the same as that populated optically, then the fluorescence spectra of these chemiluminescence systems can be used to obtain values of $\langle\tilde{\nu}^3\rangle_{F-C}$. These are given as well in Table I. The two values given might be taken to represent the average frequency of emission for the two molecular energies populated by the reactions; however, since the spectra are obtained at high pressure, energy transfer processes may have taken place and consequently the fluorescence spectra may be shifted to lower frequencies than for the resonance spectra. These values should only be considered as rough estimates of the $\langle\tilde{\nu}^3\rangle_{F-C}$ factor that should be used in applying (13) but suggest that a factor of from 10 to 100 of the "anomalously long lifetime" of NO_2 fluorescence may be due to improper estimation of this quantity. Certainly the spread in the values of the calculated lifetimes indicates the degree of caution that must be exercised in applying the radiation relation (Eq. 13) to a transition that extends over as wide a region as the present one.

B. Theory of Measurements

The theory of the phase-shift technique has been developed by previous investigators.[15,51-58] In general we may write the functional relation between the modulated concentration $\underset{\sim}{E}$ of an excited state and the modulated intensity $\underset{\sim}{I}_o$ of the excitation radiation in terms of a dimensionless complex transfer function F which is defined by the relation

$$\underset{\sim}{E} = \frac{k_a G}{k} F \underset{\sim}{I}_o \qquad (1)$$

where

k_a is the absorption cross section,
G is the concentration of molecules in the ground state,
$\underset{\sim}{I}_o = I_o e^{i\omega t}$ is the modulated excitation light,
$\underset{\sim}{E} = E e^{i\omega t}$ is the modulated concentration in the excited state, and
$\omega = 2\pi f$ is the angular frequency of the modulation.

When the kinetics are first order in a single excited state then

$$F = \frac{1}{1 + \frac{i\omega}{k}} \qquad (2)$$

where k is the total rate constant for first order decay in the absence of excitation radiation. Expressions for F for other kinetic mechanisms are given in Appendix A.

Experimentally, the transfer function $F(\omega)$ is obtained by measurements of the intensity of fluorescence and the phase shift of the fluorescent light with respect to the excitation source. For first order kinetics in a single excited state the amplitude of the modulated signal is

$$|\underset{\sim}{S}| = \alpha \gamma k_f |\underset{\sim}{E}| = \alpha \gamma k_f k_a G |\underset{\sim}{I}_o| \frac{1}{(k^2 + \omega^2)^{1/2}} \qquad (3)$$

where k_f is the fluorescence rate constant (a subset of k), where α is the fraction of the total fluorescence spectrum that is within the spectral response of the detector, and γ is a geometrical factor equal to the fraction of the emitted light which is accepted by the detector. The phase shift is given by

$$\theta = \tan^{-1} \frac{\omega}{k} \quad . \tag{4}$$

The desired rate constant k may be obtained either from the decrease in modulated amplitude or from the phase shift; both methods are expected to give the same value for k with the phase method more sensitive. This has been confirmed by Birks and Little.[51]

In two instruments which have been designed to measure the phase shift θ directly, a calibrated phase shifter was either manually set to null the observed phase shift,[52] or was mechanically swept through the null region.[53] These means of measuring the phase suffer from the limitation of short integrating times, and in the former case possible errors of judgment at low signal-to-noise. Presumably these disadvantages could be overcome by the use of a servo-driven phase shifter coupled to an integrator. An alternate technique, which is employed in the present experiment, is to measure the intensities of the in-phase and out-of-phase components of the fluorescent signal by use of a lock-in detector gated with respect to the modulation signal. In single-state kinetics the rate constant and the lifetime are obtained from the ratio of the components:

$$k = \tau^{-1} = \omega S_{0°}/S_{-90°} \tag{5}$$

The modulation amplitude is obtained in the usual way

$$|S| = (S^2_{0°} + S^2_{-90°})^{1/2} \tag{6}$$

This method has been used by Yardley and Moore[15] and Johnston and co-workers[54-56] to enable integration times to be extended arbitrarily by analog or digital means.

The inherent source of error in measurements of rate constants by the phase shift technique is the propagated error of the phase. In the present technique that error enters in setting the phase of the lock-in detector to that of the excitation light. If this error is designated as $\Delta\phi$, measured in radians, then from (4) and (5)

$$\frac{\Delta k}{k} = (R + R^{-1})\ \Delta\phi \qquad (7)$$

where $R = S_{-90°}/S_{0°}$. This result has been given by Kloss and Wendel[57] and by Bonch-Bruevich.[58]

The quantity $(R + R^{-1})$ is at a rather shallow minimum for the exactly tuned modulation frequency, $\omega = k$. The error expression (7) sets limits on the range of lifetimes that may be measured with a given frequency in order to retain a desired precision.

C. Resume' of Stern-Volmer Kinetics

The kinetic scheme of excitation to and fluorescence from a single excited state is known as Stern-Volmer kinetics.[59,60] The elementary reactions in this mechanism are:

$$G \xrightarrow{I_o k_a} E \qquad \text{excitation}$$

$$E \xrightarrow{k_f} G + h\nu \qquad \text{fluorescence}$$

$$E + M \xrightarrow{k_q} G + M \qquad \text{quenching}$$

where

G is a molecule in the ground state

E is a molecule in the excited state

M is a quenching molecule which may or may not be G

I_o is the incident intensity of excitation light, and

k_a is the absorption cross section.

The assumption of a single excited state and the conventional steady state assumption lead to the expression for the concentration of the excited state in a dc experiment:

$$E = I_o k_a G \frac{1}{k_f + k_q M} . \qquad (1)$$

The observed fluorescence signal is given by

$$S = \alpha \gamma k_f E . \qquad (2)$$

Consequently the observed signal should obey the Stern-Volmer relation:

$$(S/G)^{-1} \propto 1 + (k_q/k_f) M \qquad (3)$$

where the constant of proportionality equals the product $(I_o k_a \alpha \gamma)^{-1}$. Even if all these factors are known the dc experiment is capable of yielding only the rate constant ratio k_q/k_f. This ratio may be obtained from the same experiment without knowledge of these factors (which are difficult to obtain experimentally) as the ratio of slope to intercept in a graph of relative values of $(S/G)^{-1}$ vs. total pressure M. Such a graph should have finite and positive values for slope and intercept. Since only a single excited state participates in the fluorescence, the pressure dependence of $(S/G)^{-1}$ should be independent of the observation wavelength.

In a time resolved (flash-decay) experiment the decay in concentration of the excited state from an established concentration E (0) at

time t = 0 in the absence of excitation light is given by

$$E(t) = E(0)\ e^{-t/\tau}$$

where

$$\tau^{-1} = k_f + k_q\ M \tag{4}$$

The inverse lifetime τ^{-1} is the total first order (in E) rate of depopulation of the excited state. Consequently a graph of τ^{-1} vs. M will yield values for k_f and k_q independently as the intercept and slope respectively. The two quantities $(S/G)^{-1}$ and τ^{-1} are measured independently in different experiments. The graphs obtained from each experiment are expected to be geometrically similar; i.e., to have the same slope to intercept ratio.

An alternate graphical representation of the data may be obtained from the relations

$$(S/G)^{-1}/M \propto 1 + (k_f/k_q)\ M^{-1}$$

and (5)

$$\tau^{-1}/M = k_q + k_f\ M^{-1}$$

A graph of either of these quantities vs. the inverse of the pressure (inverse Stern-Volmer plot) should again be linear.

We wish now to treat the same mechanism in terms of the phase shift technique. This method introduces no new kinetics, but is merely an alternate method of performing the experiment. For simple Stern-Volmer kinetics the measurement of in-phase and out-of-phase signal intensities as a function of pressure, at a single modulation frequency $\omega = 2\pi f$, is equivalent to the independent measurement of lifetime and intensity as a

function of pressure. This equivalence is developed as follows. In an ac experiment the differential equation governing the population E is

$$\dot{\underset{\sim}{E}} = \underset{\sim}{I}_o \; k_a \; G - \underset{\sim}{E} \; (k_f + k_q \, M)$$

where $\underset{\sim}{I}_o$ is the incident (ac) intensity. For $\underset{\sim}{I}_o = I_o \, e^{i\omega t}$ the solution obtained for the modulated concentration in the excited state is

$$\underset{\sim}{E} = \underset{\sim}{I}_o \; k_a \; G \left(\frac{1}{k_f + k_q \, M + i\omega} \right) e^{i\omega t}$$

whence

$$\underset{\sim}{S}/G = I_o \, \alpha \, \gamma \, k_a \, k_f \left(\frac{1}{k_f + k_q \, M + i\omega} \right) e^{i\omega t}$$

$$= I_o \, \alpha \, \gamma \, k_a \, k_f \left\{ \frac{k_f + k_q \, M}{(k_f + k_q M)^2 + \omega^2} - i \times \frac{\omega}{(k_f + k_q M)^2 + \omega^2} \right\}$$

For the lock-in measurement technique

$$\underset{\sim}{S} = S_{0°} - iS_{-90°}$$

In Stern-Volmer kinetics then

$$S_{0°} = I_o \, \alpha \, \gamma \; k_a k_f \; \frac{k_f + k_q \, M}{(k_f + k_q \, M)^2 + \omega^2} \qquad (7)$$

and

$$S_{-90°} = I_o \, \alpha \, \gamma \; k_a k_f \; \frac{\omega}{(k_f + k_q \, M)^2 + \omega^2} \; , \qquad (8)$$

the in-phase and out-of-phase intensities, are the two independently measured quantities in the experiment. We now define the combinatorial quantities $R = S_{-90°}/S_{0°}$ which is dimensionless and $I = [(S_{0°})^2 + (S_{-90°})^2] \; / \; S_{0°}$ having units of intensity which, under the assumption of Stern-Volmer kinetics, should obey the relations:

$$R^{-1} = (k_f + k_q M)/\omega \quad \text{and} \quad R^{-1}/M = (k_q + k_f M^{-1})/\omega$$
$$I^{-1} \propto 1 + (k_q / k_f)M \quad \text{and} \quad I^{-1}/M \propto 1 + (k_f / k_q)M^{-1} \tag{9}$$

where, as before, the constants of proportionality take into account the product $(I_o k_a \alpha \gamma)$. The two quantitites I and R/ω are the phase shift analogs to the intensity measured in a dc experiment and the lifetime measured in a conventional flash-decay experiment, respectively.

It should be stressed that the two quantities R and I are independent. The two directly measured quantities $S_{0°}$ and $S_{-90°}$ may be written in terms of R and I

$$S_{0°} = I/(1 + R^2)$$
$$S_{-90°} = IR/(1 + R^2) \tag{10}$$

D. Summary of Previous Studies of NO_2 Fluorescence

The optically excited fluorescence of NO_2 was first observed by Norrish.[61] The fluorescence was found to extend from the wavelength of excitation into the red, and the spectrum exhibited a broad, diffuse structure. The first quantitative quenching studies of the fluorescence were made by Baxter,[62] who interpreted the results in terms of the Stern-Volmer mechanism, finding that the quenching ratio k_q/k_f was very large. The indication was that either the quenching was super-efficient or that the lifetime of the excited molecule was quite long. This question was resolved by Heil[63] who showed, from the fact that the molecules diffuse the order of 0.1 cm in their lifetime, that the lifetime was necessarily the order of 10 μsec.

The first photo-electric measurements of the fluorescence lifetime and quenching were made by Neuberger and Duncan (ND),[18] who found a lifetime of 44 μsec. ND found no dependence of the fluorescence lifetime on the wavelength of excitation for the regions 3750-4150, 4050-4700, and 4400-5000 A. Attempts were made as well to measure fluorescence lifetimes for excitation in the regions 3300-3900 and 5200-5700 A. In the former region no fluorescence was observed; this was attributed to dissociation. In the latter region fluorescence was observed, but no lifetime was capable of measurement with their equipment. This was attributed by the authors either to lack of sufficient signal or to insufficient time resolution of their equipment. ND also obtained a quenching rate constant (6.0×10^{-11} cm^3/molecule sec) which was independent of the excitation wavelength.

Douglas[20] has remeasured the fluorescence lifetime for excitation near 4300 A, and has extended the measurements to lower pressures of NO_2 (0.1 mtorr) than were used by ND. The fluorescence decay was found to be exponential with a lifetime of 44 μsec, and there was no change in the lifetime in the pressure region 0.1 to 1 mtorr.

Recent quenching measurements by Myers, Silver, and Kaufman (MSK)[19] have indicated that the lifetime is at least as long for excitation at wavelengths greater than 5000 A as for excitation at lower wavelengths. Further, the quenching ratio was found to depend on the excitation wavelength, and for a given excitation wavelength on the observation wavelength. For excitation at 4358 A the quenching ratio was reduced threefold as the wavelength of observation was changed from 4580 A to 6330 A. This observation implies that the Stern-Volmer mechanism of

of a single excited state is not obeyed, and suggests that the quenching process consists of the stepwise removal of energy from the excited molecule.

II. EXPERIMENTAL

A. Apparatus

1. General Considerations.

An apparatus was designed to excite and detect fluorescence in the visible region and to measure fluorescence lifetimes in the range 10-200 μ sec at extremely low light intensities. Since it was desired that the excitation band pass be narrow and continuously tunable throughout the region, a continuum source—monochromator combination was employed rather than an atomic line source. A block diagram of the apparatus is given in Fig. 2; the components of the apparatus are discussed below.

The phase shift method is especially suitable to lifetime measurements at low fluorescence intensities as it makes efficient use of the available excitation light (50% in the present case) and readily allows for long integration periods necessary to overcome shot noise in the optical signal. Under the conditions of the experiment, at a pressure of 1 mtorr, or 3×10^{13} molecules / cm^3 in the ground state there were typically 10^3 molecules / cm^3 in the excited state. Signal intensities were of the order of 100 counts/sec; lifetime measurements may be made at intensities well below this (e.g., 10 counts/sec) if the integrating time is sufficiently long for the desired accuracy.

For any particle detector the precision of intensity measurements is dependent on the total number of particles detected. For an ideal detector the signal-to-noise (signal to standard deviation in signal) is given by

$$S/N = (IT)^{1/2}$$

where I is the average count rate and T is the counting time. Thus for I = 100 counts/sec, T must be 100 sec for a noise-to-signal equal to 1%.

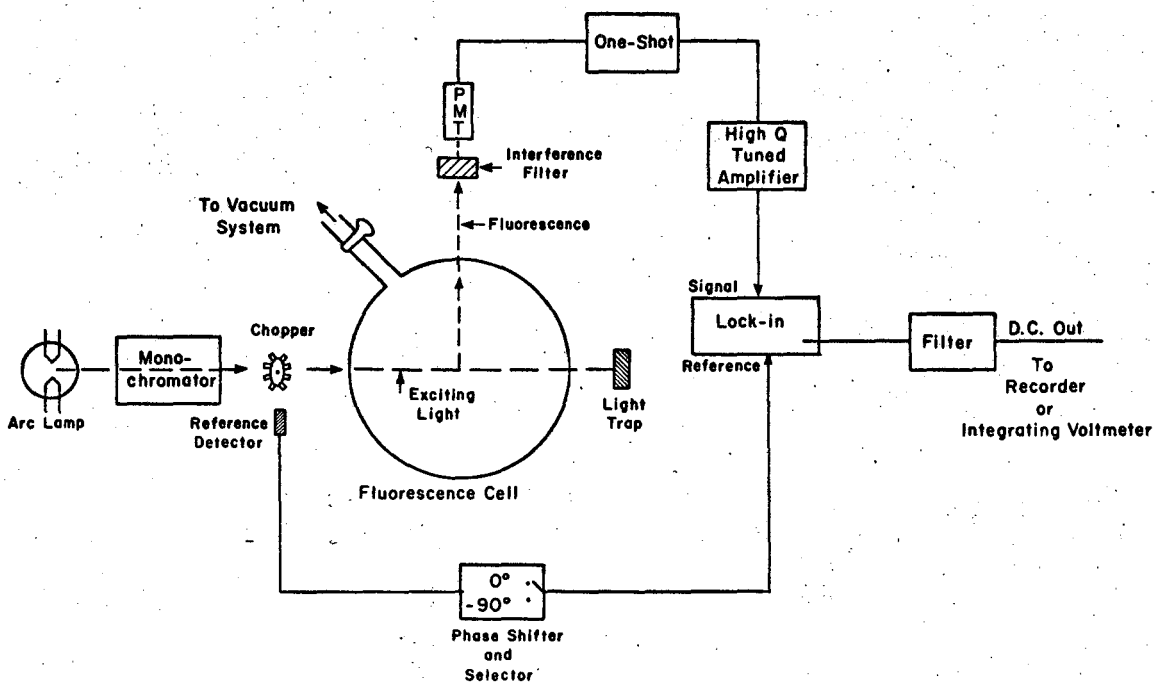

XBL 685-734

Fig. 2. Block diagram of apparatus for phase shift measurements at low light intensities.

For a real photon detector (photomultiplier and associated signal processing equipment), the signal-to-noise will be degraded from the ideal, and the necessary integrating time consequently increased.

2. Lamp.

The lamp used in these experiments was a 1600 watt dc, high pressure xenon arc (Osram Model XBO 1600), which emits a continuum over the spectral range 2400-7600 A. According to the manufacturer there is some structure to the emission spectrum of the lamp in the region 4400-5000 A, probably pressure broadened lines; however, no indication of the existence of such structure was observed in the output radiation of the source monochromators. The lamp was powered by a Christie Electric Corp. (Model MHXM-1600-2S) silicon rectifier which ran on 208 volt, three phase ac line current. The ac ripple on the dc light output was 0.7 per cent, mostly 120Hz. Although not stabilized, the lamp supply was relatively constant. During the course of an experiment lasting several hours the current was normally constant of 64.0 ± 0.7 amps. The light output varied approximately as the square of the current variation. The input to the lamp was normally 64.0 amps x 25.5 volts or 1630 watts. The lamp house (15 cm diameter) was water cooled.

According to the manufacturer the light output of the lamp is constant during its 1500 h rated life. Any decrease in the light output, if uncompensated, will lead to systematic errors in measurements of relative intensities. The measurements of fluorescence intensities reported here were made with a new lamp during the first 600 h of its life. No determination was made of any possible decrease in lamp intensity in this time, but such a long term decrease would be adequately compensated by

the use of a fluorescence intensity standard (Sec. 10). Also, for a given excitation wavelength experiments at different pressures were made in random order.

3. Monochromator.

Monochromation of the excitation light was accomplished by Bausch and Lomb 33-86-02 (compact) and 33-86-45 (500 mm) grating monochromators in series. The former, used as a pre-monochromator to reduce total scattered light, was mounted at the side slit of the larger instrument, such that the entrance slit of the second monochromator served as the exit slit of the first. Radiation from the lamp was focused on the entrance slit of the compact monochromator by a quartz condenser system supplied with the larger monochromator; this lens extended into the lamp house approximately 3 mm from the bulb.

Under the usual conditions of measurement the slit widths were 1.3 mm for the entrance slit of the compact monochromator and 0.9 mm for the slits of the 500 mm monochromator. At these slit widths the nominal full width at half maximum intensity was 11.5 A. The measured values were 15.0 ± 0.4 A. The slit function was observed by use of a Spex Industries model 1400 double grating monochromator; a profile obtained for excitation at 4300 A is given in Fig. 3. These measurements were not corrected for variation in the spectral response of the monochromator and photomultiplier in view of the narrow spectral region involved. In order to obtain a representative sampling of the beam of excitation radiation the entire beam was made to fall on a frosted glass plate, and the scattered light from this plate was observed in transmission. The frosted plate was located approximately 20 cm from the entrance slit of the Spex monochromator and no focusing was used between the plate and the entrance slit.

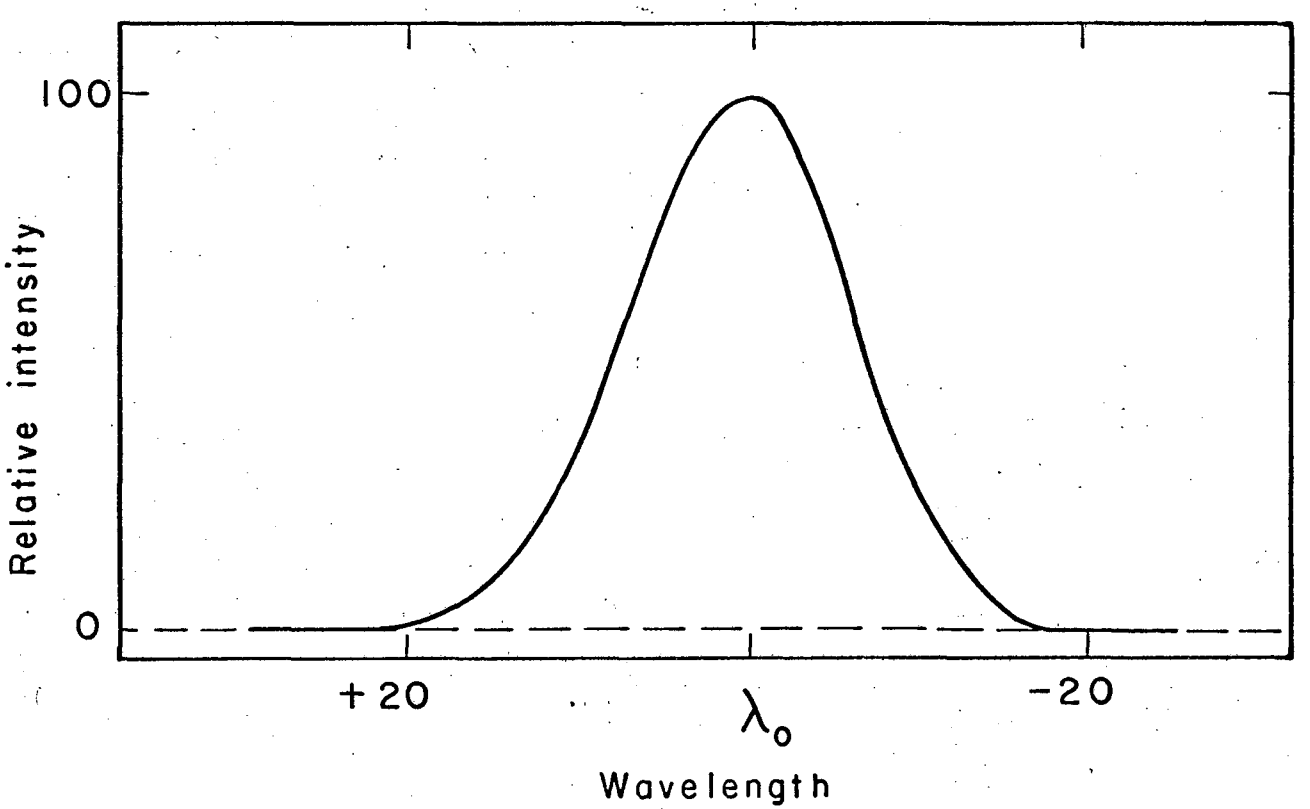

Fig. 3. Slit function of source monochromator. Normally the full width at half intensity was 15 A; the 10% width was less than 30 A and 1% width less than 40 A.

The wavelength calibration of the Spex monochromator was determined to ±0.2 A with a low pressure Hg discharge (General Electric Model No. G4T4, 4 watt) and the wavelength calibration of the excitation source determined in turn from this. The optimum tracking of the two source monochromators was determined by trial and error; at optimum tracking the band pass was fairly symmetric and the intensity approximately maximum. The difference in wavelength reading between the two monochromators for optimum tracking was constant as a function of wavelength. Repeatability in setting the source monochromators was approximately 3 A.

4. Modulator and Reference

The optical modulator consisted of a mechanical blade chopper wheel 20 cm in diameter having 60 slots recessed 1.9 cm from the circumference. The width of the slot was equal to that of the blade. The light was focused onto the plane of the blade. The image of the source monochromator slit was approximately 1 mm in width compared to 5.2 mm for the blades. It was desired to have an image of the slit focused as small as practical in order to minimize the phase spread in the excitation radiation, although this results in a greater proportion of higher harmonics in the excitation wave form.

The motor used was a 1/50 h.p. Bodine hysteresis synchronous motor (Model No. NCH-13) having a rotation speed of 60 revolutions/sec. With the 60 bladed wheel the modulation frequency produced was 3600 Hz, corresponding to a tuned lifetime (45° phase shift) of 44.21 μ sec. This frequency was confirmed by direct count and was considered to be maintained to the precision of the 60 cycle ac line frequency, which is generally better than 0.1 percent. Any significant variation in this frequency manifested itself drastically in phase shifts in the tuned amplifiers in the phase sensitive detector. There was a slight amount of jitter in the 3600 Hz signal compared to line due to the load of the

blade on the motor; this did not have any effect on the detection system.

The reference signal to drive the lock-in was taken directly from the motion of the blade by a metal distance detector (Bently Nevada Corp., Model D-152). The signal from the distance detector was filtered to remove unwanted high and low frequencies.

The filtered signal is capable of driving the lock-in directly at any given phase; however, since the lock-in used did not have a quadrature phase shifter, such a phase shifter was constructed so that reference signals separated by 90° could be obtained. The schematic of the phase shifter is given in Appendix F.

5. Fluorescence Geometry.

Because of the effect of the geometry of excitation and observation of the fluorescence it was desired to keep the observation region as large as possible. The geometrical arrangement of optical components is indicated in Fig. 4. The excitation beam B was approximately parallel throughout the cell. The two masks M served to prevent observation of any possible fluorescence by the walls themselves, and to prevent observation of molecules excited near the walls whose lifetime would be shortened by wall quenching.

In order that the photomultiplier would be able to receive radiation from the entire height of the fluorescence cell the housing was designed to accept light from a wide angle. This was accomplished by the use of an aperture plate A, which, together with the effective cathode surface diameter, defined an angle of acceptance θ ($\tan \theta = 0.31$) such that all light entrant upon the aperture within this angle would be accepted. With the geometry shown in Fig. 4 the entire height of the bulb fell within this angle of acceptance.

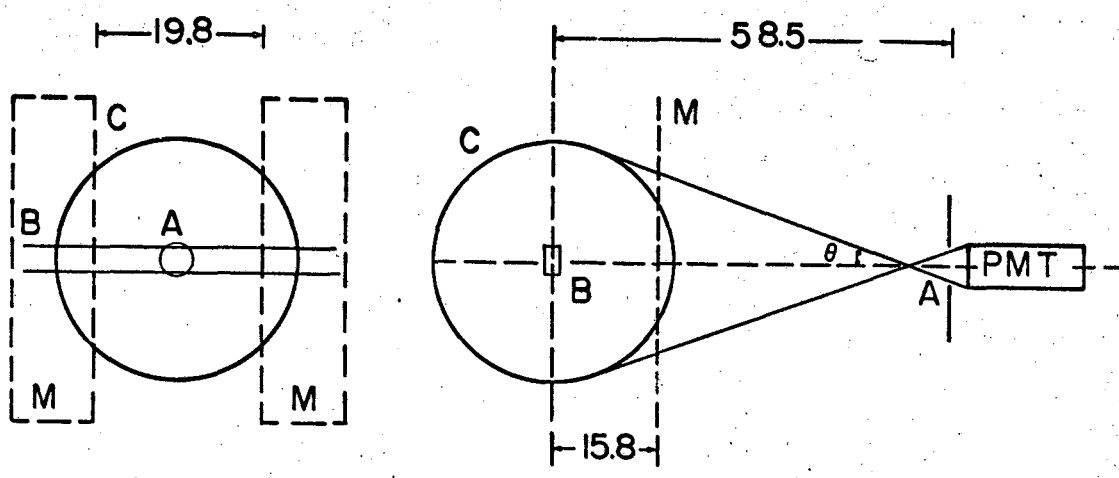

Fig. 4. Fluorescence geometry: front and side views of geometrical arrangement for excitation and observation of fluorescence. A, aperture plate, 34 mm diameter; B, excitation beam, 20 mm x 25 mm; C, fluorescence cell, 33 cm diam; M, masks.

The condition that was considered the most severe limitation of the detection efficiency at large distances from the axis was the curvature of the spherical fluorescence cell; at larger angles from the normal a higher fraction of incident light is reflected. Because of this effect the estimated dimension of the region of good detection efficiency was ±14 cm about the axis.

6. Photomultiplier.

The optical detector used in these experiments was a high gain photomultiplier having a spectral response to 8000 A (EMI 9558A, S-20 response). In use the tube was refrigerated by cold N_2 gas passing over the cathode area of the tube; the temperature, measured by a thermistor located close to the cathode was held to -56.4° ± 4°C. No dependence of the quantum efficiency of the photomultiplier was observed in this temperature range to a sensitivity of 1%. At the temperature of operation the dark current from the tube was approximately 40 counts/sec. However, this dark current was non-statistical; a significant fraction occurred in bursts of 10 or more extending over approximately 1 msec. The origin of such sources of noise has been discussed previously.[64] It is believed that these bursts may be due to disintegrations of ^{40}K in the tube window; they were not observed in a model 9558QA tube, which had a quartz window.

The high voltage power supply used was a Fluke model 408 B having a ripple less than 1 mv RMS and a stability of 0.02% per day. The photomultiplier was operated in the usual way with the cathode at negative high voltage (-1400 v) and the anode load resistor (20K) tied

to ground. A copper foil shield surrounding the dynode area of the tube was held at cathode potential.

7. Spectral Calibration.

The spectrical response of the detector (photomultiplier plus interference filters) was calibrated in order to obtain fluorescence intensity spectra. In such a calibration one uses a standard light source whose relative spectral intensity distribution is known; from the spectral distribution observed with a given detector the relative spectral response of the detector may be obtained. At a given observation wavelength the detector observes a signal

$$S_\lambda\,(\text{lamp}) = \int_\lambda I(\text{lamp})\; T(\text{filter})\; R(\text{PMT})\; d\lambda$$

where the integration is taken over the detection region, in the present case over the transmission region of the interference filter. If I(lamp) is known and is constant over the region of integration, then

$$\langle TR\Delta\lambda\rangle_\lambda = S_\lambda(\text{lamp})/I_\lambda(\text{lamp}) = \int_\lambda T(\text{filter})\; R(\text{PMT})\; d\lambda$$

Similarly, for the fluorescence signal

$$S_\lambda(\text{fluor.}) = \int_\lambda I(\text{fluor.})\; T(\text{filter})\; R(\text{PMT})\; d\lambda$$

whence

$$\begin{aligned} I_\lambda(\text{fluor.}) &= S_\lambda(\text{fluor.})/\langle TR\Delta\lambda\rangle \\ &= S_\lambda(\text{fluor.})/[S_\lambda\,(\text{lamp})/I_\lambda(\text{lamp})] \end{aligned}$$

With these assumptions the quantity $[S_\lambda(\text{lamp})/I_\lambda(\text{lamp})]$ may be taken as a measure of the spectral response at wavelength λ, Thus a calibration of the detector could be made in the usual way. The lamp

used was a tungsten ribbon filament lamp designed for this purpose (General Electric Model 30A/T24/17) powered by a photo-regulated supply.[65] The brightness temperature of the filament was measured with a Leeds and Northrup optical pyrometer (Model No. 8622-0) which had been calibrated by the LRL dc standards group. From the brightness temperature the thermodynamic temperature and spectral emissivity were determined from the data of De Vos[66] with a program written by Gabelnick.[65] The results of the calibration are given in Table II.

An examination of the assumptions concerning the constancy of I(lamp) and I(fluor.) showed that these assumptions are subject to criticism for the band pass of the interference filters used. Representative data illustrating this effect are given in Table II. The magnitude of the uncertainty in the spectral response factors for the various filters resulting from this effect is probably the order of 20% in the blue region, less in the red.

The interference filters were supplied by Baird Atomic Corp. Transmission characteristics were determined on a Cary 14 Spectrophotometer.

8. Signal Processing Electronics.

Under the conditions of these experiments the optical signal was of sufficiently low intensity ($< 5 \times 10^3$ counts/sec) that the photomultiplier signal was observable on an oscilloscope (Tektronix Model 545; rise time 20 nsec) as individual voltage pulses, or shots, corresponding to single-electron cathode events. Under these conditions a considerable advantage in signal-to-noise may be obtained by treating the signal from the photomultiplier as digital information rather than analog.[64] A possible tech-

Table II. Wavelength response of photomultiplier plus filters

Filter number	Maximum transmission frequency cm^{-1}	Band-Pass 50% cm^{-1}	Band-Pass 10% cm^{-1}	Relative response [a]	Intensity variation in calibration lamp %/100 cm^{-1}	Intensity variation in calibration lamp %/50% B.-P.
1	23200 ± 50	458	807	1.69	5.7	26.3
2	22170	260	477	1.29	5.7	14.8
3	21460	253	488	0.835		
4	20790 ± 40	238	454	(1.00)		
5	20370	274	494	0.878		
6	19960	116	239	0.428	5.6	6.5
7	19350	183	329	0.724		
8	18950	180	334	0.645		
9	17880 ± 30	189	339	0.549		
10	16960	164	293	0.405	5.3	8.6
11	15850	249	452	0.323		
12	15130 ± 20	185	342	0.371	5.2	12.6
13	14270	185	342	0.236		
14	13320	193	339	0.0633		
15	12480	177	276	0.0186	4.8	13.2

[a] Relative response (quanta/cm^{-1} sec), normalized to No. 4.

nique, thus, would be to use the pulse signal from the photomultiplier to trigger a pair of reversible counters gated in quadrature by the reference signal (digital lock-in).[54] However, this technique suffers from the disadvantage of requiring a precise knowledge of the harmonic content in the optical excitation waveform. Third, fifth, and higher harmonics have different phase shifts from the fundamental, and the contribution from these can be taken into account only if their magnitude is known.

Alternatively, an analog lock-in is capable of selecting the fundamental frequency and rejecting higher harmonics by means of a tuned amplifier in the signal channel. It was in large part for this reason that analog electronic circuitry was used in preference to digital. However, in order to retain the advantage in signal-to-noise afforded by the use of digital equipment a monostable multivibrator (one-shot) similar to that described by Akins, Schwartz, and Moore[64] was used to convert the pulses from the photomultiplier into uniform pulses suitable for subsequent analog data handling.

The design considerations involved in using this type of circuitry have been discussed previously.[64] The one shot used in the present work differs from that previously described in the addition of preamplification stages and the addition of a separate one-shot following the discriminator. It is capable of being triggered by a pulse of 1.0 mV lasting 0.1 μsec. The discriminator level was set by methods discussed previously.[64] In the present work the output pulse width was 1.0 μsec; the recovery time was 0.5 μsec. Thus coincidence loss was less that 1% for count rates up to 6×10^3 counts/sec. The output pulse voltage was attenuated to approximately 0.5V. The circuit schematic is given in Appendix F.

In order to keep the circuitry fast a transistorized current

amplifier was located at the socket of the photomultiplier tube. The schematic of this amplifier is given in Appendix F.

The output from the one-shot was fed directly into the signal channel of the lock-in amplifier (Princeton Applied Research Model JB-5). Because of the single shot characteristic of the input signal to the lock-in it was necessary to modify somewhat the usage of the amplifier; specifically it was necessary to operate at a low average dc output voltage in order to avoid saturating ac amplifiers by high transient voltages. A general discussion of the problem of dynamic range in pulse work and the advantage of using a sharply tuned circuit is given in Appendix E.

The output from the lock-in was 1) recorded directly on a potentiometer recorder (Varian, Model G-10) and 2) used to drive a voltage controlled generator (Wavetek, Model 111) which, with a counter and timer, was used to integrate the output signal.[54] The time was controlled by a crystal oscillator and provided integration periods differing by a precise factor of 2, of approximately 25, 50, and 100 sec. At signal levels sufficiently high that accurate readings of the strip chart record could be taken the signals from the recorder and the integrator were proportional to within 1%; the specified linearity of the voltage controlled generator was 0.1%.

9. Gas Handling.

The vacuum and gas handling system was a conventional greaseless metal and glass line. A 2 in. oil diffusion pump was water baffled and liquid nitrogen trapped; the pumping fluid was Dow Corning 704 silicone fluid. The section of the vacuum line used for handling and storage of

the sample was largely glass; other materials present were stainless steel, Kovar, Teflon, and Viton A. High vacuum greaseless stopcocks (Teflon plugs, O-ring seals) were used. The residual pressure prior to filling the cell was less than 4×10^{-6} torr, as measured with an ionization gauge (Consolidated Vacuum Corporation, Model GIC-10, uncalibrated).

The fluorescence cell was a 33 cm diameter, 22 liter pyrex spherical bulb; the neck was sealed against the atmosphere with a 10 mm greaseless stopcock. The cell was detachable from the vacuum line and transported to the fluorescence apparatus; the seal to the vacuum line was made with an O-ring connector. The leak rate into the sealed off fluorescence cell was less than 5×10^{-7} torr/h; most experiments were made within a period of 10 h after the cell was filled, but in a few cases measurements were continued on the next day. A cold finger was attached to the neck of the cell to allow for freezing out the sample.

Pressure measurements were made with a capacitance pressure transducer (Datametrics Model 511-10, controller Model 1014). The theory of this type of instrument has been discussed by Rony.[67] According to the manufacturer the linearity of the present instrument was better than 0.1% over the range 0 to 10 Torr; in the present experiment using analog read out (Varian G-10 recorder) measurements were precise to 1%. The finite leak rate of the transducer (approximately 0.5 mtorr cm^3/sec) through small diameter tubing to the vacuum system produced a zero offset in the pressure measurement (0.08 mtorr). Consequently, measurements of pressure were taken by difference. The impurity in the sample due to the leak rate of the transducer was estimated to be less than 0.03 mtorr; this was probably the most significant source of impurity.

Nitrogen dioxide was obtained from Matheson and had a stated purity

of 99.5%. The gas was admitted to the vacuum line to approximately 20 torr and a portion was crystallized in a cold finger at -78°C. The residual gas was pumped off and the sample pumped on. The sample was sublimed, recrystallized and pumped on several times. The crystals were at all times colorless. Following this the sample was twice distilled from -78° to -196°, the first and last fractions being discarded. The purified sample was kept in the dark at -196°. Prior to filling the cell the sample was recrystallized within the storage bulb and again pumped on at -78°. The fluorescence cell was filled by admitting NO_2 from the storage bulb at -78° into the cell until the desired pressure was attained.

The experiments were conducted at a temperature of 23.3° ± 1.3°C.

10. Procedure.

For any set of independent variables (excitation wavelength, observation wavelength, and pressure) the two measured quantities were the intensity of in-phase and out-of-phase fluorescence. In practice, however, some scattered modulated light is detected by the photomultiplier; consequently all measurements were made as a difference between signal with the fluorescing gas present and signal with the gas frozen out in the cold finger of the cell. At the higher pressures, for widely separated excitation and observation wavelengths, the scattered in-phase signal was less than one per cent of the in-phase fluorescence signal; at low pressures, for observation close to the excitation wavelength, the scattered in-phase signal was as great as ten times the in-phase fluorescence signal. Scattered out-of-phase signal was in all cases quite small. This scattered light was due to excitation light transmitted through the wings of the

filter band pass. Because of the low pressures (less than 50 m Torr) no more than 4% of the total incident radiation was absorbed in a path length of 33 cm, and correspondingly less at the lower pressures where scattered light was more important. Consequently it was concluded that the presence of the gas did not significantly affect the amount of scattered light received by the detector.

For each of the four measurements usually three to six counts were made of the output of the voltage controlled generator. The length of the integration period and the number of counts taken were determined from estimates of the signal-to-noise. It was desired to have the standard deviation of the signal less than one or two per cent.

In order to set the phase of the lock-in detector to that of the excitation radiation it was necessary to observe a representative sample of that radiation, suitably reduced in intensity. This was accomplished by:

1) The use of a ground glass scatter plate as discussed previously. The entire beam was made to fall on this plate, which was placed 40 cm from the aperture plate of the photomultiplier. No focusing was used between the frosted plate and the photomultiplier.

2) The use of neutral density filters (Oriel Optics Corp. Type G-33) in front of the aperture plate of the photomultiplier. The required density was 7 or 8.

When the lock-in is correctly phased the signal for in-phase detection is at a maximum; for out-of-phase detection, at a minimum. Measurement of the phase error $\Delta\phi$, is more sensitive in the out-of-phase channel because the error signal is linearly proportional to $\Delta\phi$. The phase error was measured as $\Delta\phi = S_{-90^\circ} / S_{0^\circ}$; the required tolerance on phase error

was 1 per cent. After several fluorescence measurements the phase error was again measured to check for any drift.

In order to rule out the effect of any drift in the amplitude response of the system (excitation intensity or instrument sensitivity) it was desired to have a reproducible fluorescence standard. A Corning yellow "sharp cut" filter (No. 3-75) was found to emit a weak fluorescence for excitation in the region 4000-5000 A; for a given excitation wavelength the fluorescence intensity was quite reproducible. Corrections resulting from the use of this standard were generally no greater than a few per cent.

B. Results

1. Effect of Size of Fluorescence Cell

In exploratory investigations it was established that the measured lifetime at low pressures was a function of the size of the fluorescence cell. After the apparatus had been adapted to use with a 33 cm spherical bulb as fluorescence cell, an experiment was conducted to obtain a quantitative measure of this effect by comparing the results of measurements obtained with cells of different size. Two cylindrical pyrex cells (4.6 cm and 9.6 cm inner diameter) were used in addition to the 33 cm spherical bulb. As with the spherical bulb, the ends of the two cylindrical cells were masked from the view of the photomultiplier so that only radiation from the central part of the cells was detected. The dimensions are given in Table III.

For this experiment the excitation beam was approximately rectangular having dimensions 2.0 x 1.5 cm. All three cells were filled to a pressure of 1.3 m Torr. Excitation was at 5175 A and the detection was

with a 2-73 filter. Each cell was adapted with a cold finger for freezing out the sample gas; correction was made for scattered source light by subtracting the signal obtained when the NO_2 was frozen out. The lifetimes were computed under the assumption of a single excited state and are given in Table III.

2. Fluorescence Lifetime as a Function of Excitation Wavelength

In this study the fluorescence cell was filled to a low pressure (1.3 ± .1 mtorr) and the fluorescence lifetime was measured for excitation wavelengths from 3975 A to 6000 A. The excitation band-pass was approximately 25 A, full width at half maximum. The fluorescence was observed through a Corning 2-73 filter for excitation wavelengths shorter than 5400 A, or the appropriate "sharp-cut" filter for higher excitation wavelengths to reduce scattered light from the source. At the extremes of the excitation region the fluorescence was quite weak, and consequently the uncertainty in the measurements is increased. The measured lifetimes were 60-90 μsec throughout the excitation region. The data are given in Table IV and Fig. 5. Figure 5 also shows the results of several individual measurements for excitation in the region around 5175 A with an excitation band-pass of 12 A.

The lifetimes were computed on the assumption of a single excited state and were not corrected for quenching. Since an observed lifetime at finite pressure is shorter than the radiative lifetime these measurements represent a lower bound to the radiative lifetime. However at the pressure of these measurements quenching would not shorten the lifetime by more than ten or twenty per cent.

Considerable attention was paid to the possibility that systematic

Table III

Effect of size of fluorescence cell on measured lifetime

Cell Diameter cm	Overall length cm	Length of cell visible to PMT cm	Apparent lifetime μsec
4.6	7.5	3.0	44
9.6	12.5	5.5	68
33, spherical	---	19.8	80

Table IV. Fluorescence lifetimes for NO_2 at 1.3 mtorr for excitation 3975 - 6000 A

Excitation wavelength A	Lifetime μsec
3975	58 ± 4
4000	55.7 ± 1.2
4100	59.8
4200	60.4
4300	62.4
4400	59.4
4475	63.3
4500	63.2 ± 2.2
4575	65.3
4675	62.7
4775	69.0
4875	71.7
4975	72.9
5075	73.2
5125	71.3
5175	79.8 ± 2.2
5225	74.5 ± 1.5
5275	72.8
5325	79.3
5375	85.3
5450	73.4
5500	74.0
5600	90 ± 3
5700	73.6 ± 1.8
5800	80 ± 3
5900	70 ± 4
6000	77 ± 4

Table IV (continued)

Excitation band-pass was approximately 25 A, full width at half maximum. Observation was with Corning 2-73 filter for excitation wavelengths shorter than 5400 A and the appropriate "sharp cut" filter at higher wavelengths. Errors given are typical and represent two standard deviations of the mean as determined from the scatter of the data.

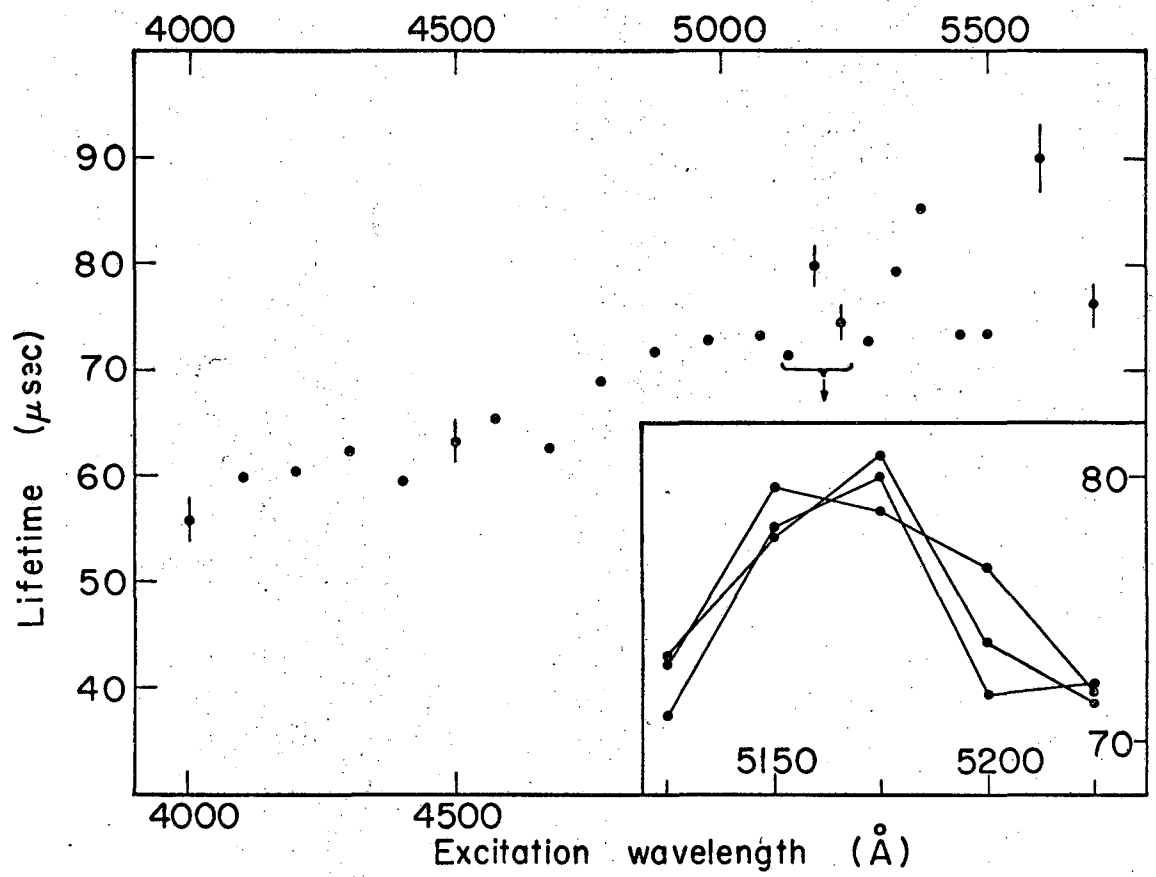

Fig. 5. Fluorescence lifetime of NO_2 gas at 1.3×10^{-3} torr pressure as a function of excitation wavelength. Half width of excitation light was approximately 25A. Error bars are typical and were determined from the scatter of several experiments. Inset shows individual data points for the region around 5175A, excited with 12A half width. Data points for the same run are connected; points within a run were taken in random order.

errors might be responsible for observed fluctuations in the measured lifetime. To avoid this possibility measurements of lifetimes at different excitation wavelengths within a narrow region were made in random order, and the phase of the instrument was checked frequently and at different wavelengths.

In addition to low pressure studies exploratory investigations were made at a higher pressure (36.0 mtorr) to extend the range of excitation wavelengths to wider limits. The higher pressure was necessitated by the decrease in fluorescence signal in the extended region. At the higher pressure the lifetimes were of course shortened signficantly from the radiative lifetimes by quenching processes. At 36 mtorr, it was possible to observe fluorescence with the excitation wavelength set as low as 3950 A. The fluorescence signal decreased by a factor of approximately 4000 between excitation at 4050 A and 3950 A. The absorption coefficient and the lamp intensity are relatively constant in this region. Consequently this decrease in intensity represents a decrease in the quantum yield of fluorescence. However the observed lifetime (with Corning Filter 3-70) remained relatively constant (± 25%) in this region. These data are given in Table V.

At high wavelengths it was possible to measure fluorescence lifetimes for excitation as far to the red as 6800 A, (Table VI). The observed lifetime was relatively constant as a function of excitation energy for excitation extending throughout the region.

3. Pressure Dependence of Fluorescence Lifetime and Intensity.

These studies were conducted over the pressure range 0.5 to 50 m Torr for three excitation wavelengths, 4000, 4300 and 4800 A. For each

Table V. Fluorescence lifetimes for NO_2 at 36 mtorr, excited near the dissociation threshold

Excitation wavelength, A	Lifetime, μ sec	Quantum yield, relative to 4050 A
4050	14.1 ± 1	1
4000	18.3 ± 1	.3
3980	22.8 ± 1	.04
3970	23.2 ± 1	9×10^{-4}
3960	20.0 ± 1	5×10^{-4}
3950	15.5 ± 4	2.5×10^{-4}

Observation was with Corning 3-70 filter. Errors in lifetimes are evaluated from Eq. (I-B-5) and the scatter of the data and represent estimated tolerance limits. Excitation band pass was 20 A, full width at half maximum. Quantum yields are calculated assuming constant lamp intensity and absorption coefficient.

Table VI

Fluorescence lifetimes for NO_2 at 36 mtorr for excitation wavelengths 4000-6800 A.

Excitation Wavelength, A	Filter, Corning CS No.	Lifetime, μ sec
4000	3-70	18.3±1
4500	2-73	15.6±1
5000	2-73	13.7±1
5500	2-63	9.4±1
6000	2-58	13.7±1
6400	2-64	11.0±2
6800	7-69	12.0±4

set of experimental conditions (excitation wavelength, observation wavelength, and pressure) the raw data from the counter were averaged and appropriate differences taken to correct for scattered light from the empty cell. The quantities thus obtained, $S_{0°}$ and $S_{-90°}$ were the uncorrected in-phase and out-of-phase signal intensities. These intensities were normalized by dividing by the pressure of the absorbing gas and corrected for the amplitude response of the system and for the wavelength response of the system for the interference filter used. These corrected data were used to compute the intensity ratio, $R^{-1} = S_{0°}/S_{-90°}$, and the inverse Stern-Volmer intensity, $I^{-1} = S_{0°}/(S^2_{0°} + S^2_{-90°})$. (See Sec. I-C). The uncertainties (fractional sample standard deviations) in these quantities were computed from the spread in the original data from the counter. All of these quantities are given in Table D-I, as are the apparent lifetimes, computed by the expression $\tau = \omega^{-1} R$.

For each set of measurements with a given excitation and observation wavelength the quantities I^{-1} and R^{-1} were graphed as a function of pressure and fitted by the method of least squares. These quantities were selected to be fitted because of the theoretical prediction of linearity for Stern-Volmer kinetics. Any deviations from linearity were expected to be small and readily fitted with a small number of parameters.

The purposes of least squares fitting were:

1) to obtain values of zero pressure intercepts and high pressure slopes by extrapolation and to make quantitative estimates of the uncertainties in these quantities and functions of these quantities.

2) to reduce the error in the estimated values of the quantities I, R, $S_{0°}$, $S_{-90°}$, etc. by using all the data, and to be able to estimate these quantities at arbitrary values of the pressure.

3) to make quantitative estimates of the magnitude of deviations from linearity in the data.

The fitting functions used and the criteria for selecting the "best" fit to the data are given in Appendix D.

The detailed interpretation of these data will be discussed in Sec. III.-C. This interpretation is based on the discussion of multi-state kinetics as developed in Appendices A and B. However, there are a number of immediate qualitative observations that may be made.

The fluorescence was found not to obey Stern-Volmer (single excited state) kinetics. The measured lifetimes were different at different observation wavelengths. The quantities R^{-1} and I^{-1} exhibited pressure dependences that were different from one observation wavelength to another and from one another at the same observation wavelength. Further, the graphs of these quantities as a function of pressure were, in general, not linear. Considered as a function of fluorescence frequency, the observed lifetimes at high pressures were much shorter at high frequencies, close to the excitation energy, than at low frequencies. The fluorescence spectra showed a considerable shift toward lower energy (red shift) as the pressure was increased. These results will be discussed in more detail in the remainder of this section.

We consider first the intensity ratio or "lifetime" data. In Fig. 6 are given conventional Stern-Volmer plots of such data for the three excitation wavelengths. The zero pressure intercepts of these graphs should, in the single state assumption, correspond to the fluorescence rate constants (inverse radiative lifetimes). If an observed state is excited both directly and by a pressure dependent cascade process, the zero pressure intercept should still be the fluorescence rate constant for

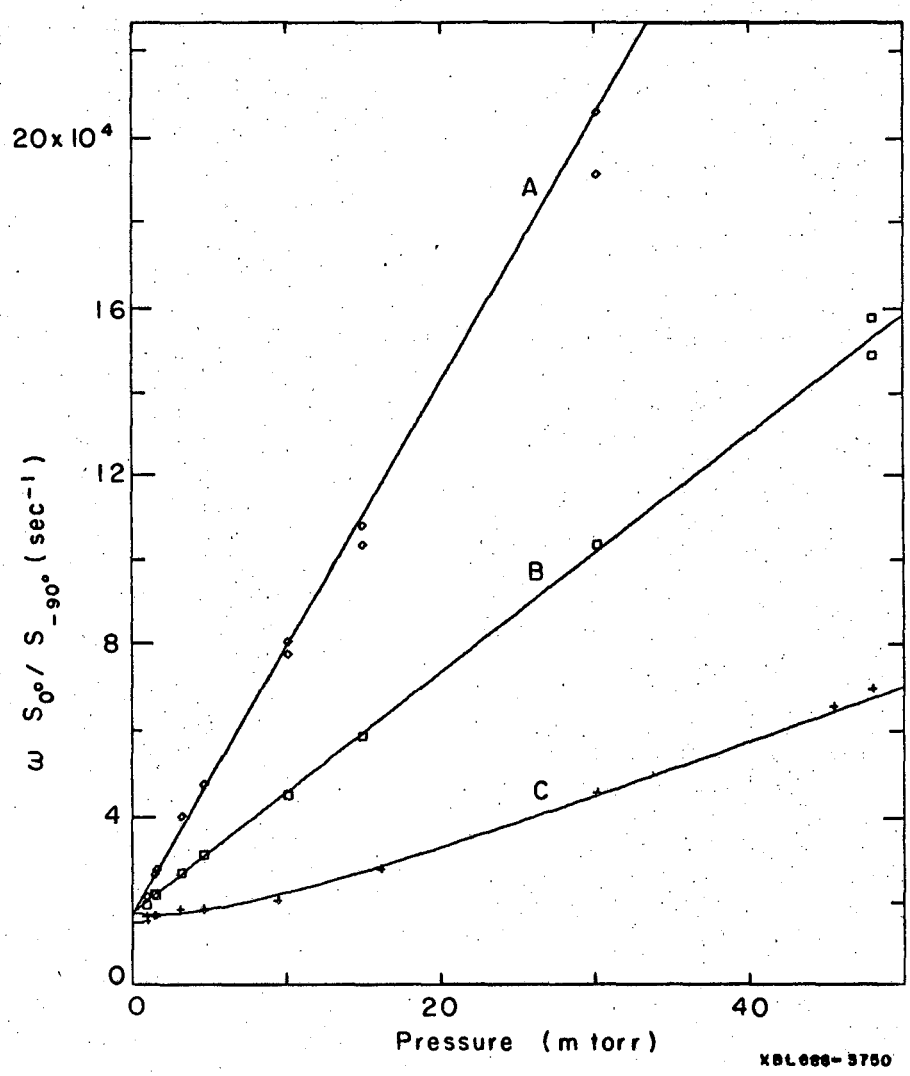

Fig. 6a Stern-Volmer graphs of lifetime data. Excitation energy: 4000 A or 25000 cm^{-1}. Observation energy: A, 23200; B, 20370; C, 14270 cm^{-1}.

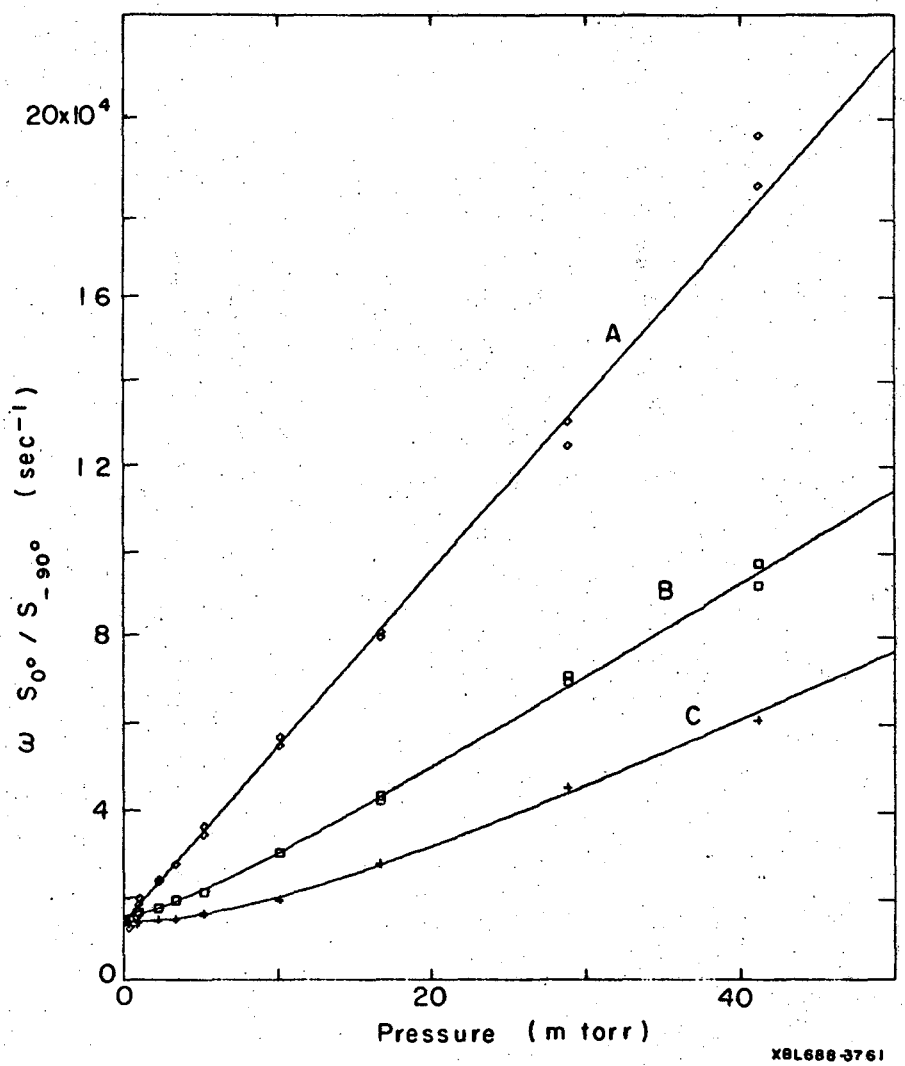

Fig. 6b. Stern-Volmer graphs of lifetime data. Excitation energy: 4300 A or 23260 cm^{-1}. Observation energy: A, 22170; B, 17880; C, 14270 cm^{-1}.

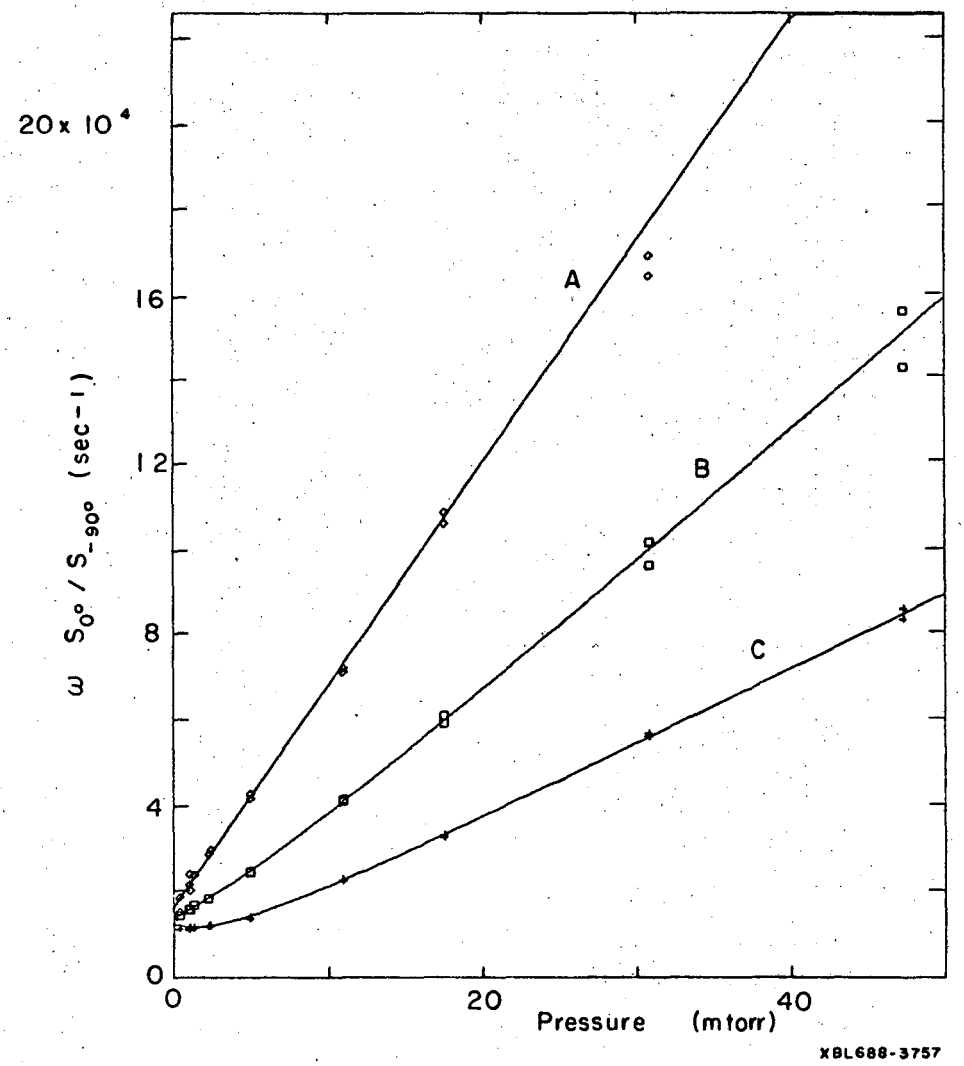

Fig. 6c. Stern-Volmer graphs of lifetime data. Excitation energy: 4800 A or 20830 cm^{-1}. Observation energy: A, 19960; B, 17880; C, 14270 cm^{-1}.

the initially populated state. However, as may be seen from Table VII there is a significant amount of variance in these zero pressure intercepts (for a given excitation wavelength) indicating that molecular states of considerably different lifetimes are directly populated by the excitation light within the band-pass of the monochromator. Since the observations yield an average of the detected fluorescence rates the observed variance sets a lower limit to the variance in the rate constants of the individual quantum states.

We now consider the pressure dependence of the lifetime data. For observation close to the excitation wavelength the appparent quenching rate constants (slopes of Stern-Volmer graphs) are steeper than when observation is at lower energies. If we assume that the interpretation of Stern-Volmer kinetics is valid for the fluorescence at the highest observed energies, then the slopes of these graphs may be considered to be equivalent to quenching rate constants. The rate constants obtained in this way for the three excitation wavelengths are given in Table VIII.

From the fitted functions for observations at each frequency the lifetimes at various pressures were computed and plotted as a function of frequency (Fig. 7). The points were connected by means of Lagrangian interpolation; these interpolations are given as merely suggestive and do not represent actual measurements.

The lifetime data were also plotted according to the inverse Stern-Volmer relation (τ^{-1}/M vs. $1/M$). Examples of such plots are given in Fig. 8. Such a graph allows extrapolation of the data to infinite pressure ($1/M = 0$); the infinite pressure slopes of the conventional Stern-Volmer plots become intercepts of these inverse plots. A finite,

Table VII. Spread in radiative lifetimes

Excitation wavelength A	Radiative lifetime μ sec	Spread %
4000	58-64	10
4300	62-76	20
4800	60-80	30

Lifetimes were obtained from extrapolation of Stern-Volmer curves to zero pressure. Values given indicate extremes measured at different fluorescence wavelengths.

Table VIII. Apparent quenching rate constants for fluorescence at energy close to energy of excitation

Energy of excitation A	Energy of excitation cm^{-1}	Energy of observation cm^{-1}	k_q (apparent) cm^3/molecule sec	P
4000	25000	23200	1.92×10^{-11}	0.84
4300	23260	22170	1.26×10^{-11}	0.55
4800	20830	19960	1.60×10^{-11}	0.70

Quenching rate constants were computed from slopes of Stern-Volmer lifetime graphs. P is "quenching" probability per gas kinetic collision, computed using molecular diameter from Ref. 86.

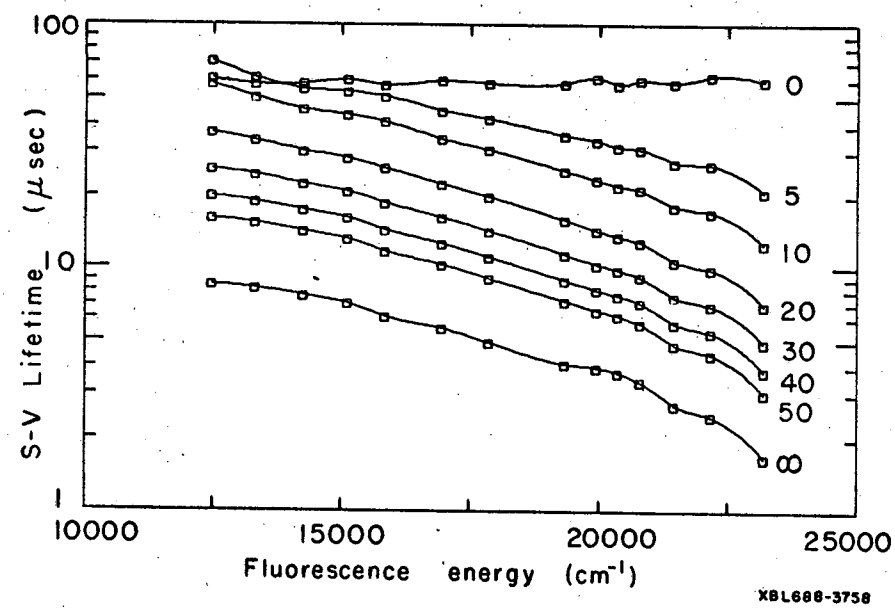

Fig. 7a. Lifetime spectra as a function of pressure. Lifetimes were computed from fitted curves of R^{-1} by the Stern-Volmer relation $\tau = \omega^{-1} S_{-90°}/S_{0°}$. The running index gives the pressure in m torr. The relative lifetime distribution obtained from the infinite pressure extrapolation is not scaled with respect to the ordinate. Excitation energy, 4000 A or 25000 cm^{-1}.

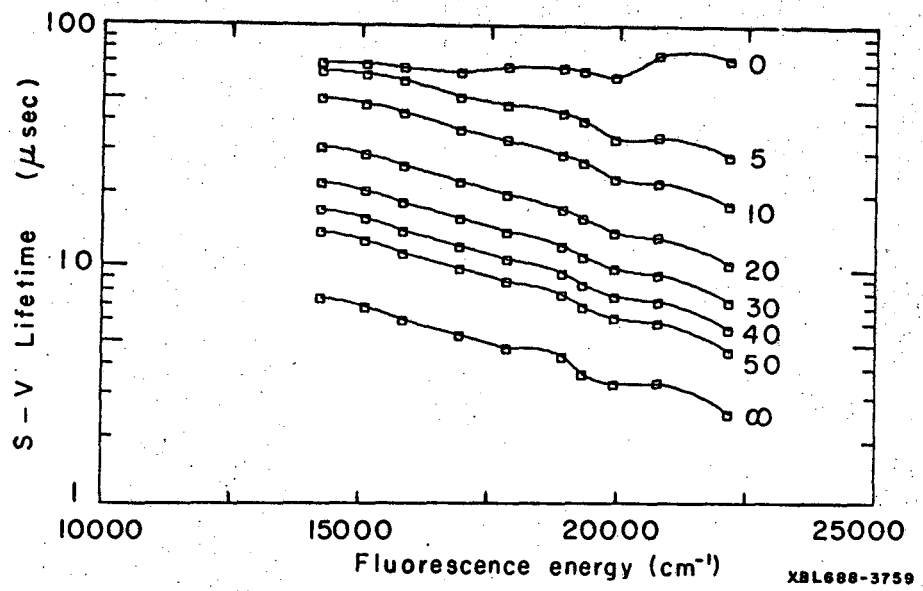

Fig. 7b. Lifetime spectra as a function of pressure. Lifetimes were computed from fitted curves of R^{-1} by the Stern-Volmer relation $\tau = \omega^{-1} S_{-90°}/S_{0°}$. The running index gives the pressure in m torr. The relative lifetime distribution obtained from the infinite pressure extrapolation is not scaled with respect to the ordinate. Excitation energy, 4300 A or 23260.cm^{-1}.

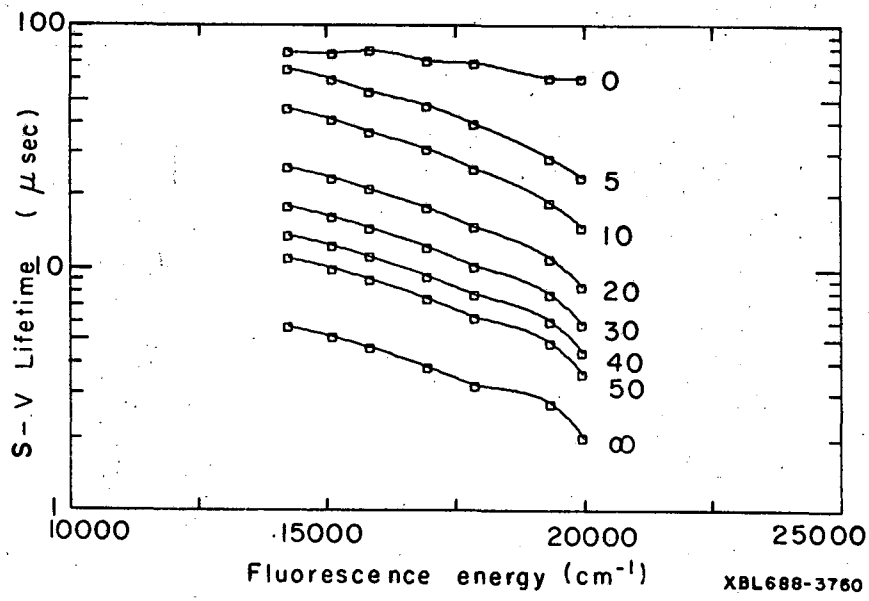

Fig. 7c. Lifetime spectra as a function of pressure. Lifetimes were computed from fitted curves of R^{-1} by the Stern-Volmer relation $\tau = \omega^{-1} S_{90°}/S_{0°}$. The running index gives the pressure in m torr. The relative lifetime distribution obtained from the infinite pressure extrapolation is not scaled with respect to the ordinate. Excitation energy 4800 A or 20830 cm^{-1}.

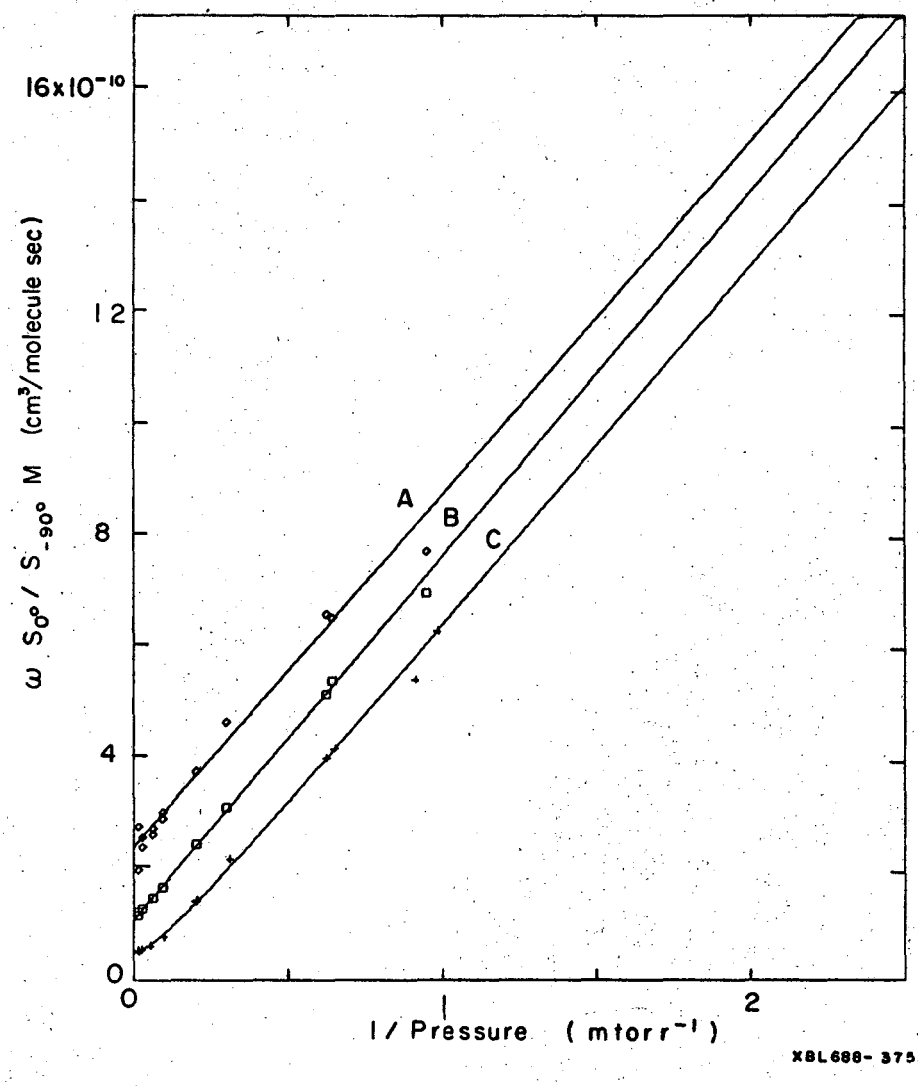

Fig. 8a. Inverse Stern-Volmer graphs of lifetime data. Excitation energy: 4000 A or 25000 cm^{-1}. Observation energy: A, 23200; B, 20370; C, 14270 cm^{-1}.

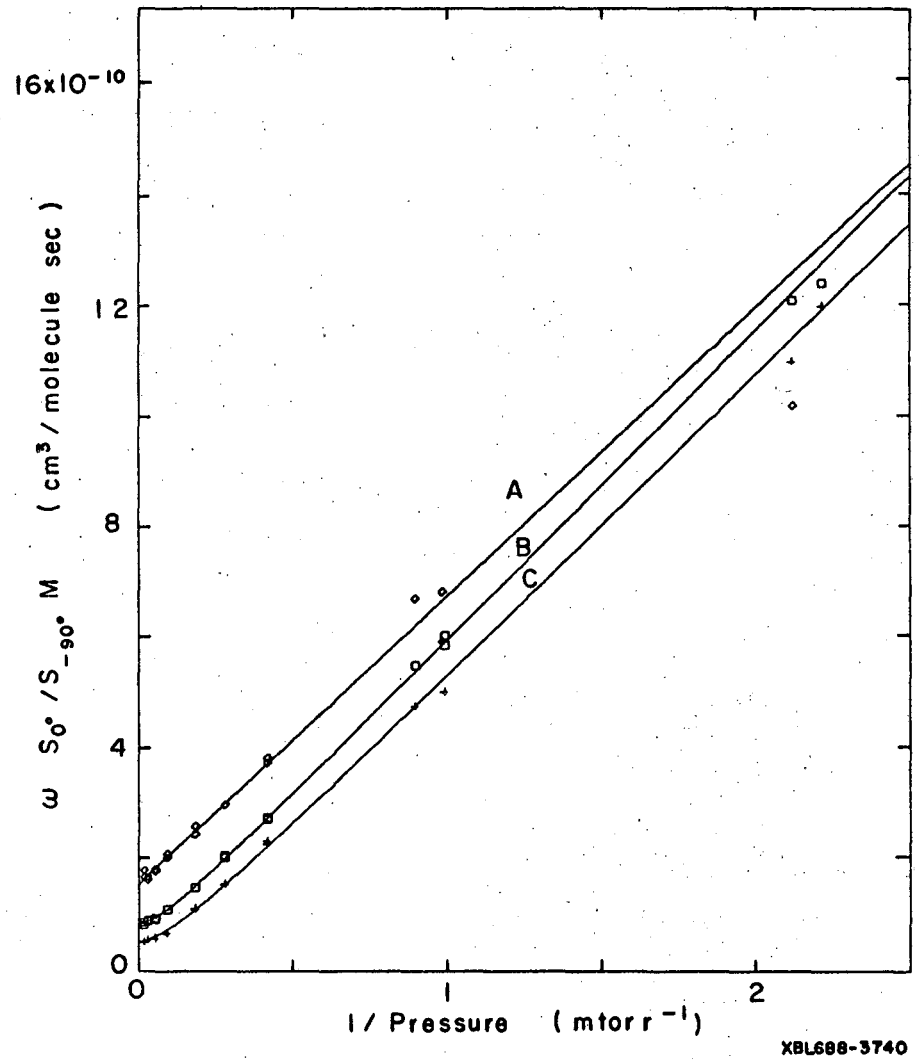

Fig. 8b. Inverse Stern-Volmer graphs of lifetime data. Excitation energy: 4300 A or 23260 cm^{-1}. Observation energy: A, 22170; B, 17880; C, 14270 cm^{-1}.

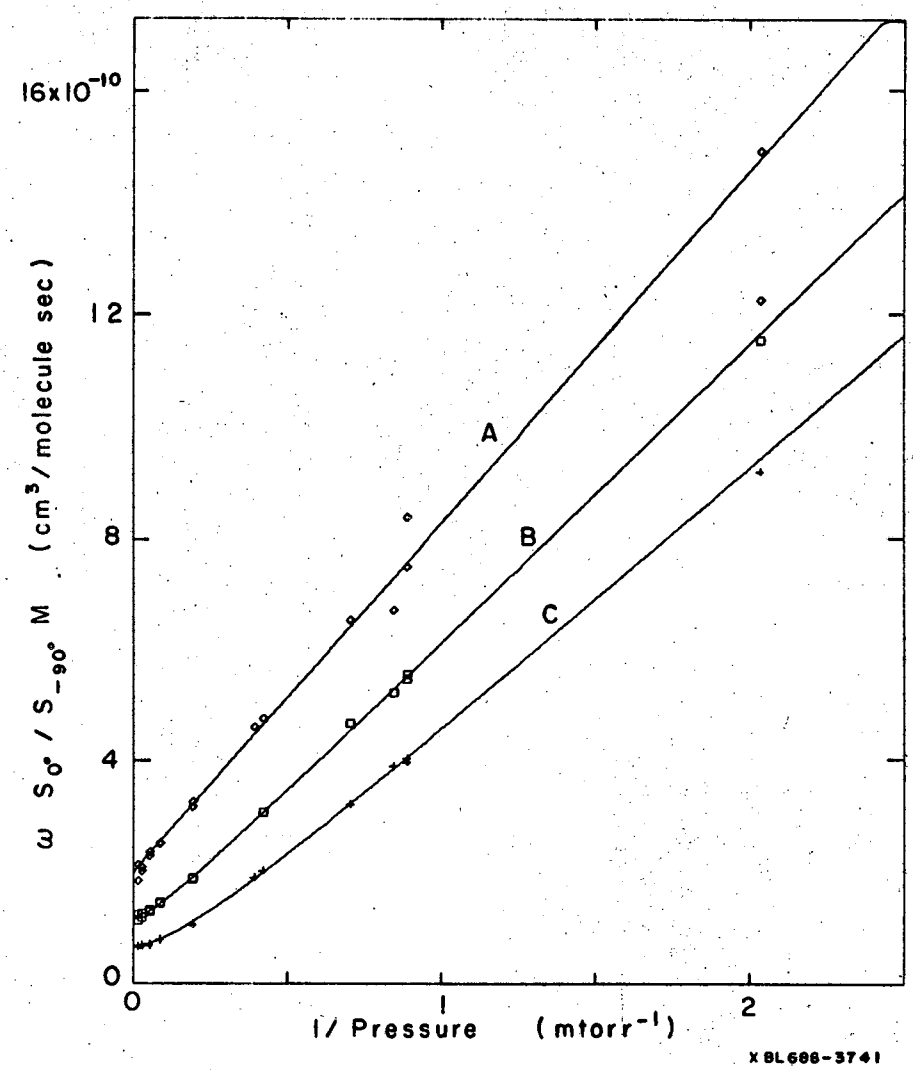

Fig. 8c. Inverse Stern-Volmer graphs of lifetime data. Excitation energy: 4800 A or 20830 cm^{-1}. Observation energy: A, 19960; B, 17880; C, 14270 cm^{-1}.

non-zero intercept in such a plot indicates that there is a first order dependence of the inverse lifetime upon pressure at the high pressure limit; this was found to be the case in all instances. The high pressure slopes (k_q apparent) were computed from the fitted functions and are given in Table D-I. From the inverse of these slopes the infinite pressure limit of τM is obtained. Spectra of these limiting lifetimes are given in Fig. 7.

The inverse intensity data were graphed according to the Stern-Volmer theory in the same way as the inverse lifetime data. Since intensity data are relative, these graphs were necessarily normalized, and it was chosen to normalize the zero intercepts to unity. The intensity data exhibited finite intercepts in both the conventional and inverse Stern-Volmer plots, indicating that the quenching at high pressures was first order in total pressure, (Figs. 9, 10).

As with the lifetime data the intensities from the fitted functions were graphed as a function of wavelength, (Fig. 11). In these graphs (for the first time in the presentation of the data) the relative response factors of the detector for the various interference filters have been employed; consequently any error in the determination of these response factors. (Sec. II-A-7) will enter into the intensity spectra. Such error will appear as the systematic raising or lowering (by a fixed amount) of the intensity at one observation frequency relative to that at another. Again, from the high pressure slopes of the data it was possible to calculate infinite pressure limits to the intensity spectra. These data are given in Fig. 11.

It should be pointed out here that the fluorescence spectra extended in all cases beyond the limit of observation (7000 to 8000 A). This was

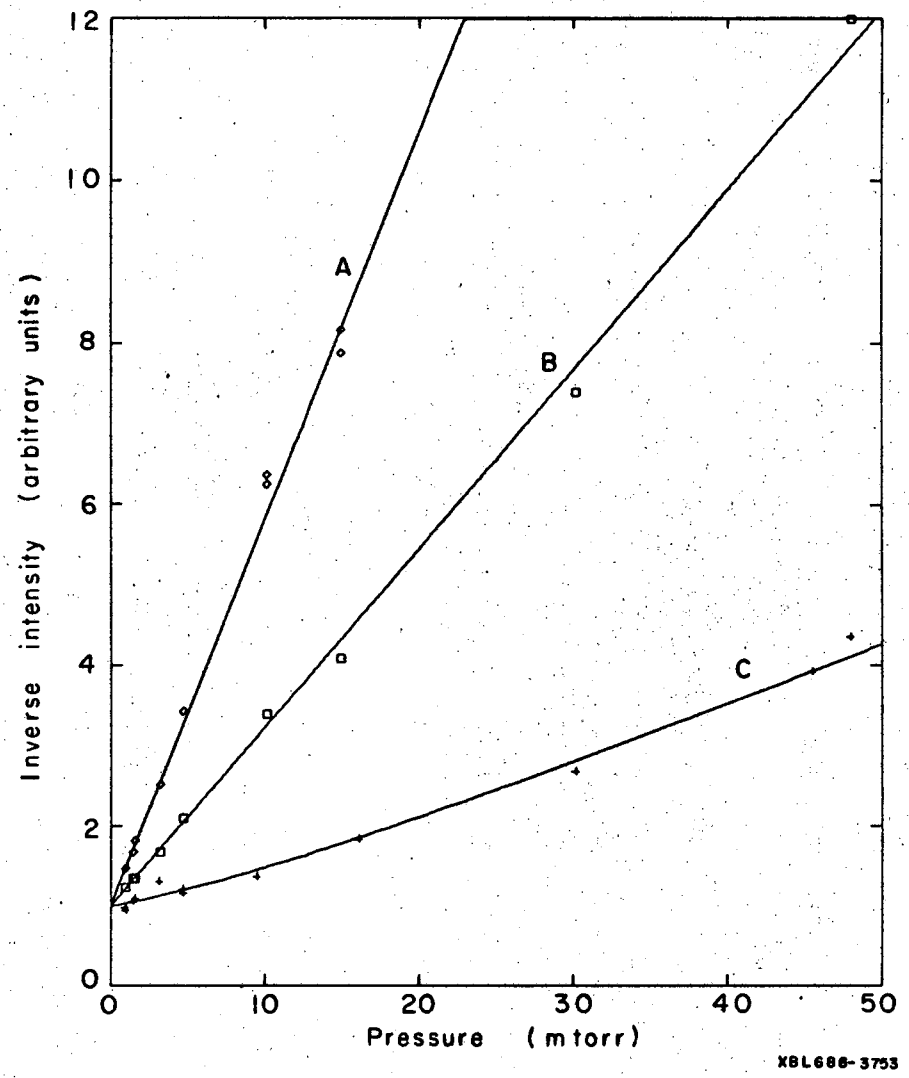

Fig. 9a. Stern-Volmer graphs of intensity data. Excitation energy: 4000 A or 25000 cm^{-1}. Observation energy: A, 23200; B, 20370; C, 14270 cm^{-1}.

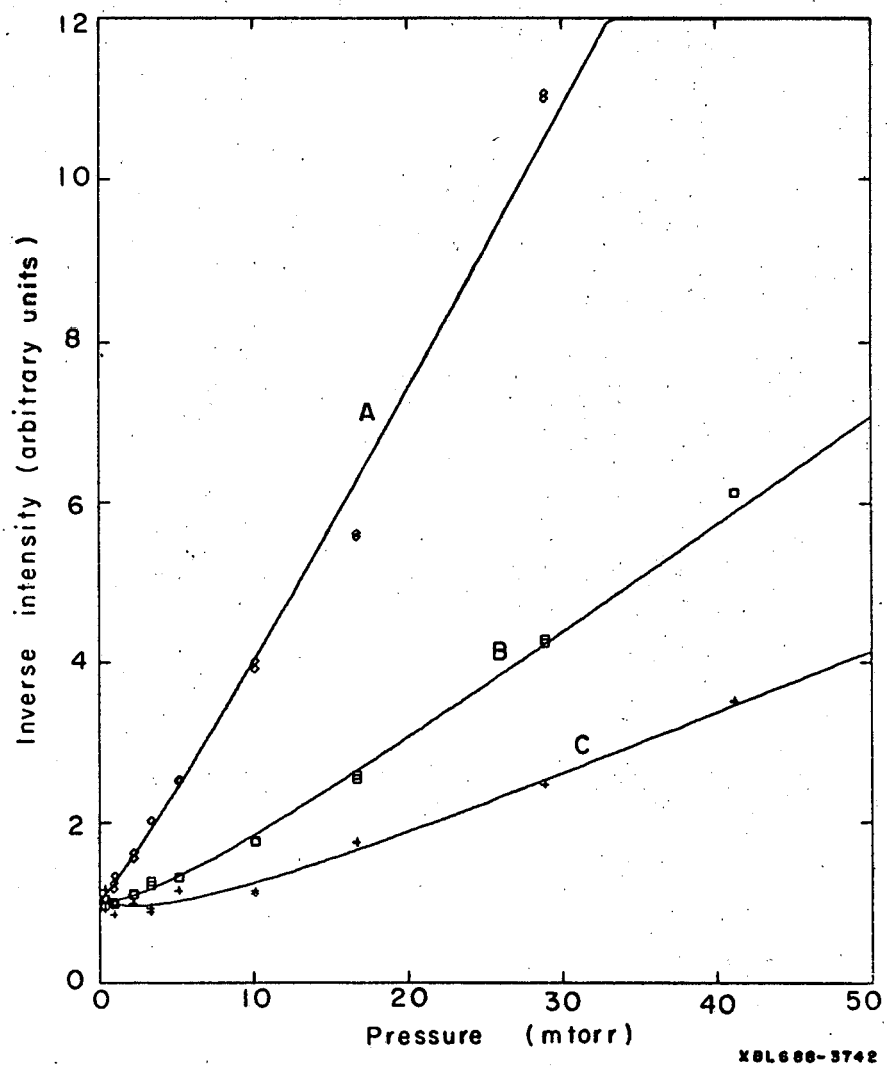

Fig. 9b. Stern-Volmer graphs of intensity data. Excitation energy: 4300 A or 23260 cm^{-1}. Observation energy: A, 22170; B, 17880; C, 14270 cm^{-1}.

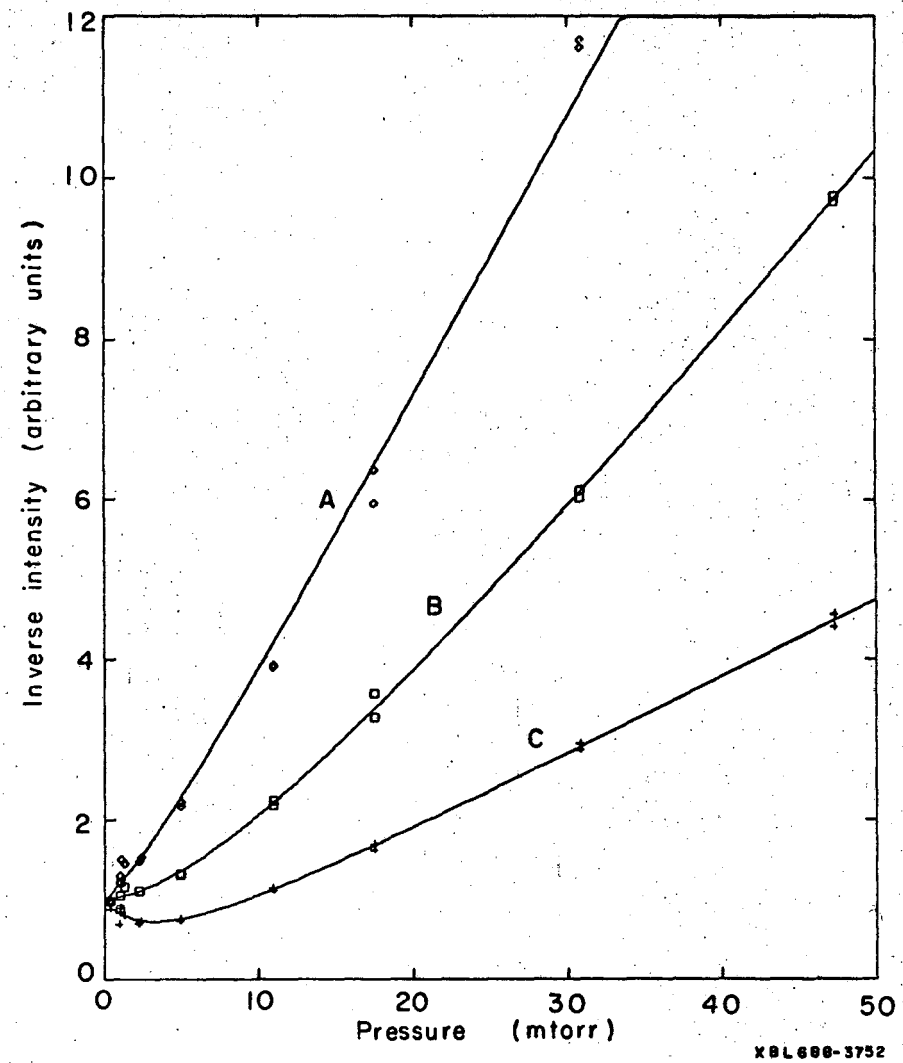

Fig. 9c. Stern-Volmer graphs of intensity data. Excitation energy: 4800 A or 20830 cm^{-1}. Observation energy: A, 19960; B, 17880; C, 14270 cm^{-1}.

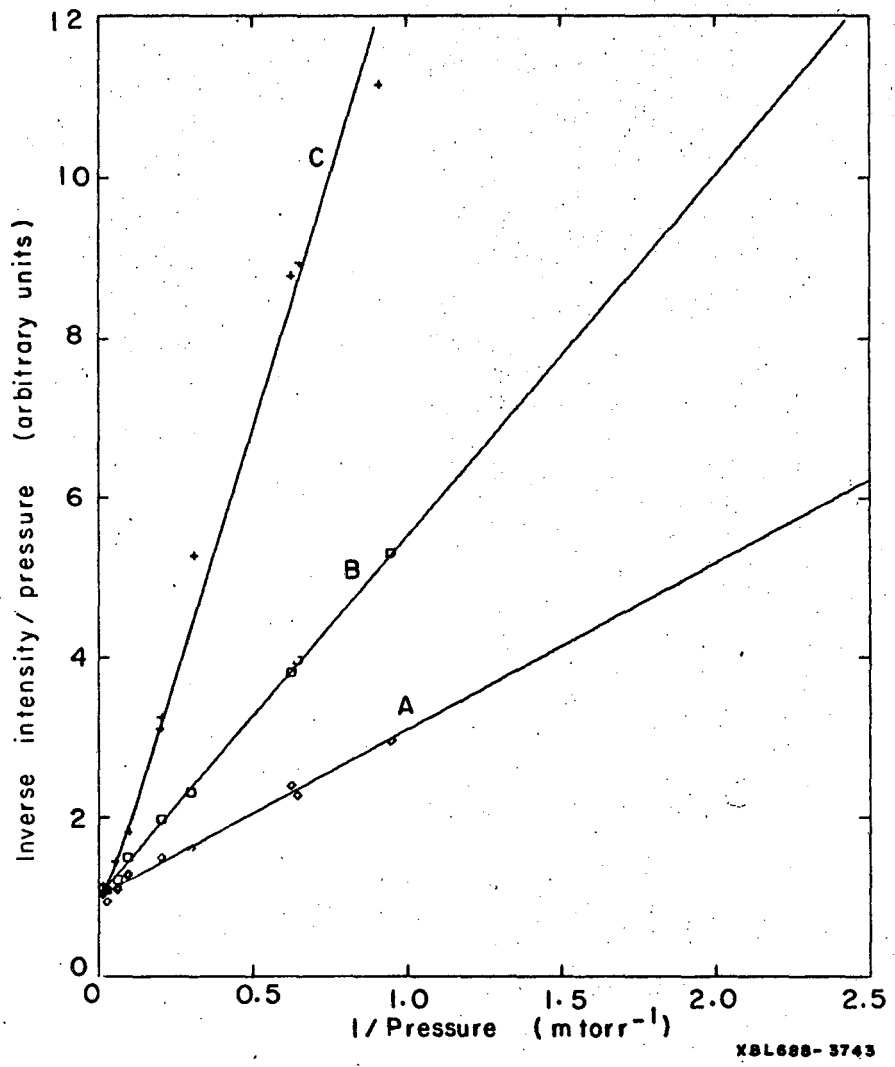

Fig. 10a. Inverse Stern-Volmer graphs of intensity data. Excitation energy 4000 A or 25000 cm^{-1}. Observation energy: A, 23200; B, 20370; C, 14270 cm^{-1}.

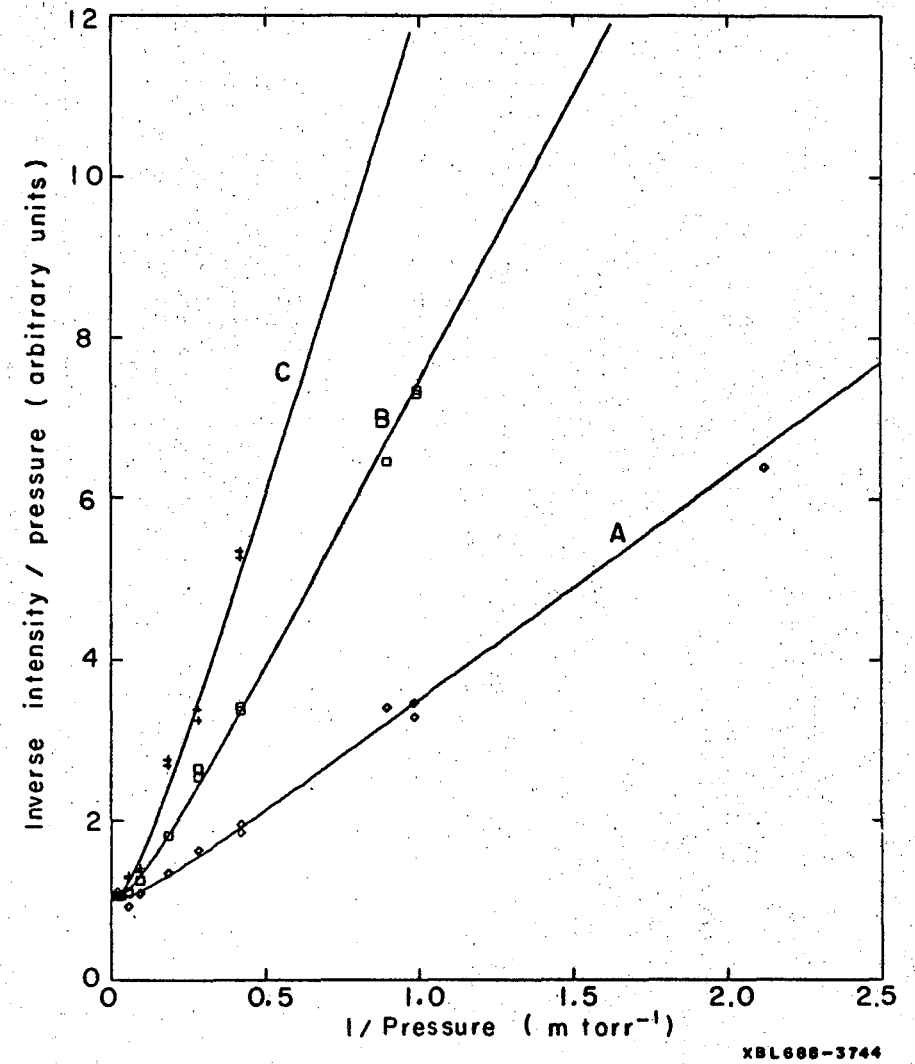

Fig. 10b. Inverse Stern-Volmer graphs of intensity data. Excitation energy: 4300 A or 23260 cm^{-1}. Observation energy: A, 22170; B, 17880; C, 14270 cm^{-1}.

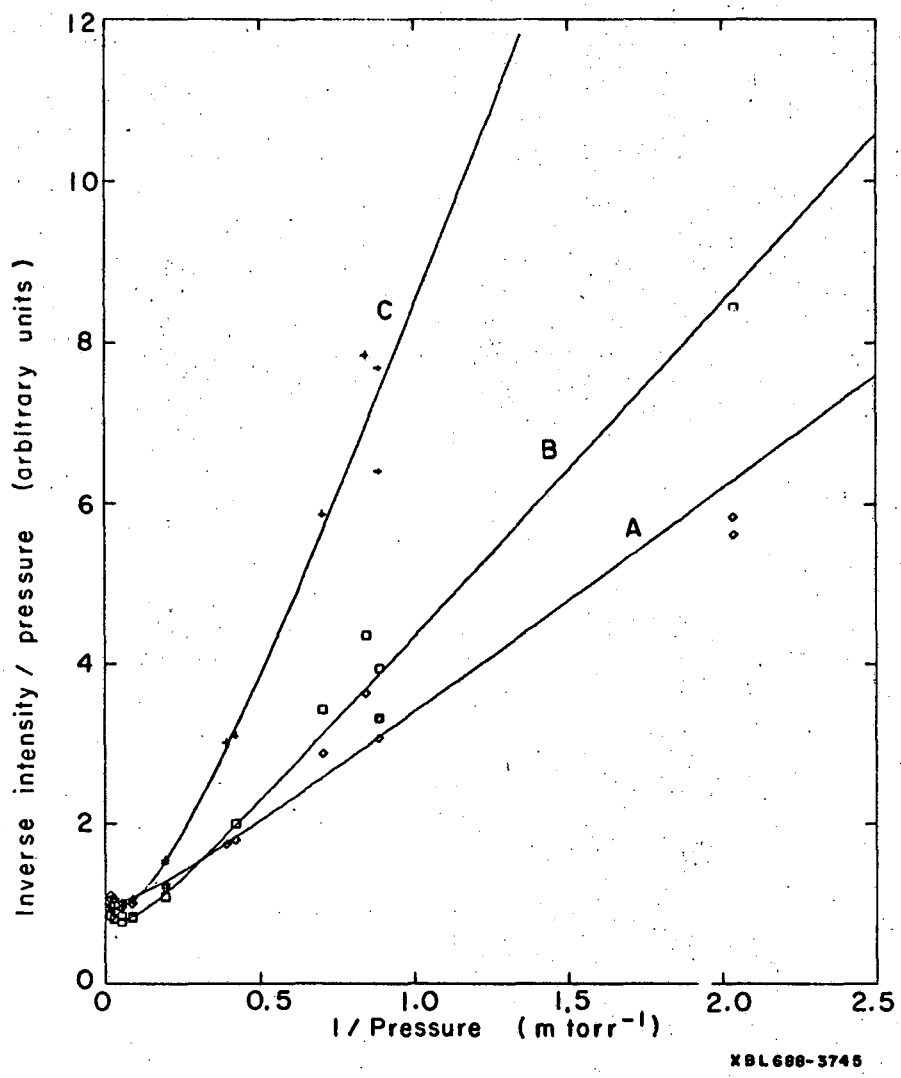

Fig. 10c. Inverse Stern-Volmer graphs of intensity data. Excitation energy: 4800 A or 20830 cm^{-1}. Observation energy: A, 19960; B, 17880; C, 14270 cm^{-1}.

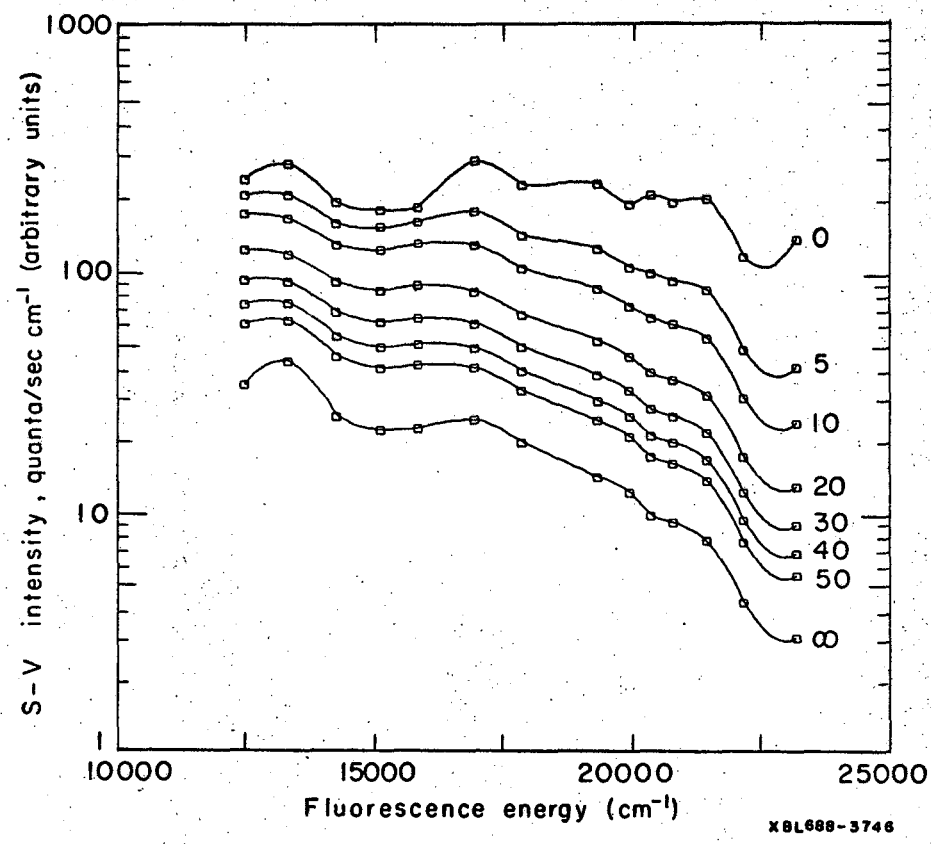

Fig. 11a. Intensity spectra as a function of pressure. Intensities were computed from fitted curves of I^{-1} where I is the Stern-Volmer intensity, $(S^2_{0°} + S^2_{90°})/S_{0°}$. The running index gives the pressure in m torr. The spectral distribution obtained from the infinite pressure extrapolation is not scaled with respect to the other spectra. Excitation energy 4000 A or 25000 cm^{-1}.

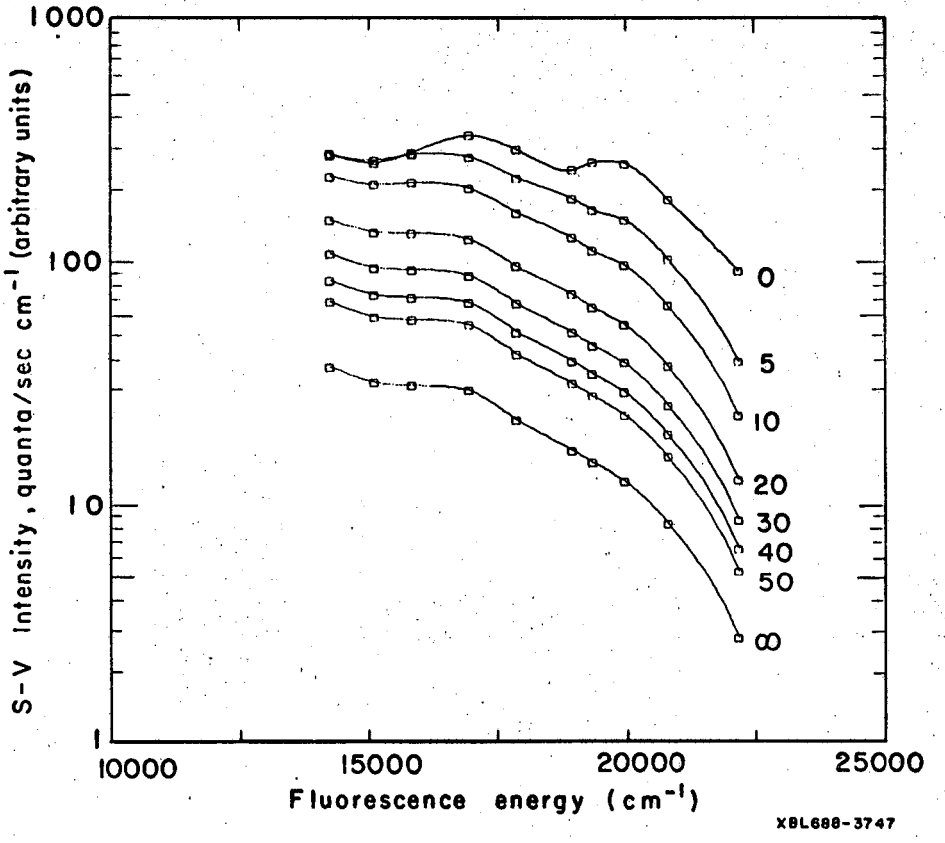

Fig. 11b. Intensity spectra as a function of pressure. Intensities were computed from fitted curves of I^{-1} where I is the Stern-Volmer intensity $(S^2_{0°} + S^2_{-90°})/S_{0°}$. The running index gives the pressure in m torr. The spectral distribution obtained from the infinite pressure extrapolation is not scaled with respect to the other spectra. Excitation energy, 4300 A or 23260 cm^{-1}.

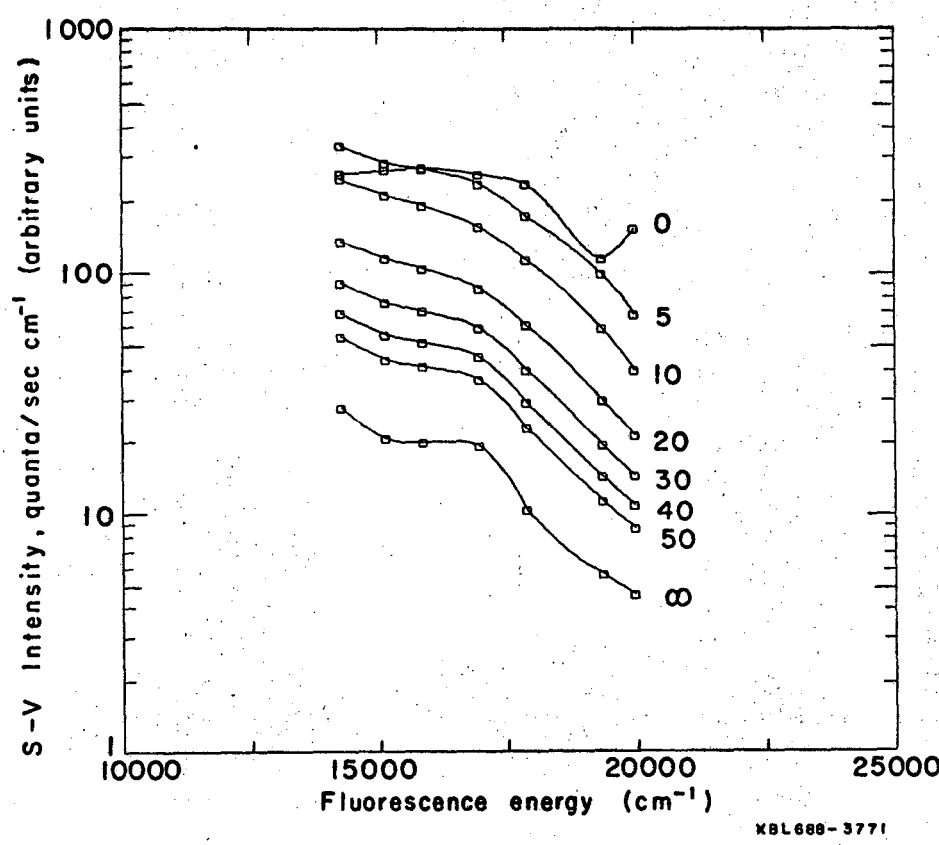

Fig. 11c. Intensity spectra as a function of pressure. Intensities were computed from fitted curves of I^{-1} where I is the Stern-Volmer intensity, $(S_0^{2\circ} + S_{-90^\circ}^2)/S_0^\circ$. The running index gives the pressure in m torr. The spectral distribution obtained from the infinite pressure extrapolation is not scaled with respect to the other spectra. Excitation energy, 4800 A or 20830 cm^{-1}.

true for the resonance fluorescence (zero pressure) spectra as well as those at higher pressures, indicating that a broad spectrum is a property of molecules within a localized energy region and not merely the consequence of a broad distribution function of molecular energies.

The change in the shape of the fluorescence spectra indicates a changing distribution function of the excited molecules. The fact that fluorescence at high energies is more strongly quenched than at low energies is suggestive of energy transfer processes that remove energy stepwise from the excited molecules rather than deactivation of the excited molecules in a single step. This interpretation is strengthened by the observation of fluorescence enhancement at long wavelengths for the case of excitation at 4800 A (Fig. 9c). In this figure enhancement is evidenced by a negative slope in the Stern-Volmer plot at low pressures. States fluorescing at the observation wavelength are collisionally populated (as pressure is increased) before overall quenching becomes dominant.

III. DISCUSSION

A. Effect of Molecular Migrations on Lifetime Measurements

The low pressure lifetimes in the present experiment (55-90 μsec) are significantly longer than have been reported previously by Neuberger and Duncan[18] and by Douglas,[20] (44 μ sec). While the technique of measurement is different in the present experiment (phase shift) from that previously used (flash decay), it is concluded that the longer lifetimes measured are due to the use of a fluorescence cell of sufficiently large diameter that the measured lifetime is not governed by wall collisions, or by collision free migration of excited molecules outside the region of observation. This conclusion is based on the following considerations:

1) A calculation of the effect of molecular migration with assumed quenching on wall collision (Appendix C) led to the prediction of considerably shorter apparent lifetimes when the radius of the fluorescence cell is less than 5 or 6 times the product $r = v_p \tau$ where v_p is the most probable molecular velocity. For NO_2 at 295°K, assuming a value for the lifetime of 80 μsec, the distance r is 2.7 cm. The radius of observation used in the present experiment was 14 cm or 5r. Thus the error in the lifetime from molecules leaving the region of observation would be no more than a few percent. The previous investigators did not state the dimensions of their fluorescence geometry, so that a direct evaluation from Fig. C-1 of possible shortening of their measured lifetimes is not possible.

2) The measured lifetimes showed a significant (50%) dependence upon the excitation wavelength. While the existence of such a dependence does not demonstrate that the dimensions of the observation region have been

extended sufficiently, it does suggest that the measured lifetimes are at least approaching the true values.

3) The measurements of fluorescence lifetimes made with cells of smaller dimensions were significantly reduced from the lifetimes with the 33 cm cell and were consistent with the predictions of Fig. C-1. This may be taken as direct evidence of the effect of molecular migration of the order of 5 cm, and of quenching upon collisions of excited molecules with the walls of the cell.

With respect to the existing values of the lifetimes of SO_2 fluorescence it was felt that molecular migration might be responsible for errors in these values as well. Greenough and Duncan[68] have reported a value of 44 μsec for the lifetime of the $\tilde{A}^1B_1$ state of SO_2 excited in the wavelength region 2700-3100 A. The radius of the fluorescence cell in these experiments was $\rho = 3.8$ cm; the dimensions of the excitation beam and of the region of observation are not explicitly stated. Assuming that the lifetime of SO_2 is in fact 44 μsec, then $R/\rho = 3$; the resulting error in the lifetime would be at least 15%. Douglas[20] has reported a measurement of the SO_2 lifetime which is 50% greater than that of Greenough and Duncan and has indicated the existence of some dependence on the excitation wavelength. Again, the dimensions of the fluorescence geometry are not given. Mettee[69] has inferred from measurements of quenching of SO_2 fluorescence that the lifetime may change by an order of magnitude as excitation increases from 2650 to 3130 A. The lifetime of SO_2 fluorescence should certainly be remeasured under conditions in which the observation region is sufficiently large that the lifetime is not governed by molecular migration.

B. Fluorescence Lifetime of NO_2

The present experiments yielded values for radiative lifetimes of 55 to 90 μsec for excitation in the region 3975 to 6000 A and indicated that the lifetime continues to be long to the low energy limit of excitation energies used, 6800 A, and that there is a definite trend in the lifetime as a function of excitation energy (longer lifetimes at lower excitation energies). (Figure 5, Table IV). The observations were at variance from the predictions of molecular radiation theory as developed in Sec. I-A in several ways:

1) The absolute magnitudes of the fluorescent lifetimes were greater than predicted from the absorption and emission spectra by a factor of 3 to 40, depending on the choice of the average emission frequency $\langle\tilde{\nu}^3\rangle_{F-C}$; because of considerations which are developed in Sec. G, the latter value is thought to be a fair estimate of the factor by which the lifetimes are anomalously long.

2) The ratio in observed lifetimes at the extremes of excitation energies used (4000 to 6000 A) was only 1.6, whereas, other things being equal, the energy difference would lead to a prediction of the order of $(6000/4000)^3 \approx 3.4$.

3) Distinct fluctuations were observed in the radiative lifetimes as a function of excitation energy and also for the narrow spread in excitation energy in the monochromator band pass (60 cm^{-1} full width at half maximum).

For these reasons we must consider the radiation relation for molecular transitions (Eq. I-A-13) inadequate to predict the radiative lifetime and the assumptions upon which it was derived inadequate to

describe the molecular dynamics of the excited state of NO_2. Such a conclusion has previously been reached by Douglas.[20] The inadequacies of the relation may be considered in terms of the assumptions that were made in the derivation (Sec. I-A):

1) The Born-Oppenheimer (B-O) approximation.

2) The invariance of transition moment.

Assumption 2) has been the subject of considerable investigation in diatomic molecule spectroscopy. Nicholls and co-workers have interpreted the transition moment as a slowly varying function of the centroid $\langle \psi_{v'} | r | \psi_{v''} \rangle$ of the vibronic levels. As a consequence of the variance of the transition moment the lifetime is somewhat dependent upon the level of the upper state, aside from the frequency-cubed factor. A review of the r-centroid approach has been given by Nicholls and Stewart.[70]

The same type of approach could in principle be extended to polyatomic molecules, but the approach until the present time has been entirely qualitative. On the basis of correlation diagrams between bent (90°) and linear configurations of AB_2 molecules Walsh[41] has predicted the energy dependence on bending angle for triatomic molecular orbitals; see also Ref. 46b. In such a molecular orbital picture NO_2 may be considered as a CO_2 "nucleus" plus one additional electron. This additional electron is in a $(a_1\text{-}\pi_u)$ m.o. which falls sharply in energy as a function of bending angle. The low lying electronic transition in NO_2 corresponds to the promotion of this electron to the $(b_1\text{-}\pi_u)$ m.o. whose energy is much less strongly a function of bending angle; consequently the molecule is expected to be in a linear, or more linear, configuration in the upper

state, and this expectation is confirmed by the analysis of the absorption spectrum.[42] Thus a decrease in the transition moment with the bending coordinate will decrease the radiative rate constant. This possibility has been suggested by Mulliken[71] to account for the long fluorescence lifetime of NO_2. If such a mechanism were responsible for the long lifetime, however, the lifetime would be expected to decrease rather strongly with increasing vibrational quantum number in the bending coordinate, and correspondingly with the energy of the upper state. Since the observed lifetimes were more constant as a function of excitation energy than expected, this mechanism does not appear to be the reason for the increased radiative lifetime.

Jortner and coworkers[26-28] have recently considered the validity of the Born-Oppenheimer approximation in molecular transitions. If there exist perturbations between the upper electronic state and any other electronic state having an appreciable level density in the absorption region then the B-O wave functions will not adequately describe the upper state. Rather the true molecular wave functions must be written as a superposition of B-O wave functions, which may be used as a basis set:

$$\psi_{true} = \sum_i \psi^i_{BO} \langle \psi^i_{BO} | \psi_{true} \rangle$$

The transition moment to the ground state, which in the B-O approximation would belong to a single excited vibronic state is, under these conditions, spread out among a number of true vibronic states. The total transition moment, as measured by the absorption coefficient integrated over the electronic transition, is conserved; however, the transition moment to

the ground state from a given true vibronic level, which determines the radiative lifetime, is reduced by the factor $|\langle\psi_{BO}|\psi_{true}\rangle|^2$. If the perturbation is small, this factor will be ≈1. The magnitude of such a factor is, lacking an exact solution of the molecular Hamiltonian, estimated by the density of the true molecular levels and the magnitude of the coupling matrix element. Such estimations have been discussed by Jortner and Berry.[27]

In the case of NO_2 there exists a strong perturbation of the upper vibronic levels by Renner effect coupling with the excited vibrational levels of the ground electronic state.[42] The Renner effect is due to the interaction of the angular momentum of the bending vibration with the electronic angular momentum. As a consequence of this interaction the two electronic states $^2A_1$ and $^2B_1$, which are non-degenerate in the bent configuration but which correlate with the degenerate $^2\Pi_u$ states in the linear configuration, are coupled with each other. A given vibronic level may thus not be assigned uniquely to either of the two Born-Oppenheimer potential energy surfaces corresponding to the two states. This subject is discussed in detail in Ref. 46c.

In the upper vibronic levels of the B_1--A_1 transition of NO_2 the magnitude of the perturbation is such that, aside from a few simple subbands for which the perturbation is forbidden, no regularity of any kind has been observed. The perturbation is very sensitive to isotopic substitution, so that aside from the few bands that were analyzed, the spectrum of $^{15}NO_2$ could not be correlated with that of $^{14}NO_2$. The bands that were analyzed accounted for some of the strongest individual lines in the spectrum, but for only a very small fraction of the total number

of lines in the spectrum and for only a small fraction of the total absorption. These analyzed lines all terminate in $K_a = 0$ sub levels of the upper electronic state for which there is no Renner effect interaction with levels of the ground state.[42,46c] From this qualitative consideration of the magnitude of the perturbation in NO_2, it appears that the mechanism which has been outlined will be very important in increasing the lifetime of the excited state.

A consequence of the above discussion is that lifetimes from level to level might vary significantly since the magnitude of the coupling to the ground state would not be expected to be constant. In particular, the unperturbed levels might be expected to exhibit significantly shorter lifetimes in an experiment in which only such levels are excited. In an experiment such as the present one such short lived states would contribute to the total fluorescent intensity only in proportion to their absorption, and would not be detected in the presence of a much greater signal from states having a long lifetime. If such short lived states contributed significantly to the total signal intensity, their presence would lead to Stern-Volmer plots whose (positive) slope decreased with pressure; no such behavior was observed.

Related to the theory of intra-molecular lengthening of lifetimes that has been outlined is an inter-molecular process that has been proposed by Jortner and Berry.[27] The dense manifold of states which are not optically connected to the ground state is collisionally populated at finite pressures and the apparent lifetime of fluorescence is consequently lengthened. Jortner and Berry do not indicate the magnitudes of collision cross-sections that might be expected for this type of

process. However, such a mechanism would imply that, at sufficiently low pressures, the fluorescence lifetime would be short. Similarly, Robinson[25] has proposed that measurements of benzene fluorescence[72] may not have been performed at sufficiently low pressures to observe resonance fluorescence. This question is, of course, open to further experimentation either at lower pressures or in collision free molecular beams. However, we should like to point out that the present measurements were performed at pressures such that the average molecule at the assumed long lifetime suffered as few as 0.2 gas kinetic collisions; if the "resonant" lifetime were significantly shorter than 60 μsec, the number of collisions of the average molecule would be correspondingly reduced. In no case, for either I^{-1} or R^{-1} data, was there any indication of a discontinuity in the pressure dependence of the data which would cause us to question the extrapolation to the limit of zero pressure.

C. Energy Transfer in Excited NO_2

In this section we wish to analyze the results of the pressure dependent studies in terms of an energy transfer mechanism. The model chosen is a multi-step, constant energy per step, model as previously proposed by Rabinovitch and coworkers (step-ladder model);[10] the step size is not fixed, but is to be determined from the analysis. According to this highly simplified model we may index the states of the molecule 1 . . . . n, where 1 is the index of the initially populated state. The energy of state n is given by

$$\mathcal{E}_n = \mathcal{E}_1 - (n-1)\,\mathcal{E}_c \qquad (1)$$

where $\mathcal{E}_c$ (the efficiency) is the energy transferred per effective collision.

We now wish to relate this model to the expressions which are developed for high pressure limits in Appendix B. In Appendix B the high pressure limit for the ratio of in-phase to out-of-phase components of the population is shown (under conditions of series-parallel population of state k) to approach the limit

$$E_k^{0°}/E_k^{-90°} = \omega^{-1} \frac{\langle k_a \rangle}{\langle k_a/k_q \rangle} M = \omega^{-1} k_{qk}^* M \tag{2}$$

where

$$\langle k_a \rangle_k = k_{ka} + \sum_i k_{ia} \frac{k_{ki}}{k_{qi}} + \sum_{ji} k_{ja} \frac{k_{ij}}{k_{qj}} \frac{k_{ki}}{k_{qi}} + \cdots \tag{3}$$

and

$$\langle k_a/k_q \rangle_k = \frac{k_{ka}}{k_{qk}} + \sum_i k_{ia} \frac{k_{ki}}{k_{qi}} \left(\frac{1}{k_{qi}} + \frac{1}{k_{qk}} \right)$$

$$+ \sum_{ji} k_{ja} \frac{k_{ij}}{k_{qj}} \frac{k_{ki}}{k_{qi}} \left(\frac{1}{k_{qj}} + \frac{1}{k_{qi}} + \frac{1}{k_{qk}} \right) \tag{4}$$

$$+ \cdots$$

In these expressions

k_{ia} is the absorption coefficient into state i, and

k_{ij} is the energy transfer into state i from state j, a subset of

k_{qj}, the total rate constant for depopulation of state j.

The summations are taken over all intermediate states populating the

(observed) state k. Combining these expressions we may write

$$\frac{\langle k_a/k_q\rangle_k}{\langle k_a\rangle_k/k_{qk}} = \frac{k_{ka} + \sum_i k_{ia}\frac{k_{ki}}{k_{qi}}\left(1+\frac{k_{qk}}{k_{qi}}\right) + \sum_{ji} k_{ja}\frac{k_{ij}}{k_{qj}}\frac{k_{ki}}{k_{qi}}\left(1+\frac{k_{qk}}{k_{qj}}+\frac{k_{qk}}{k_{qi}}\right)+\cdots}{k_{ka} + \sum_i k_{ia}\frac{k_{ki}}{k_{qi}} + \sum_{ji} k_{ja}\frac{k_{ij}}{k_{qj}}\frac{k_{ki}}{k_{qi}} + \cdots} \qquad (5)$$

If we now make the assumption that the quenching rate constants are equal ($k_{qi} = k_{qj} = \cdots = k_{qk}$), then

$$\frac{\langle k_a/k_q\rangle_k}{\langle k_a\rangle_k/k_{qk}} = \frac{k_{ka} + 2\sum_i k_{ia}\frac{k_{ki}}{k_{qi}} + 3\sum_{ji} k_{ja}\frac{k_{ij}}{k_{qj}}\frac{k_{ki}}{k_{qi}} + \cdots}{k_{ka} + \sum_i k_{ia}\frac{k_{ki}}{k_{qi}} + \sum_{ji} k_{ja}\frac{k_{ij}}{k_{qj}}\frac{k_{ki}}{k_{qi}} + \cdots} \qquad (6)$$

The expression on the right hand side of (6) (which has a lower limit of unit may be interpreted as an average $\langle n\rangle$ of the number of states leading to the observed state k, where the average is taken over paths populating the state k. Hence for the observed high pressure quenching rate constant we have

$$k^*_{qk} = \frac{\langle k_a\rangle_k}{\langle k_a/k_q\rangle_k} = \frac{k_{qk}}{\langle n\rangle} \; ; \qquad (7)$$

the apparent quenching rate constant is decreased $\langle n\rangle$ fold from the microscopic quenching rate constant. Or, for an observed state having a high pressure limiting slope k^*_{qk} and a microscopic quenching rate constant k_{qk} then the average number of states is given by

$$\langle n\rangle = k_{qk}/k^*_{qk} \; . \qquad (8)$$

If the spectroscopy is not resolved, then the limiting slope may only be considered to be a qualitative measure of the number of sequentially populated states prior to the emission of light at the observation wavelength.

Returning now to the discussion of the step-ladder model, we see that the quantity $\langle n \rangle$ which is obtained from the analysis of the high pressure inverse lifetime data may be identified with the index n of the step-ladder model. Hence we may write

$$\frac{1}{k^*_{qk}} = \frac{1}{k_t}\left(1 + \frac{\Delta\mathcal{E}}{\mathcal{E}_c}\right) , \tag{9}$$

where the use of the symbol k_t implies that all removal of excited molecules takes place through the mechanism of energy transfer. In (9) we have used $\Delta\mathcal{E}$, which is defined as the energy difference between the initial and final states,

$$\Delta\mathcal{E} \equiv \mathcal{E}'_1 - \mathcal{E}_n . \tag{10}$$

Hence in the assumptions of the model a graph of $1/k^*_{qk}$ vs $\Delta\mathcal{E}$ should be linear with intercept k_t^{-1} and slope $(k_t \mathcal{E}_c)^{-1}$. From such a graph it should be possible to obtain both the product of the energy transfer rate constant times the energy transfer per collision, and the magnitude of the energy transfer rate constant.

In terms of the present experiment there is one additional consideration that must be made, namely that the spectroscopic observation is neither resolved nor assigned to states of known energies and that the resonance spectrum of all vibrational levels is quite broad. Consequently

there is not a direct relation between the fluorescence energy (cm^{-1}) and the energy of the molecules.

As an approach to this problem we may write down the average energy $\langle \mathcal{E}_k \rangle_{\tilde{\nu}}$ of all molecules contributing to the fluorescence at the observation energy $\tilde{\nu}$:

$$\langle \mathcal{E}_k \rangle_{\tilde{\nu}} = \frac{\sum_k E_k \, k_{fk} \, \alpha_{k\tilde{\nu}} \, \mathcal{E}_k}{\sum_k E_k \, k_{fk} \, \alpha_{k\tilde{\nu}}} \tag{11}$$

This average is taken over molecules that fluoresce per unit time and is weighted by the relative contributions of the various levels to the fluorescence at the observation energy. If we now consider fluorescence at a second observation energy, then we may relate the average molecular energies to the average fluorescence energies by

$$\langle \mathcal{E}_k \rangle_{\tilde{\nu}} - \langle \mathcal{E}_k \rangle_{\tilde{\nu}'} = (\tilde{\nu} - \tilde{\nu}') \, U \tag{12}$$

where

$$U \equiv \frac{\langle \mathcal{E}_k \rangle_{\tilde{\nu}} - \langle \mathcal{E}_k \rangle_{\tilde{\nu}'}}{\tilde{\nu} - \tilde{\nu}'} \tag{13}$$

is a measure of the error in the direct relation

$$\Delta \mathcal{E}_{\text{molecules}} = \Delta \mathcal{E}_{\text{fluorescence}} \tag{14}$$

Thus if $U = 1$, (14) is valid. The exact value of U is of course impossible to evaluate in the present experiment, but it is possible, with rather plausible assumptions, to estimate the magnitude of this quantity and to set stringent limits on the estimated value.

The assumption upon which we shall rely is that the resonance

fluorescence spectra of the various energy levels participating in the fluorescence are broad and flat throughout the region of observation. This assumption is justified in a rough way by an examination of the zero pressure fluorescence intensity spectra (Fig. 11), for excitation at energies of 21000 to 25000 cm^{-1}. Under the assumption of a flat fluorescence spectrum the value of U may be computed for an assumed distribution function of molecular populations, y. For observation at energy $\tilde{\nu}$ the average molecular energy is given by

$$\langle \mathcal{E}_k \rangle_{\tilde{\nu}} = \int_{\tilde{\nu}}^{\tilde{\nu}_e} y\, \tilde{\nu} d\tilde{\nu} \Big/ \int_{\tilde{\nu}}^{\tilde{\nu}_e} y\, d\tilde{\nu} \qquad (15)$$

and similarly for $\langle \mathcal{E}_k \rangle_{\tilde{\nu}'}$. Hence

$$U = \frac{1}{\tilde{\nu} - \tilde{\nu}'} \left\{ \frac{\int_{\tilde{\nu}}^{\tilde{\nu}_e} y\tilde{\nu} d\tilde{\nu}}{\int_{\tilde{\nu}}^{\tilde{\nu}} y d\tilde{\nu}} - \frac{\int_{\tilde{\nu}'}^{\tilde{\nu}_e} y\, \tilde{\nu} d\tilde{\nu}}{\int_{\tilde{\nu}'}^{\tilde{\nu}} y d\tilde{\nu}} \right\} \qquad (16)$$

and U may be evaluated either algebraically or graphically. However, the point of the present analysis is only to show that the value of U approaches unity and is quite insensitive to the distribution y.

For a simple model in which y is taken as proportional to some power, p, of the difference between excitation energy and molecular energy, $y(\nu) \propto (\nu_e - \nu)^p$, then the value obtained for U is

$$U = \frac{p+1}{p+2} \qquad (17)$$

In Fig. 12 are given distribution functions for p = 0, 1/2, 1, 2, and 4. The values obtained for U are respectively 0.5, 0.6, 0.67, 0.75, and 0.83. The flat distribution A(p=0) assumes that relaxation has populated all energy levels equally; for higher values of p the relaxation has preferentially populated the lower energy states. As this relaxation becomes more and more complete, U approaches more closely the value of unity. With reference to the present experiment, we observe in Fig. 11 that there is a shift in the spectral distribution of the intensity taking place at higher pressures. This shift corresponds to a pressure dependent relaxation process which is taking place; from the fact that the intensity becomes greater at the lower fluorescence energies we may infer that the relaxation preferentially populates the lower energy states. Thus, interpreting the experimental results in terms of this simple model we may conclude that p probably has the value of $\gtrsim 1$, although it is not possible to state the value of p with precision.

Also given in Fig. 12 is an exponential distribution for an assumed value of kT = 200 cm^{-1}. This distribution corresponds to total relaxation to the translational temperature, neglecting the effects of degeneracy on the density of states. For such an exponential distribution, given by $y \propto e^{-a\tilde{\nu}}$, the average energy $\langle \mathcal{E}_k \rangle_{\tilde{\nu}} = (\tilde{\nu} + 1/a)$ for observations such that $\tilde{\nu}_e - \tilde{\nu} \gg 1/a$. Hence, in this limit

$$\langle \mathcal{E}_k \rangle_{\tilde{\nu}} - \langle \mathcal{E}_k \rangle_{\tilde{\nu}'} = \tilde{\nu} - \tilde{\nu}'$$

that is, U = 1, and Eq. (14) is valid. Examination of the high pressure limits of the fluorescence spectra indicates that this limit is not reached the spectral distributions are not so steep as required by this model.

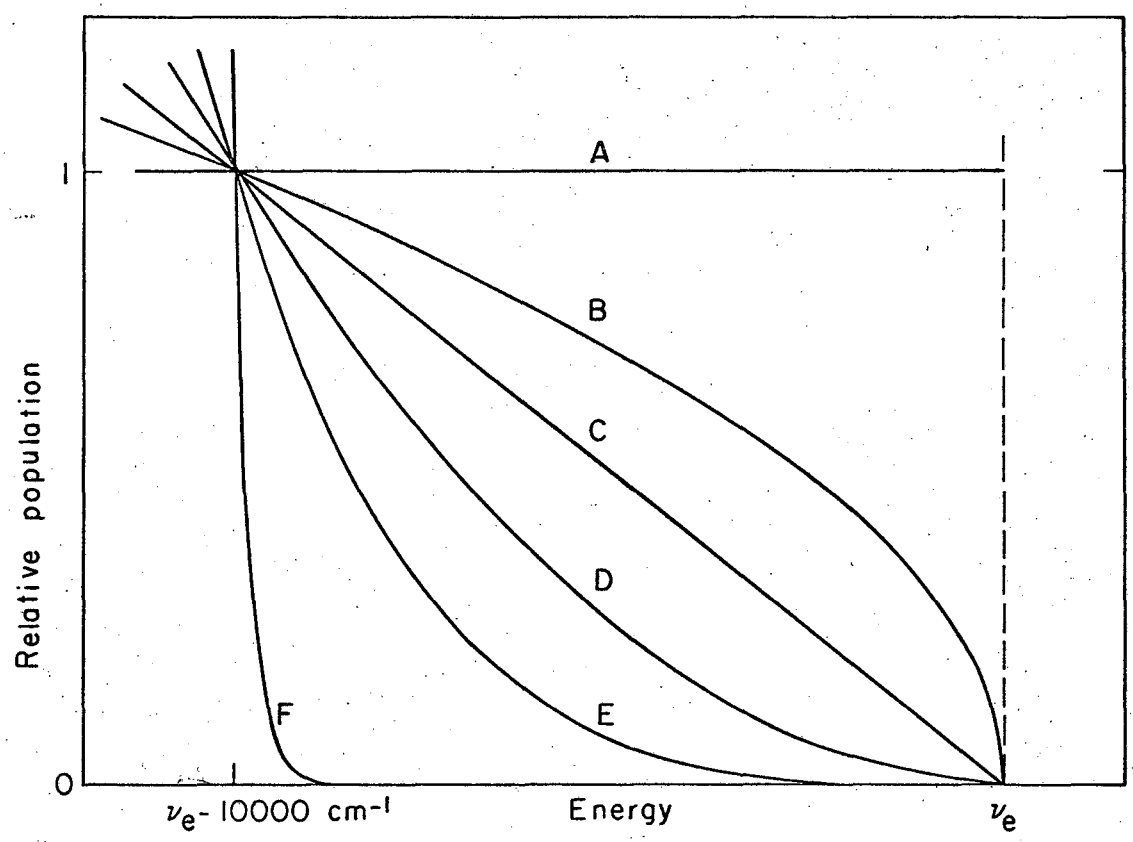

XBL688-3776

Fig. 12 Model distribution functions for excited state populations. Population (y) is plotted as a function of energy. A-E: $y \propto (\tilde{\nu}_e - \tilde{\nu})^p$ where p = 0, 1/2, 1, 2, and 4. F: $y \propto \exp(-\tilde{\nu}/200\ \text{cm}^{-1})$.

However, as indicated earlier, the value of U is quite insensitive to the choice of model, and to the steepness of the distribution function. Consequently, we feel that it is reasonable to accept Eq. (14) as valid (U = 1), but to admit to a possible lower limit of 0.7 to the value of U.

With the foregoing assumptions we consider Fig. 13 which shows graphs of $1/k^*_{qk}$ vs $(\mathcal{E}_{excite} - \mathcal{E}_{fluorescence})$ for the three excitation energies. In all three cases the data appear to be satisfactorily fitted by a straight line as predicted by Eq. (9). The energy transfer rate constants and efficiencies computed from the least squares linear fits through the three sets of data points are given in Table IX. For excitation at 4300 and 4800A the apparent energy transfer rate constants (col. 2) and efficiencies (col. 4) computed from the intercepts of Fig. 13 are quite close to each other and to the gas kinetic collision rate constant. For excitation at 4000 A the rate constant is significantly larger than gas kinetic and the apparent efficiency is correspondingly reduced. We are somewhat hesitant to extrapolate the 4000 A data to $\Delta\mathcal{E} = 0$, and the rate constant obtained in this way shows a rather large error. However, a qualitative interpretation of a larger total quenching rate constant for excitation near the dissociation limit might be given through the mechanism of dissociative quenching. For molecules that have suffered one non-dissociative, energy-transferring collision the effective energy transfer cross section would not be expected to be anomalously large; when $\mathcal{E}_c$ is computed using the gas kinetic cross section a value is obtained which is closer to the values obtained in the same way for excitation at the two lower energies (col. 5). For this reason we are inclined to conclude that the magnitude of k_t is approximately gas kinetic in all three cases,

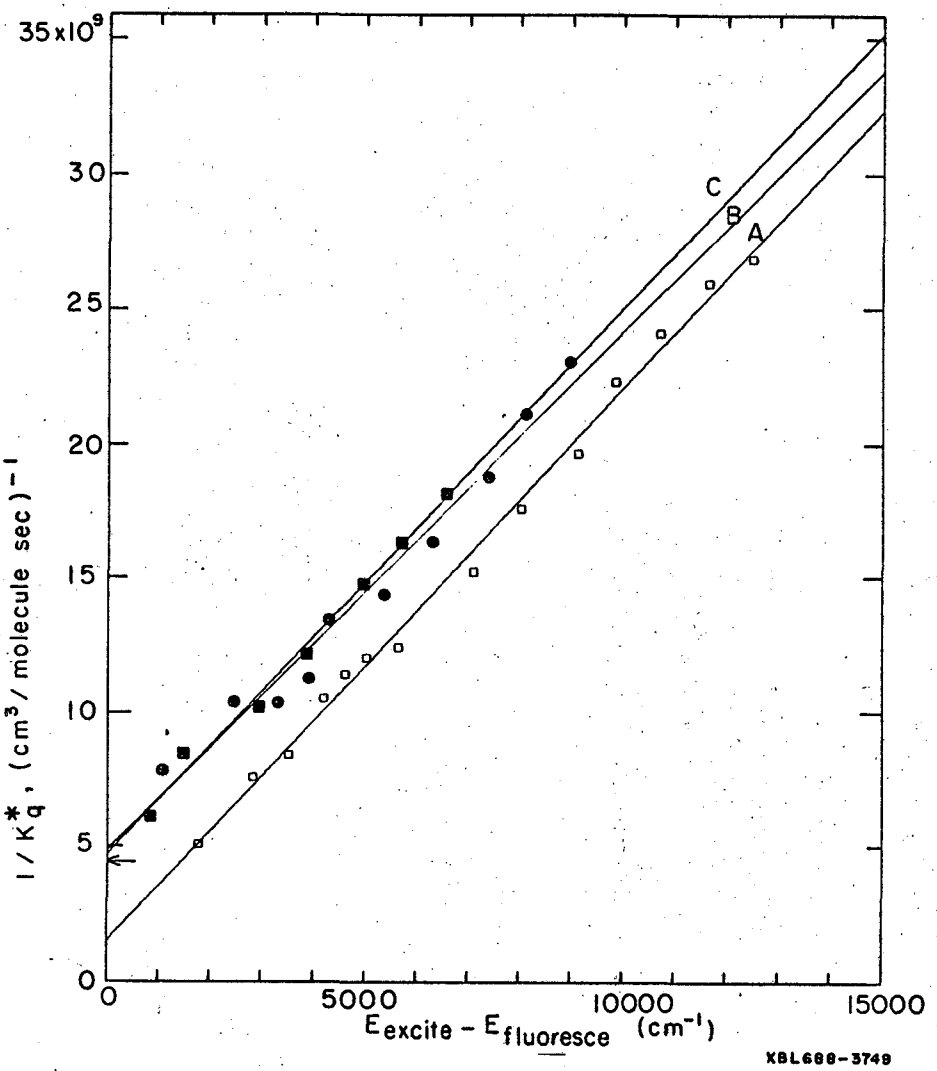

Fig. 13. Energy transfer in excited NO_2. The inverses of the high pressure limiting values of the slopes of Stern-Volmer lifetime graphs are plotted as a function of the energy difference between excitation and observation. Linear least squares fits to the data are also given. Arrow on ordinate indicates the inverse of the gas kinetic rate constant.

Open squares, A: Excitation at 4000 A or 25000 cm^{-1}.

Closed circles, B: Excitation at 4300 A or 23260 cm^{-1}.

Closed squares, C: Excitation at 4800 A or 20830 cm^{-1}.

Table IX. Energy transfer rate constants, probabilities per gas kinetic collision, and efficiencies, as computed from high pressure data

Excitation wavelength A	$k_t(\Delta\mathcal{E}=0)$ cm^3/molec sec	$P^{(a)}$	$\mathcal{E}_c^{(b)}$ cm^{-1}	$\mathcal{E}_c^{(c)}$ cm^{-1}
4000	$(6.5 \pm 2.7^{(d)}) \times 10^{-10}$	2.9 ± 1.2	740 ± 340	2120 ± 85
4300	$(2.02 \pm 0.57) \times 10^{-10}$	0.89 ± .22	2550 ± 900	2270 ± 260
4800	$(2.08 \pm 0.33) \times 10^{-10}$	0.91 ± .14	2400 ± 600	2150 ± 190

a Probabilities are computed from rate constant for gas kinetic collisions, 2.28×10^{-11} cm^3/molec sec, derived from collision diameter 3.73×10^{-8} cm (Ref. 86).

b Computed from k_t $(\Delta\mathcal{E}=0)$ (column 2)

c Computed per gas kinetic collision

d Errors represent two standard deviations

and that the energy transfer per collision is approximately 2300 cm^{-1}.

At this point we wish to review the assumptions that have gone into the estimation of the efficiency per collision.

1) In the derivation of the expression for k^*_{qk} (Appendix B) we specifically neglected the possibility of "back-up" transitions. The occurrence of such transitions to any large degree would have the effect of reducing the apparent k^*_{qk} at small $\Delta\mathcal{E}$, i.e., increasing the slope in Fig. 13, and decreasing the apparent efficiency. In view of the direction of this error and the magnitude of the energy per step compared to thermal energy kT, the neglect of "back-up" transitions seems justified.

2) In the interpretation of k_{qk}/k^*_{qk} as a measure of $\langle n \rangle$ the number of states leading to state k, we specifically assumed that all microscopic quenching constants were identical. Any major trend in the relative magnitude of k_{qk} as a function of energy will distort this interpretation. However, as noted above, the results at 4300 and 4800 A seem to indicate an approximate constancy of k_{qk}.

3) We have assumed a step-ladder model for energy transfer; as shown by Rabinovitch et al.,[10] the assumption of more realistic statistical models of energy transfer may change the interpretation of efficiencies in chemical activation studies by a factor of approximately two. The corresponding analysis for fluorescence kinetics has not been carried out.

4) The assumption was made that $\Delta\mathcal{E}_{molecules} = \Delta\mathcal{E}_{fluorescence}$. The experimental data are a measure of $\Delta\mathcal{E}_{fluorescence}$. If, for some reason, the fluorescence spectra of energy transfer states are red shifted by amounts much greater than the energy difference of the collision, then

this effect will contribute to the apparent energy transfer efficiency. Such a phenomenon might be expected if the originally populated states were qualitatively different from the energy transfer states(as in the case of collision induced internal conversion). However, for the reasons given in Sec. B, this possibility is considered unlikely. Further, the slope of $1/k^{*}_{qk}$ is constant over a range that corresponds to $\Delta\langle n\rangle$ as high as 4 (excitation at 4000 A). This linearity would require an interpretation in which successively populated states had additional amounts of intra-molecular red shifting. As a part of this assumption the population distributions were assumed to be strongly weighted toward the lower energies. If this effect were not so great as assumed, the true values of the efficiency might be as much as 30% less than those we have calculated. The ultimate resolution of this question will have to await experiments in which the spectroscopy is resolved and analyzed.

No attempt was made to interpret the energy transfer data in terms of specific quantum transitions in the upper state, since knowledge of the spectroscopic constants is not sufficiently refined to allow this. The magnitudes of the vibrational quanta of the upper state are not known, with the exception of ν_2. Douglas and Huber[42] have assigned 880 cm^{-1} to this frequency if the upper state is bent in the equilibrium conformation; if the upper state is linear this frequency corresponds to $2\nu_2$.

The origin of the electronic transition has been placed between the limits 11500-15500 cm^{-1} from the magnitude of the isotope shift of the absorption spectrum.[42] If we take these limits and we assume that the vibrational and electronic energies are separable, then the vibrational

energies are 9500 to 13500 cm^{-1} for excitation at 4000 A, and 5300 to 9300 cm^{-1} for excitation at 4800 A; the vibrational energy transferred per collision is thus a very significant fraction of the total vibrational energy. However, in view of the mixing of electronic states which results from the vibrational motion, it may be more appropriate to consider the effective vibrational energy to be considerably greater than these estimates, approaching the total excitation above the lowest vibrational level of the ground state (21000 to 25000 cm^{-1}). With this interpretation the energy transferred per collision would be the order of ten percent of the total vibrational energy of the molecule.

D. Comparison with Other Studies of Inter-Molecular Energy Transfer

The present data on energy transfer fit into a developing picture that energy rich molecules are collisionally deactivated by heat bath molecules with large cross-sections and/or high efficiencies (energy per collision) as compared to the low effective cross-sections in diatomic and small polyatomic molecules in low vibrational levels of the ground state.[7,8,11,15] These results are consistent with the strong collision assumptions of theories of unimolecular reactions,[73] but are in contradiction to the predictions of Mahan,[74] based on an extrapolation of energy transfer theories developed for low energy vibrational transitions, that such cross-sections and energies should be quite small (deactivation probabilities the order of 0.1 and energies per collision the order of 10 cm^{-1}). In this discussion we shall consider the results of energy transfer studies on highly excited molecules and review briefly the methods used in these investigations. Of most significance here are fluorescence studies and chemical activation studies.

There are no other direct measurements of vibrational energy transfer in highly excited tri-atomic molecules with which to compare the results of the present work. In a dc study of SO_2 fluorescence Mettee[69] has observed vibrational relaxation in the $\tilde{A}\ ^1B_1$ state but data were not available for the quantitative evaluation of energy transfer rate constants; the relaxation appeared to take place with high probability similarly to the present observations on NO_2.

A prototype fluorescence study of energy transfer in a diatomic molecule is that of Steinfeld and Klemperer[14a] on I_2 excited to the v' 25 level of the $B^3\Pi_{0u+}$ state. This study was not time resolved; time normalization was obtained from independent lifetime measurements.[75] Because the observation was spectrally resolved it was possible to obtain relative rate constants into specific transfer states for both rotational and vibrational energy transfer. The probabilities obtained for single quantum vibrational energy transfer with various collision partners (0.1 to 0.6 per collision) were much greater than probabilities for such energy transfer in low levels of ground state I_2.[76] Probabilities per collision for two quantum transitions were also relatively large, approximately one-fifth as great as for single quantum transitions.

Existing theories of energy transfer were found to be inadequate when applied to the calculation of the vibrational-translational energy transfer probabilities for collisions of the highly excited I_2 molecules with rare gas molecules.[14b] Since the collision probabilities were large, simple perturbation theory broke down and led to over-estimation and non-conservation of these probabilities. On the other hand, quantum mechanical calculations, based on the method of Schwartz, Slawsky, and Herzfeld,[7]

tended to underestimate the collisional probabilities, and also failed to reproduce the observed dependence on the reduced mass of the collision pair.

With respect to polyatomic molecules, a very important series of investigations in the experimental verification of highly efficient collisional energy transfer was that of Neporent[77] and of Boudart and Dubois[78] on the fluorescence stabilization of β-napthylamine. These studies were also not time resolved; the first order, pressure independent lifetime upon which the calculations of efficiencies were based was the rate constant for internal conversion to a non-fluorescent state. It was possible to obtain relative values for this rate constant, which is a strong function of the vibrational energy of the molecule, from the temperature dependence of the paramagnetic quenching of the fluorescence by O_2. The absolute magnitude of the internal conversion rate constant was fixed by the assumption of unit efficiency for gas kinetic collisions in the oxygen quenching.

Energy transfer determinations were made for several M gas identities. The relative amounts of energy transfer per gas kinetic collision were determined experimentally from the slope of a Stern-Volmer like plot. This slope was a function of the energy transfer since the internal conversion rate constant was a strong function of the vibrational energy. From the analysis of Neporent's and their own data, Boudart and Dubois found values for energy transfer per collision ranging from 70 cm^{-1} (H_2, He) to 1690 cm^{-1} ($n\text{-}C_5H_{14}$) for vibrational energy of the excited molecule equal to 10200 cm^{-1}. The energy transfer per collision increased as the energy of vibration increased but decreased as the temperature was increased.

The results of these and other large-molecule studies have been reviewed by Stevens.[17]

Schlag and coworkers[79,80] have recently given preliminary reports of direct measurements by the phase-shift technique of energy transfer studies from β-napthylamine fluorescence with propane and propene as collision partners. The total cross sections for removal of vibrational energy were 0.04 to 0.13 times gas kinetic. The amount of energy transfer per collision was not reported.

Stockburger[81] has obtained results on energy transfer in naphthalene that are qualitatively different from those of Boudart and Dubois. Naphthalene was excited to a high vibrational level (~ 8000 cm^{-1}) in an excited electronic state which exhibited collisionally induced vibrational deactivation but apparently did not suffer electronic quenching. From the degree of population in the ground vibrational level as a function of M gas pressure it was possible to calculate the energy transfer efficiency per gas kinetic collision using lifetime values for fluorescence determined independently. The values obtained ranged from 6 cm^{-1} (He) to 220 cm^{-1} ($n\text{-}C_6H_{14}$).

We now consider the results of some chemical activation studies. Rabinovitch and coworkers[10] have studied several such systems to obtain data on energy transfer from the pressure dependence of the relative rates of competing chemical reactions. Typically the first order rate constant to which the rates of collisional processes are compared is the decomposition of the activated species. The efficiency of collisions in deactivating this species so that the first order process does not occur is obtained by a Stern-Volmer like analysis of the relative yields

of the two reactions.

A prototype study is that of sec-butyl-d_1 radical excited by the addition of D atom to cis-butene-2.[82] The first order decomposition rate was estimated by the method of direct counting of the density of vibrational levels.[83] The data were analyzed in a manner that is equivalent to examination of Stern-Volmer data for curvature. The analysis allows an estimation of the number of collisions responsible for deactivating the molecule. From the absence of curvature it was shown that the parent molecule is capable of removing 8-12 kcal (2800-4200 cm^{-1}) in a single collision. In other studies based upon an analysis of the curvature in "quenching" graphs it was possible to set limits on the energy transfer per collision $\mathcal{E}_c$ (efficiencies) and upon the cross sections of the collision (probabilities). The exact values of $\mathcal{E}_c$ were dependent on the model used for the analysis, but model-to-model the differences were within a factor of two. For sec-butyl radicals (E = 14000 cm^{-1}) rare gases and diatomic molecules exhibited $\mathcal{E}_c$ from 900 to 1200 cm^{-1}; polyatomic molecules were capable of removing at least 3000 cm^{-1} per collision. Similar studies with excited cyclopropane (E = 35000 cm^{-1}) showed $\mathcal{E}_c$ values ranging from 2000 (He, Ne, Ar) to 4000 cm^{-1} (C_2H_4).[84] In general in these studies the data indicated a cross-section of the order of gas kinetic, but occasionally a lower value was indicated.

E. Considerations Concerning the Dependence of Energy Transfer Rates on the Identity of the Collision Partner

In the various studies of energy transfer from polyatomic molecules the results have tended to show that the efficiency $\mathcal{E}_c$ (energy transfer per collision) where measured, or the product of efficiency times the probability of deactivation per collision increases with increasing complexity of collision partner M. (See preceding section.) If M is monatomic then only vibration → translation processes may take place. If M is diatomic or polyatomic then vibration → rotation and vibration → vibration processes may also take place, and the existence of these other possible modes of energy transfer may account for the increased efficiencies of polyatomic collision partners.

In their study of quenching of NO_2 fluorescence Myers, Silver, and Kaufman[19] noted an increase in the apparent quenching rate constant with molecular complexity. Since the present work has been able to provide a much more detailed picture of the energy transfer processes in excited NO_2 these studies are being extended to additional collision partners in order to obtain relative and absolute efficiencies for other M gas identities.

The question also arises whether NO_2 plays a special role as an energy transfer partner with excited NO_2 because of the identity of the species, and the possible resonant phenomena that may be associated with NO_2-NO_2 collisions and also because of the existence of a stable dimer.

An answer to this question may be obtained from the data of MSK (Table X) on the relative (per collision) quenching efficiencies of M gas partners. Since the identity of the quantum states observed will be a

Table X. Relative quenching cross sections as a function of collision partner

Quenching gas M	k_f/k_q $torr^{-1}$	P, relative to NO_2 = 1
He	29	0.17
Ar	30	0.33
N_2	44	0.42
O_2	48	0.54
H_2	62	0.25
NO	82	0.83
CH_4	82	0.67
N_2O	91	1.00
NO_2	100	(1.00)
CO_2	105	1.13
SF_6	155	1.46
CF_4	160	1.63
H_2O	280	2.00

Data are from Myers, Silver, and Kaufman (Ref. 19). Values of k_f/k_q are experimental values of quenching ratio. Values of P have been computed per collision, relative to NO_2 = 1. Excitation wavelength was 4358 A.

function of the spectral sensitivity of the detector, and since the apparent dc quenching ratio will be a function of the states observed, the values given in Table X can only be taken as having (at best) relative significance. However, it may still be inferred that NO_2 as a collision partner does not play a role which is significantly different from that of collision partners of comparable complexity.

In the experiments conducted with spectral resolution of the fluorescence MSK used Ar as well as NO_2 as a collision partner. While the magnitudes of the quenching ratios varied by a factor of three, the quenching ratios of Ar remained constant relative to those of NO_2.

As an additional examination of a possible special role of NO_2 as a collision partner, a calculation was made of the probability of complex formation in binary collisions of ground state NO_2 molecules. This calculation was made using data on the unimolecular decomposition of N_2O_4. This reaction may be considered in terms of the elementary processes:

$$N_2O_4 + M \underset{c}{\overset{d}{\rightleftharpoons}} N_2O_4^* + M$$

$$N_2O_4^* \underset{a}{\overset{b}{\rightleftharpoons}} NO_2 + NO_2$$

where $N_2O_4^*$ denotes an excited complex with energy sufficient for dissociation. The observed rate for decomposition is given (at the high pressure limit) by:

$$\text{Rate} = k_{\text{decomp}} (N_2O_4) = \frac{db}{c} (N_2O_4) .$$

The equilibrium constant K for this reaction is given by

$$K = \frac{db}{ac} .$$

Consequently, a, the rate constant for complex formation may be obtained by

$$a = k_{decomp}/K \quad .$$

The data of Carrington and Davidson[85] for the dissociation constant and Verhoek and Daniels[49] for the equilibrium constant were used; the value for a which was obtained was 8.6×10^{-13} cm^3/molec sec. Since the observed energy transfer rate constants were of the order of gas kinetic (2.3×10^{-10}), it was concluded that N_2O_4 complex formation did not play a special role in the energy transfer process.

F. Fluorescence Near the Dissociation Limit and the Mechanism of Dissociation

It was observed that the fluorescence lifetime remained relatively constant (± 25%) as the excitation was swept through the dissociation threshold (≈ 3980 A) whereas the apparent quantum yield for fluorescence, Φ_f, decreased by a factor of approximately 4000. From this we may assert that there are two sets of excited molecules present: one set fluoresces and does not dissociate; the other dissociates and does not fluoresce. This assertion may be proved by assuming the contrary mechanism and showing that this leads to a contradiction with the observations:

$$G \xrightarrow{I_o k_a} E$$

$$E \xrightarrow{k_f} G'$$

$$E \xrightarrow{k_q M} G'$$

$$E \xrightarrow{k_d} \text{dissociation products}$$

The rate constant for dissociation k_d is zero below an energy threshold and non-zero above this threshold. From this mechanism we may write

$$\tau = (k_f + k_d + k_q M)^{-1}$$

$$\Phi_f = k_f/(k_f + k_d + k_q M) \quad .$$

We now define the quantities y_Φ and y_τ as the ratios in quantum yields and lifetimes, respectively, for excitation at energies greater than and less than the dissociation threshold:

$$y_\Phi = \Phi_f \text{ above threshold}/\Phi_f \text{ below threshold}$$
$$y_\tau = \tau \text{ above threshold}/\tau \text{ below threshold}$$

It was observed experimentally that $y_\Phi \ll 1$; consequently $k_d \ll (k_f + k_q M)$. The assumed mechanism requires that $y_\Phi = y_\tau$. Therefore this mechanism must be rejected. Further, if there is a significant proportion of the fluorescence coming from molecules which are capable of both fluorescence and dissociation, the overall observed lifetime will be correspondingly reduced. Therefore the greatest part of the observed fluorescence for excitation energies in the threshold region must be from molecules which cannot dissociate. The remaining excited molecules must dissociate at a rate much greater than the fluorescence rate. Thus the assertion of two sets of excited molecules is proved.

We now wish to consider the nature of these two different sets of states. Certainly, if there are two different electronic states involved as proposed by Pitts, et al.,[87] the kinetic mechanism will be supported. However, this mechanism requires that the absorption coefficient for the

lower, non-dissociative state vanish rather sharply and the dissociative state begin at the threshold at the same value to continue the smooth total absorption curve (Fig. 1). Alternately, we may explain the observed behavior by assuming that the two sets of states are within the same electronic state. Those states which are capable of dissociating do so in a time so short compared to the fluorescence lifetime that they make no contribution to the fluorescence intensity. Those states which are observed in fluorescence are not capable of dissociating (presumably because they lack sufficient energy). The fluorescence observed with excitation at 3950 A is all due to molecules of energy less than required for dissociation, excited by light in the low energy "tail" of the excitation band pass.

With this interpretation we may consider the results of Table V as a measure of the dissociation threshold of NO_2. This may be set at 3980 A with tolerance limits of ±30 A due to the width of the excitation source, and the smearing of the threshold because of hot ground state molecules. This is in good agreement with determinations of this dissociation limit by other means, Table XI.

This aspect of the present work was not undertaken as an attempt to obtain a better value for this dissociation limit but to confirm the mechanism of dissociation, namely that molecules that are capable of dissociating do not fluoresce. This result is strongly indicated by the results of the predissociation study of Douglas and Huber,[42] who found no unbroadened lines (in absorption) at higher energies than 25125 cm^{-1}. A rate constant for dissociation may be estimated from the width of the broadened absorption line by uncertainty considerations. Douglas and Huber

Table XI. Dissociation of NO_2 to O (^3P) and NO ($^2\Pi$)

Energy cm^{-1}	Method	Reference
25105±10	Thermodynamics: $NO_2 = NO + 1/2\ O_2$	a
	NO, O_2 dissociation	b
25112±20	Break-off in magnetic rotation spectrum	c
25125±7	Predissociation in absorption; last unbroadened line	d
25157±20	Break off in NO + O luminescence spectrum	e
25146±70	Quantum yield for dissociation, 4047A photolysis	f
25160±500	Break off in luminescence from shock heated NO_2	g,h
25125±120	Break off in fluorescence quantum yield	present work

a. Ref. 91
b. Ref. 90
c. Ref. 92
d. Ref. 42
e. Ref. 29; see also Ref. 93, p. 60
f. Ref. 87
g. Ref. 93
h. Ref. 94

do not state the width of observed predissociated absorption lines. However, a lower limit to this width may be set by the Doppler width of a line.

$$\Delta\tilde{\nu} \geq \Delta\tilde{\nu}_{\text{Doppler}} = 2.8\times10^{-2} \text{ cm}^{-1}$$

From the reproduction of their absorption spectrum at 3910 A an upper limit to this width may be set:

$$\Delta\tilde{\nu} \leq 1.0 \text{ cm}^{-1}$$

Hence, from the uncertainty relation,

$$k_d = 1/\tau_d \approx \Delta\nu = c\Delta\tilde{\nu}$$

We may set limits on the value of the rate constant for dissociation, k_d:

$$8\times10^{8} \text{ sec}^{-1} \lesssim k_d \lesssim 3\times10^{10} \text{ sec}^{-1}$$

Doppler width $\lesssim 1/\tau \lesssim$ Uncertainty width

These limits may be compared with the value for k_d estimated by the technique of Marcus and Rice.[83] From lack of knowledge of the frequencies of the excited state of NO_2 this calculation was based on the ground state frequencies of the molecule,[88] and assumed a bent configuration (s = 3). For an assumed electronic energy of the excited state of 13500 cm^{-1} (see Sec. C) and for molecular excitation 200 cm^{-1} greater than the dissociation energy, the value computed was $k_d = 5\times10^{10}$ sec^{-1}, which is in close agreement with the limits estimated above.

In conclusion, the several estimates of k_d have given values which are five to seven orders of magnitude greater than the measured fluorescence rate constant, 1.6×10^{4} sec^{-1}. Virtually every molecule which is energetically

capable of dissociation will dissociate and consequently will not contribute to the observed fluorescence intensity or lifetime; the fluorescence quantum efficiency will have the approximate limits $(0.5\text{-}20)\times10^{-6}$. This interpretation is in agreement with the interpretation of NO_2 photolysis which has been given by Ford and Jaffe[89] that dissociation takes place with unit quantum efficiency at energies greater than the dissociation energy.

The discussion thus far has not accounted for the intra-molecular mechanism whereby the excited molecule dissociates; the fact that the electronic absorption to the $^2B_1$ state extends far beyond the dissociation limit has given additional support to interpretations of the NO_2 photolysis and fluorescence kinetics as requiring an additional electronic state. Figure 14 shows a set of pseudo-diatomic molecule potential energy curves that may be taken as representative of curves used in these interpretations.[29,87] State $\tilde{A}$ is responsible for the electronic absorption; it is drawn as extending well above the dissociation limit to account for absorption at these energies. $\tilde{B}$ is required to account for predissociation, and its presence is used to explain the anomalously long fluorescence lifetime by an internal conversion mechanism.

A diagram such as this is misleading, however, because it excludes the possibility of an alternate mechanism for predissociation, namely predissociation by vibration.[46d] This mechanism is not available in diatomic molecules, which have only one mode of vibration. This mechanism is of particular importance in the dissociation of symmetric molecules. Because of the C_2 symmetry the Franck-Condon factors in absorption will be concentrated almost exclusively in the symmetric vibrations (ν_1 and

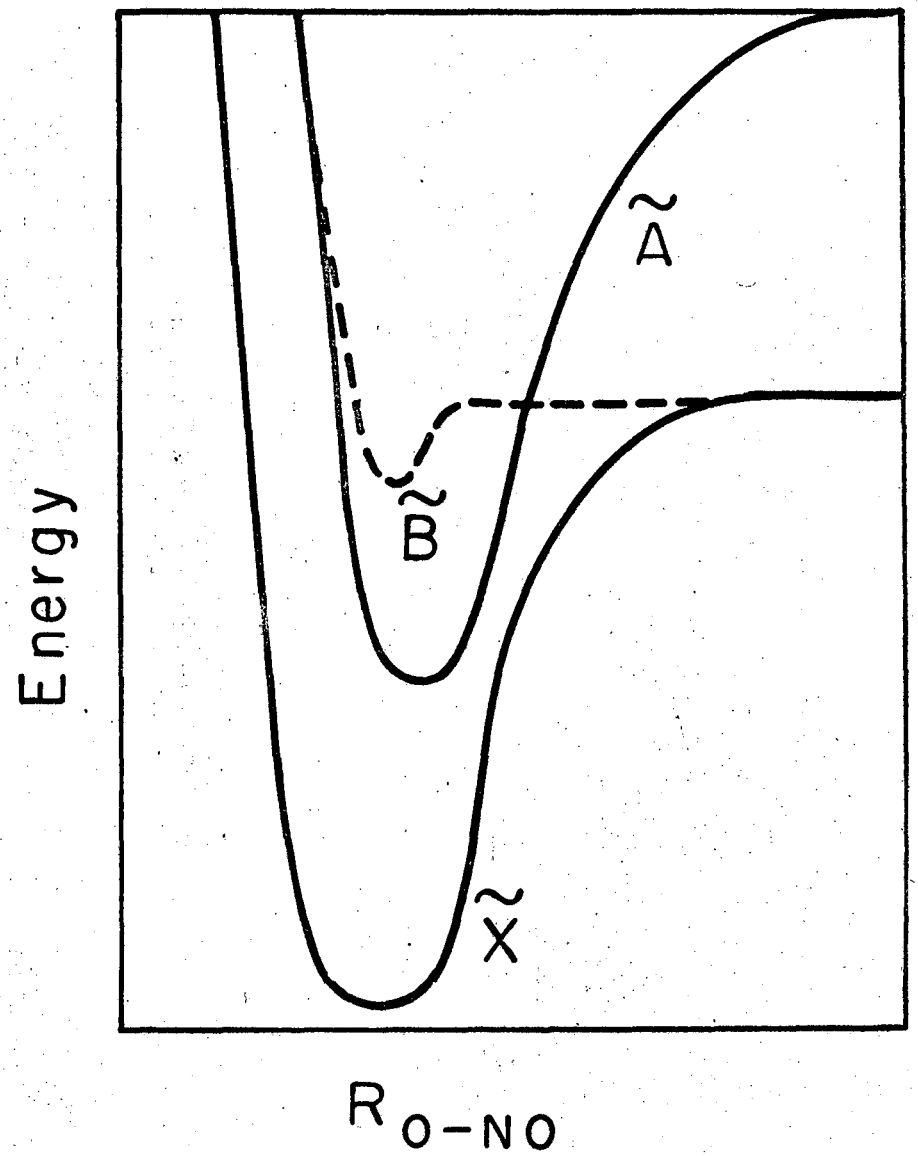

XBL688-3762

Fig. 14. One-dimensional potential energy curves for NO_2 as a pseudo-diatomic molecule. $\tilde{A}$ is the lowest excited electronic state and is strongly connected to the ground state by an optical transition. $\tilde{B}$ is weakly connected to A by a perturbation.

ν_2); i.e., absorption in ν_3 is Franck-Condon forbidden. The symmetric stretch, which leads to the dissociation products O + N + O, extends to a dissociation limit (77500 cm^{-1})[90] which is much higher than that for dissociation into O + NO, and thus can account for vibrational structure in the absorption spectrum beyond the lower value. The dissociation into O + NO must take place by asymmetric vibrations which can be populated only by mixing of the normal modes following the excitation. This mechanism allows for predissociation without requiring the presence of an additional electronic state.

G. Relation of Fluorescence and Chemiluminescence Studies

The two chemiluminescent reactions

$$NO + O\ (^3P) \rightarrow NO_2 + h\nu$$

and

$$NO + O_3 \rightarrow NO_2 + O_2 + h\nu$$

have previously been interpreted as involving the same excited electronic state of NO_2 as that populated optically and observed in fluorescence.[22,32] These interpretations have been based on the similarity of the spectral distributions and kinetic (quenching) behavior in the three systems. Since the same electronic state participates in all systems, then information obtained from the various studies can be applied to the other studies. Particularly, fluorescence studies because of time and energy resolution, are capable of direct measurement of radiative and energy transfer (quenching) rate constants. However, the complete spectral distribution of the fluorescence has not yet been measured in a fluorescence system, whereas these distributions are available from both chemiluminescent systems.

The reaction of nitric oxide and oxygen atom (the air afterglow) has been interpreted in terms of two distinct types of mechanisms:

I. Stabilization by Radiation

$$NO + O \underset{k_d}{\overset{k_a}{\rightleftharpoons}} NO_2^*$$

$$NO_2^* \xrightarrow{k_f} NO_2 + h\nu$$

$$I_f = (k_a/k_d)k_f\,(NO)(O)$$

II. Collisionally stabilized excited state; the simplest mechanism of this type that may be written is:

$$NO + O + M \underset{-1}{\overset{1}{\rightleftharpoons}} NO_2^* + M$$

$$NO_2^* \xrightarrow{k_f} NO_2 + h\nu$$

$$NO_2^* + M \xrightarrow{k_q} NO_2 + M$$

$$I_f = \frac{k_1\, k_f (NO)(O)(M)}{k_f + k_{-1}(M) + k_q(M)}$$

For pressures greater than 1 torr the chemiluminescent intensity has been found to obey the relation[31,95,96]

$$I_f = k^*\,(NO)(O) \quad .$$

This has led to the proposal of mechanism I.[34-36] However, this mechanism has been disputed because:

1) The value of k^* has shown somewhat of a dependence on the identity of M.[95,96]

2) The spectrum of the chemiluminescence has a sharp cut off at the

enthalpy of recombination (See Sec. F) and does not have a tail to thermal energies above that value.

A simple mechanism such as II can account for these observations, since at high pressures ($k_q M + k_{-1} M \gg k_f$),

$$I_f = \frac{k_1 k_f (NO)(O)}{k_{-1} + k_q} .$$

This expression has the required dependence on the total pressure M, and since reactions (1) and (q) are not detailed balance inverses, k^* might be expected to have a dependence on the identity of M.

Mechanism II does predict, however, a dependence on the total pressure M at pressures less than 100 m torr; such a dependence has recently been reported.[32,33] The dependence may, by analogy to Stern-Volmer kinetics, be expressed as a quenching ratio $(k_q + k_{-1})/k_f$. The values reported are in good agreement with the fluorescence quenching data.[19] We should like to stress that as the Stern-Volmer mechanism is inadequate for the interpretation of fluorescence data at low pressures because of energy transfer process in the excited state, mechanism II should similarly be inadequate for the interpretation of the air afterglow at low pressures. Quenching plots -- $I_f/(NO)(O)(M)$ vs. (M) -- should not be linear and should have high pressure slope to intercept ratios which are a function of the observation wavelength. The dependence of the quenching ratio upon the observation wavelength has been observed, with lower quenching ratios at higher observation energies.[32,33] Mechanism II may be tested for consistency by estimation of k_1 from the known value of k^* [31] and the quenching ratio k_q/k_f.[19] From these quantities k_1 is computed to be 6×10^{-32} $cm^6/molecule^2$ sec, which is in good agreement with the values

reported by Kaufman[96] for the overall rate constant (at high pressures) for the reaction $NO + O + M \rightarrow NO_2 + M$. Such a comparison is necessarily artificial since k_q/k_f is a function of observation wavelength, but suggests that a major proportion of NO_2^* formed by (1) is capable of fluorescence at sufficiently low pressure.

In Fig. 15 are given the low resolution fluorescence spectra obtained in the present experiment (high pressure limit spectra) and on the same scale the spectrum of the air afterglow,[31] all normalized to the same intensity at 7000 A. While the three fluorescence distributions are generally close to the air afterglow distribution, that obtained for excitation at 4300 A most closely approximates this distribution. We wish to speculate semi-quantitatively about the possible reason for this. If we consider the air afterglow spectrum as due principally to molecules at energies of 4300 A or 23300 cm^{-1} rather than from molecules at $\Delta H = 25100$ cm^{-1}, then this energy difference of approximately 2000 cm^{-1} is equal to the energy transfer efficiency of one collision. That is, the three body reaction (1) may be thought of as two sequential two body processes

$$NO + O \underset{k_d}{\overset{k_a}{\rightleftharpoons}} NO_2^{**}$$

$$NO_2^{**} + M \xrightarrow{k_s} NO_2^{*} + M$$

where the stabilization reaction (s) is quite analogous to the energy transfer process of the stabilized species at slightly lower energies. By virtue of this similarity a similar dependence on the identity of M might be expected. This would account for the slight dependence of k^*

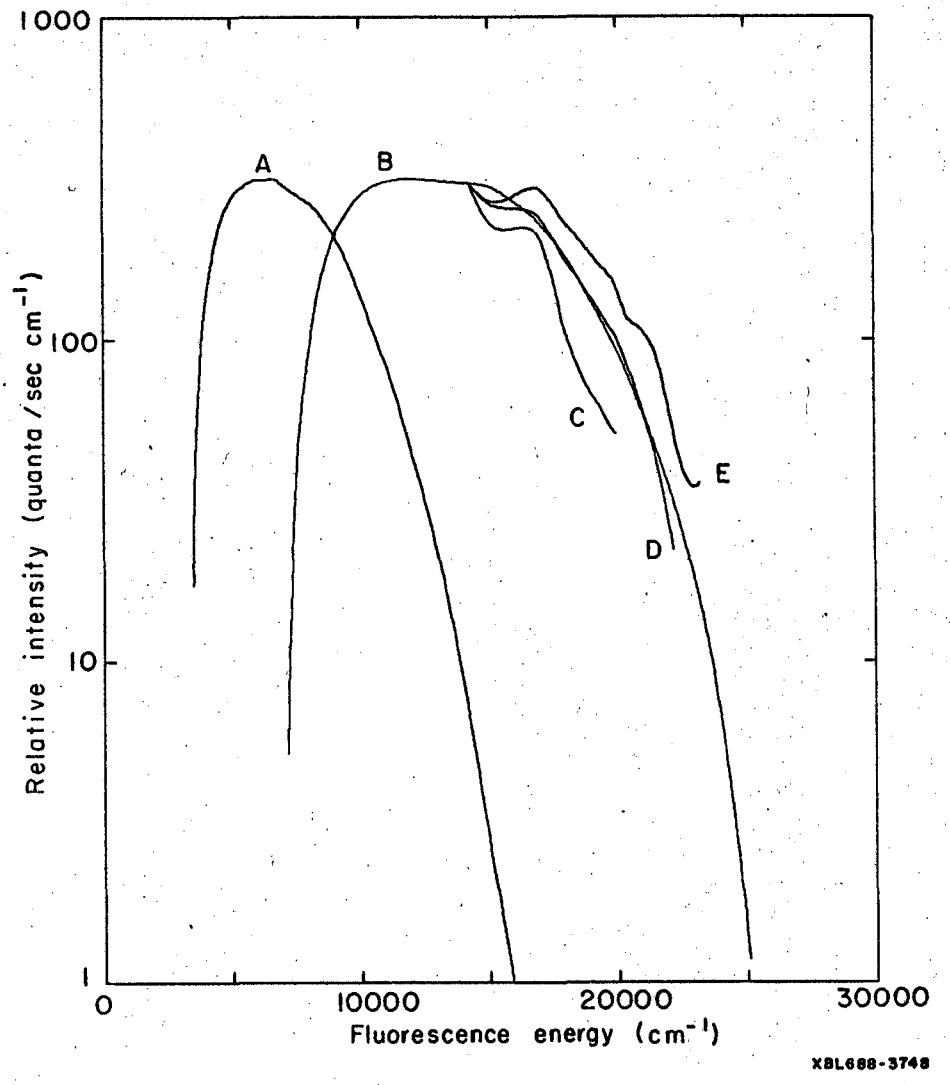

Fig. 15. Fluorescence and chemiluminescence spectra. A: NO + O_3; total pressure, 5-60 mtorr data of Ref. 21. B: NO + O; total pressure 0.1-5 torr; data of Ref. 31. C, D, E: NO_2 fluorescence spectra for excitation at 4800, 4300 and 4000 A respectively; high pressure limit spectra (P > 50mtorr); present work. The fluorescence spectra are normalized to the NO + O spectrum at 14270 cm^{-1}.

on M identity, despite the widespread differences in quenching efficiencies in fluorescence experiments. Thus CO_2 and Ar were equally efficient as M gases in the air afterglow reaction,[96] whereas CO_2 is 3.5 times as efficient as Ar in fluorescence quenching.[19] From this mechanism we may write the complex rate constant k_1 in terms of the elementary rate constants:

$$k_1 = \frac{k_a k_s}{k_d} .$$

If we assume values of 1×10^{-10} for k_a (Ref. 2b) and k_s (M = Ar; k_{NO_2} from present experiment and $k_{Ar}/k_{NO_2} = 0.33$, Ref. 19) and the value 5×10^{10} sec^{-1} for k_d (see Sec. F), then we obtain $k_1 = 20\times10^{-32}$, which is in good agreement with the experimental value considering the very approximate values of rate constants assumed.

We turn now to the nitric oxide -- ozone reaction. Clough and Thrush[21,22] have interpreted this luminescence in terms of the mechanism

$$NO + O_3 \xrightarrow{k_b} NO_2^* + O_2$$

$$NO_2^* + M \xrightarrow{k_q} NO_2 + M$$

$$NO_2^* \xrightarrow{k_f} NO_2 + h\nu$$

which is analogous to II above and to the Stern-Volmer mechanism of fluorescence. The emission spectrum of this system, which has been reported not to change with pressure in the range 5 to 60 m torr, is given in Fig. 15. The ratio of the values of $\langle\tilde{\nu}^3\rangle_{F-C}$ for the two systems (≈ 8) is much greater than would be predicted from the relative enthalpy values of the two reactions: $(25100/16700)^3 \approx 3.4$; this factor is even

lower (≈ 2.6) if we take the energy of NO_2^* as equal to the enthalpy plus the activation energy for the luminescence (18158 cm^{-1}).[22]

Although spectra for fluorescence excited at energies in this region (5500-6000 A) were not obtained, fluorescent lifetimes were obtained which exhibit less than the expected dependence on excitation energy. Consequently we infer that most of the NO_2^* formed in the bimolecular atom transfer reaction (b) has energy substantially lower than the enthalpy of the reaction, in distinction to the air-afterglow reaction, in which NO_2^* has energy close to the enthalpy of reaction. In the ozone reaction the oxygen molecule may be formed with significant amounts of vibrational energy, which would leave the NO_2^* with reduced energy. The high energy luminescence, which extends to 17600 cm^{-1} would have to be interpreted as coming from the tail of the distribution function of NO_2^* energies. However, the existence of a distribution of energies of NO_2^* would require that the apparent quenching be different at different observation wavelengths, in contradiction to the observations of Clough and Thrush.[22] The resolution of these questions will have to await further experimentation on the NO_2 fluorescence excited at the lower energies corresponding to the enthalpy of the ozone reaction.

Appendix A: Transfer Functions

In this appendix we shall develop some expressions for transfer functions between a modulated excitation source and excited states populated by the source and some general rules for the propagation of transfer functions. In all cases the discussion will be limited to linear systems. Thus we shall rule out any reactions between two excited species and also shall restrict our experiment to moderate light intensities at which the ground state is not significantly depleted. Such nonlinearities introduce components of the population at harmonics of the modulation frequency as well as a nonlinear dependence of the concentration on the intensity of the modulation source. The solution of this problem has been discussed by McGraw and Johnston.[56] A general expression for excited state populations in linear kinetics, developed in a somewhat different context, has been given by Gordon.[97]

The simplest mechanism is that of a single excited state decaying with a single lifetime, which was discussed in the text. The elementary reactions in this mechanism are:

$$G \xrightarrow{k_a I_o} E \qquad \text{excitation}$$

$$E \xrightarrow{k} G' \qquad \text{de-excitation}$$

The differential equation governing the system is:

$$\dot{\underset{\sim}{E}} = k_a \underset{\sim}{I_o} G - k \underset{\sim}{E} \tag{1}$$

where $\underset{\sim}{I_o} = I_{dc} + I_o (e^{i\omega t})$ is the incident intensity, including the dc term. Since the differential equation (1) is linear, and we are concerned

only with the modulated concentration of E, we may drop the dc term and write $\underset{\sim}{I}_o = I_o e^{i\omega t}$. The solution of (1) at times long compared to k^{-1} gives[98]

$$\underset{\sim}{E} = \frac{I_o k_a G}{k} \frac{1}{1 + \frac{i\omega}{k}} e^{i\omega t} = \frac{\underset{\sim}{I}_o k_a G}{k} \cdot \frac{1}{1 + \frac{i\omega}{k}} \qquad (2)$$

consequently the transfer function, which is defined as the ratio of the population at frequency ω $E(\omega)$ to that at zero frequency $E(0)$, is

$$F = \frac{1}{(1 + i\omega/k)}$$

When $\omega = 0$, $F = 1$, and the solution to (1) reduces to the steady state solution as required. The phase of the state E_1 with respect to I_o is required to be in the first quadrant.

We now consider two state series kinetics.

$$G \xrightarrow{k_a \underset{\sim}{I}_o} E_1$$

$$E_1 \xrightarrow{k_1} E_2$$

$$E_2 \xrightarrow{k_2} G'$$

From (2) we may immediately write

$$E_1 = \frac{I_o G k_a}{k_1} \frac{1}{1 + \frac{i\omega}{k_1}}$$

E_2 is governed by the equation

$$\dot{\underset{\sim}{E}}_2 = k_1 \underset{\sim}{E}_1 - k_2 \underset{\sim}{E}_2$$

Consequently

$$E_2 = \frac{k_1 E_1}{k_2} \frac{1}{1 + \frac{i\omega}{k_2}} = \frac{I_o G k_a}{k_2} \frac{1}{1 + \frac{i\omega}{k_1}} \frac{1}{1 + \frac{i\omega}{k_2}}$$

This result has been given previously by Birks, et al.,[99] and by Schlag, et al.[79] It has been used by Yardley and Moore[15] to determine the rate constants k_1 and k_2 in a three level system by observation of fluorescence from E_2. The result may be expressed as a product rule in transfer functions for levels excited in series (series-product rule):

$$F(E_2,G) = F(E_1,G) \cdot F(E_2, E_1)$$

The extension to an arbitrary number of levels populated in series follows by induction. The phase lag between any two successive states is required to be between 0° and -90°.

In the dc limit the expression for E_2 reduces as required to the steady state expression:

$$E_2 = \frac{I_o G k_a}{k_2} .$$

At this point it might be worthwhile to mention an analogy to ac electrical circuits, in the study of which are encountered identical differential equations to those of linear kinetics. An analogy to the single excited state system is given by a simple RC low pass filter, Fig.A-1a. The voltage response of this circuit to ac excitation at an angular frequency ω is given by

$$E_1 = E_o \frac{1}{1 + i\omega\tau}$$

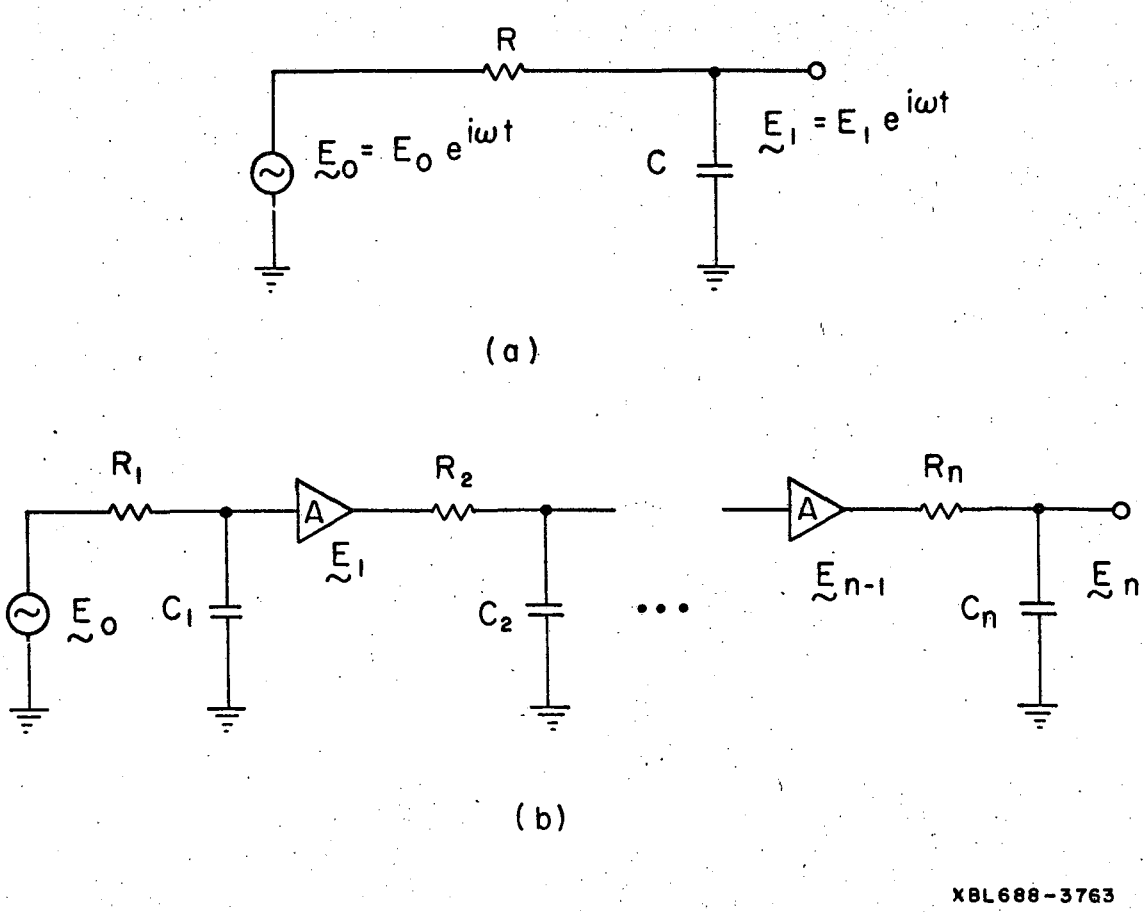

Fig. A1. Electrical circuit analogs to fluorescence kinetics. a. Single excited state. b. States excited in series. A represents an ideal buffer amplifier to isolate successive stages.

where $\tau = RC$ is the discharge time of the circuit in the absence of an applied voltage. The electrical circuit analogy to n state series kinetics is given by n isolated low pass filters connected in series, Fig. A-1b.

A second important result concerning fluorescence kinetics comes as a direct consequence of the linearity, namely that the contributions from two or more parallel paths are additive. There is no interaction resulting from the existence of parallel paths populating a given state. An analogous electrical circuit could be constructed by the use of voltage summing amplifiers (Fig. A-2). This result may be called the parallel-sum rule.

With these two rules we may consider the problem of cascade kinetics. Here there are two parallel paths, one of which excites the observed state (E_2) directly, and one of which goes via an intermediate state (E_1) which has a finite lifetime.

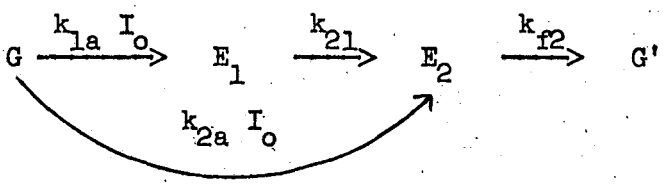

We may now write immediately

$$E_2 = \frac{I_o G}{k_{f2}} \left(k_{1a} \frac{1}{1 + \frac{i\omega}{k_{21}}} \frac{1}{1 + \frac{i\omega}{k_{f2}}} + k_{2a} \frac{1}{1 + \frac{i\omega}{k_{f2}}} \right) ,$$

a result previously obtained by Lawrence and Savage.[100]

The problem of radiation trapping may be treated by summation of an infinite series.

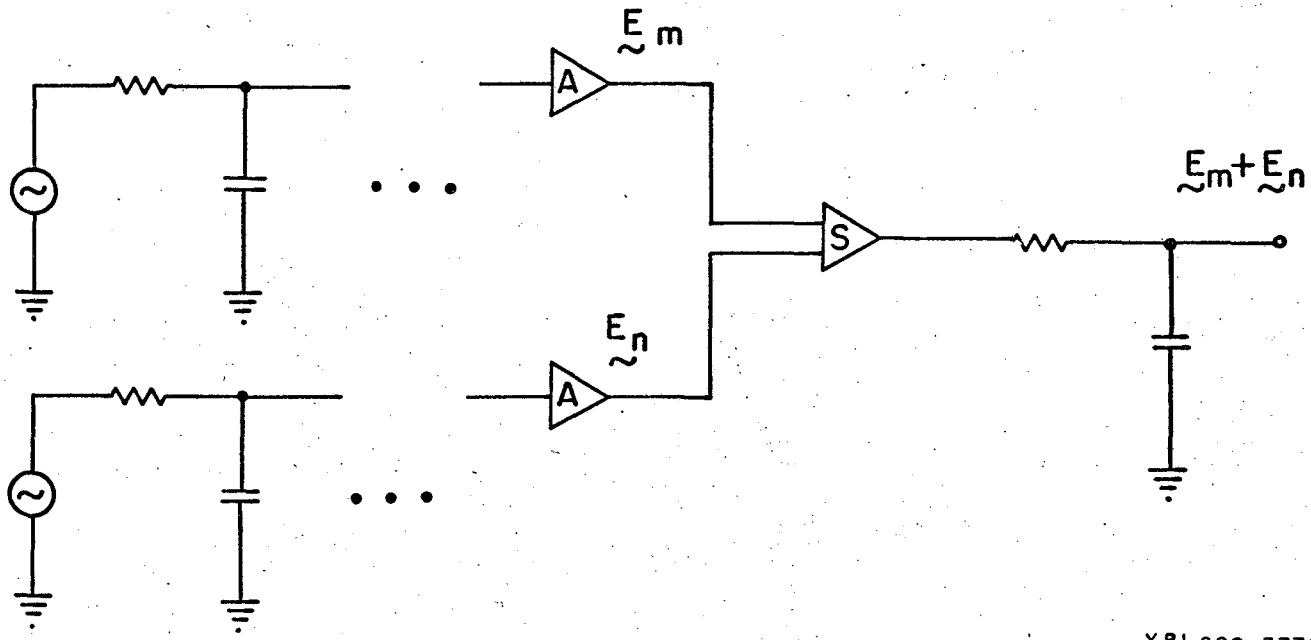

Fig. A 2. Electrical circuit analog to the parallel mechanism in fluorescence kinetics. S represents an ideal voltage-summing amplifier.

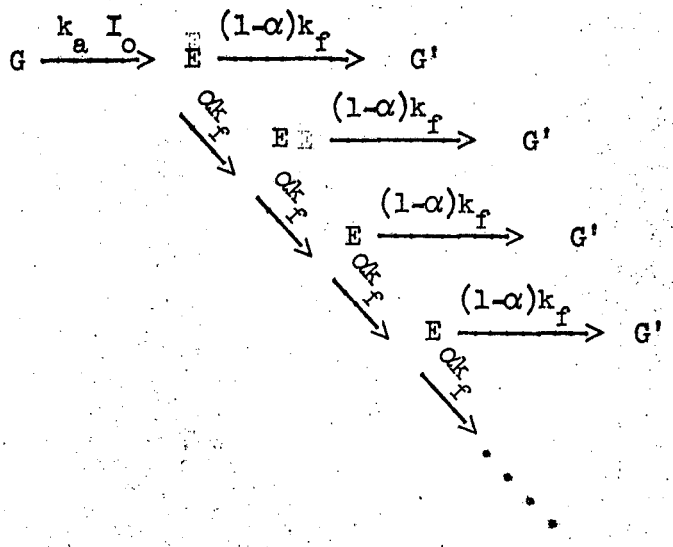

Here α is the fraction of the emitted radiation that is reabsorbed by other molecules in the system. By summing contributions to E,

$$E = I_o G \frac{k_a}{k_f+i\omega} \left\{ 1 + \frac{\alpha k_f}{k_f+i\omega} + \left(\frac{\alpha k_f}{k_f+i\omega}\right)^2 + \cdots \right\}$$

$$= I_o G \frac{k_a}{k_f+i\omega} \cdot \frac{1}{1 - \frac{\alpha k_f}{k_f+i\omega}}$$

$$= I_o G k_a \frac{1}{(1-\alpha) k_f + i\omega} .$$

The system behaves as a single state system with its fluorescence rate constant reduced by the factor $(1-\alpha)$. The system has the correct dc limit:

$$E = \frac{I_o G k_a}{(1-\alpha)k_f} .$$

As a final example we consider a situation involving two coupled excited states.

$$G \xrightarrow{I_o\, k_a} E_1 \underset{\beta k_2}{\overset{\alpha k_1}{\rightleftharpoons}} E_2$$

$$E_1 \xrightarrow{(1-\alpha)k_1} G'$$

$$E_2 \xrightarrow{(1-\beta)k_2} G'$$

Rewriting this in a form suitable for summation in an infinite series:

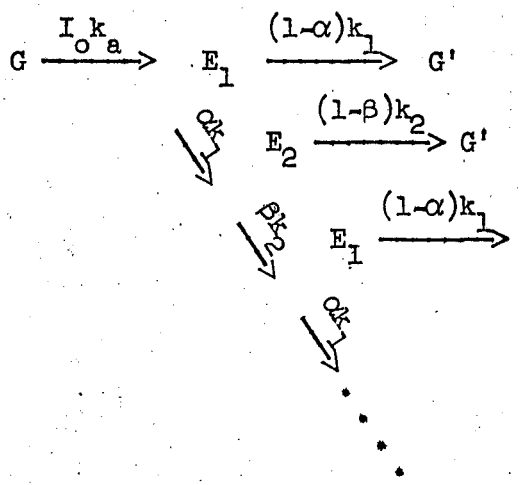

By direct sum,

$$E_1 = I_o\, G\, \frac{k_a}{k_1+i\omega} \left\{ 1 + \left(\frac{\alpha k_1}{k_2+i\omega} \quad \frac{\beta k_2}{k_1+i\omega} \right) + \left(\quad \right)^2 + \cdots\cdots \right\}$$

$$= I_o\, G\, k_a \left\{ \frac{(k_2 + i\omega)}{(k_1+i\omega)(k_2+i\omega) - \alpha\, k_1\, \beta\, k_2} \right\}$$

$$E_2 = I_o\, G\, \frac{k_a}{k_1+i\omega} \quad \frac{\alpha k_1}{k_2+i\omega} \left\{ 1 + \left(\frac{\alpha k_1}{k_2+i\omega} \quad \frac{\beta k_2}{k_1+i\omega} \right) + \left(\quad \right)^2 + \cdots\cdots \right\}$$

$$= I_o k_a G \left\{ \frac{\alpha\, k_1}{(k_1+i\omega)(k_2+i\omega) - \alpha\, k_1\, \beta\, k_2} \right\} .$$

It is interesting to note that E_2 obeys the usual phase relation to E_1, but that E_1 does not have a simple relation to I_o.

At $\omega = 0$ (dc excitation) the appropriate steady state expressions are obtained:

$$E_1 = I_o G \frac{k_a}{k_1 (1-\alpha\beta)}$$

$$E_2 = I_o G \frac{k_a \alpha}{k_2 (1-\alpha\beta)}$$

From these examples it may be seen that the phase shift method is a rather natural extension of steady state kinetics. The simplicity of the expressions developed is in great distinction to the expressions arising from a flash-decay experiment, in which the solution to the set of coupled differential equations depends strongly on a knowledge of the initial conditions or on the assumption (often not valid) that the duration of the flash has been sufficient to establish steady state conditions.[101] The simplicity results from the fact that only a single modulation frequency is involved and also that the kinetics are linear in the modulated species.

It has been observed[102] that the phase shift method at a single frequency does not provide a test that the fluorescent mechanism is first order in a single state (exponential decay). The reason for this is that the phase shift method probes the fluorescent system with a single frequency. This is in contrast to a sharply cut-off flash, which contains "all" frequencies, and which consequently provides a direct test for "exponentiality". The functional dependence of the transfer function on frequency may, however, be obtained directly from phase shift studies

by varying the modulation frequency, and tests of the assumed mechanism may be made in this way. Further, the frequency dependence of the transfer function may be used to elucidate the mechanism where this is not known. The analogy to electrical circuits may be carried further: The use of flash-decay methods is analogous to determining the characteristics of an unknown circuit from its time response to transient signals. The phase shift study is analogous to characterizing the circuit by its frequency response. The use of a single modulation frequency in the investigation of a chemical system where the assumed mechanism is not that of a single excited state does not invalidate the study. The frequency response of the system may be calculated for an assumed mechanism and the measurements interpreted in terms of that mechanism. However, conducting the studies at more than one modulation frequency would provide a valuable check on the assumed mechanism.

Appendix B: High Pressure Limits in Fluorescence Kinetics

In a system of n collisionally coupled quantum states the pressure dependence of the concentrations depends, in general, on a large number (order n^2) of rate constants. Jenkins[103] has given solutions for a system consisting of two excited states for steady state experiments in which one or both states are excited or observed. If the data are sufficiently precise the complete set of rate constant ratios may be evaluated by regression techniques.

In instances where a large number of quantum states are involved it is useful to develop approximations from the general expression for concentrations in order to predict or explain the pressure dependence of fluorescence lifetimes and intensities. This is readily done at high pressures by an expansion in inverse powers of the total pressure M. The development of approximate expressions is particularly necessary for the interpretation of experiments of low spectral resolution in which an observed signal is almost inevitably due to contributions from many quantum states.

In this discussion we shall assume a set of n excited states E_1, E_2, ..., E_n populated in a series mechanism. We shall consider first the steady state or dc situation. From Appendix A we have

$$E_1 = I_o G \frac{k_{1a}}{k_{f1} + k_{q1} M} = \frac{I_o G}{M} \cdot \frac{k_{1a} M}{k_{f1} + k_{q1} M} \quad . \qquad (1)$$

Here k_{1a} is the absorption coefficient into state E_1; k_{f1} is the fluorescence rate constant from state E_1; and k_{q1} is the total rate constant for collisional depopulation of state 1. For a second

generation excited state

$$E_2 = \frac{I_o G}{M} \cdot \frac{k_{1a} M}{k_{f1} + k_{q1} M} \cdot \frac{k_{21} M}{k_{f2} + k_{q2} M} \quad . \qquad (2)$$

Here k_{21} is the transfer rate constant from state E_1 to state E_2, a subset of k_{q1}. For a third generation excited state

$$E_3 = \frac{I_o G}{M} \cdot \frac{k_{1a} M}{k_{f1} + k_{q1} M} \cdot \frac{k_{21} M}{k_{f2} + k_{q2} M} \cdot \frac{k_{32} M}{k_{f3} + k_{q3} M} \qquad (3)$$

and so on for subsequent generations of states.

More generally, a second generation state E_2 may be populated by contributions from more than one first generation state, so that we have

$$E_2 = \frac{I_o G}{M} \sum_i \frac{k_{ia} M}{k_{fi} + k_{qi} M} \cdot \frac{k_{2i} M}{k_{f2} + k_{q2} M} \qquad (4)$$

where the summation is over all states populated directly by absorption of incident radiation. Similarly for a third generation state

$$E_3 = \frac{I_o G}{M} \sum_{ji} \frac{k_{ja} M}{k_{fj} + k_{qj} M} \cdot \frac{k_{ij} M}{k_{fi} + k_{qi} M} \cdot \frac{k_{3i} M}{k_{f3} + k_{q3} M} \qquad (5)$$

where the summation is over all first and second generation quantum states. We now introduce the (very real) possibility of cascading, in which case we can no longer state that a quantum state E_k is uniquely a given number of generations removed from the initially populated state. Thus

$$E_k = \frac{I_o G}{M} \left\{ \frac{k_{ka} M}{k_{fk}+k_{qk} M} + \sum_i \frac{k_{ia} M}{k_{fi}+k_{qi} M} \cdot \frac{k_{ki} M}{k_{fk}+k_{qk} M} \right.$$

$$\left. + \sum_{ji} \frac{k_{ja} M}{k_{fj}+k_{qj} M} \cdot \frac{k_{ij} M}{k_{fi}+k_{qi} M} \cdot \frac{k_{kj} M}{k_{fk}+k_{qk} M} + \cdots\cdots \right\} \quad (6)$$

where k is now used merely as an index and does not signify the generation of the state. The ellipsis signifies summations representing contributions to the population having greater numbers of intermediate states. It should be pointed out here that the expression (6) is still not completely general, as it neglects the possibility of "back-up" transitions. If the energy per step is sufficiently large compared to kT, this neglect is justified. This point is discussed in the text. The existence of "back-up" transitions would not affect the existence of high pressure limits (equation 7).

It is the expression (6) which we wish to take to the high pressure limit, at which $k_{qi}M \gg k_{fi}$ for all i. At sufficiently high pressure the fluorescence rates will be negligible in all denominators in (6). Under this condition the expression reduces to

$$E_k = \frac{I_o G}{M} \left\{ \frac{k_{ka}}{k_{qk}} + \sum_i \frac{k_{ia}}{k_{qi}} \frac{k_{ki}}{k_{qk}} + \sum_{ji} \frac{k_{ja}}{k_{qj}} \frac{k_{ij}}{k_{qi}} \frac{k_{ki}}{k_{qk}} + \cdots\cdots \right\} . \quad (7)$$

Thus at high pressures the concentrations in all quantum states have the same (inverse first order) dependence on the total pressure M. Since the spectral distribution of the fluorescence from each quantum state is a function of that state, the total fluorescence spectrum has a "high

pressure limit" in which the relative intensities at all observation wavelengths are independent of pressure. At sufficiently high pressures, for dc excitation the system of arbitrarily many quantum states will have a single quenching behavior. The inverse intensity at any wavelength will vary linearly with pressure, just as is the case with single-state (Stern-Volmer) kinetics.[78] The comparison with Stern-Volmer kinetics is facilitated by rewriting (7)

$$E_k = \frac{I_o G}{k_{qk} M} \left\{ k_{ka} + \sum_i k_{ia} \frac{k_{ki}}{k_{qi}} + \sum_{ji} k_{ja} \frac{k_{ij}}{k_{qj}} \frac{k_{ki}}{k_{qi}} + \cdots \right\} \quad . \tag{8}$$

If we define

$$\langle k_a \rangle_k \equiv \left\{ k_{ka} + \sum_i k_{ia} \frac{k_{ki}}{k_{qi}} + \sum_{ji} k_{ja} \frac{k_{ij}}{k_{qj}} \frac{k_{ki}}{k_{qi}} + \cdots \right\}$$

then

$$\frac{1}{E_k} = \frac{k_{qk} M}{I_o G \langle k_a \rangle_k} \quad . \tag{8a}$$

This is to be compared to the high pressure limit of the Stern-Volmer equation

$$\frac{1}{E_k} = \frac{k_q M}{I_o G k_a} \tag{8b}$$

We may also consider the ratio of the high pressure limiting slope to the zero pressure intercept, or its inverse. The intercept/slope ratio, which has units of pressure, is given by

$$P^*_{dc} = \frac{\langle k_a \rangle_k}{k_{ka}} \frac{k_{fk}}{k_{qk}} \quad . \tag{9}$$

This quenching pressure is increased by the ratio $\langle k_a \rangle_k / k_{ka}$ over that

for direct excitation into the state E_k. It should be observed that this ratio is defined only for $k_{ka} \neq 0$.*

A further remark should be made at this point with reference to a low resolution experiment. At low resolution the detector does not observe the fluorescence from a single quantum state, but rather a sum of fluorescences from many states:

$$I_\lambda = \sum_k \alpha_{\lambda k} k_{fk} E_k \qquad (10)$$

where $\alpha_{\lambda k}$ takes into account the overlap of the fluorescence of the state E_k with the spectral response of the detector at wavelength λ. Consequently the preceding and subsequent discussion should be in terms of I_λ rather than E_k. This extension follows readily and does not change the conclusions which we have reached.

---

* Further qualitative information available from dc experiments is obtained from the low pressure limit in quenching curves. A Taylor's series expansion of (6) at low pressure yields the result

$$\frac{d}{dM}\left(\frac{1}{E_k(M)}\right)_{M=0} = \frac{k_{fk}}{I_o G\, k_{ka}}\left[\frac{k_{qk}}{k_{fk}} - \sum_i \frac{k_{ia}}{k_{ka}}\,\frac{k_{ki}}{k_{fi}}\right]$$

The quantity in brackets will be positive or negative depending on whether the state k is populated at low pressures predominately by direct excitation or by energy transfer from initially excited states.

For ac excitation the analysis of the kinetic mechanism is similar. Here

$$E_1 = I_o G \frac{k_{1a}}{k_{q1} M + k_{f1} + i\omega} = \frac{I_o G}{M} \frac{k_{1a} M}{k_{q1} M + k_{f1} + i\omega} \quad . \qquad (11)$$

At this point we shall neglect all k_{fi} with respect to k_{qi} M so that

$$E_1 = \frac{I_o G}{M} \frac{k_{1a} M}{k_{q1} M + i\omega} = \frac{I_o G}{M} \frac{\frac{k_{1a}}{k_{q1}} \left[1 - \frac{i\omega}{M} \left(\frac{1}{k_{q1}} \right) \right]}{1 + \left(\frac{\omega}{k_{q1} M} \right)^2} \quad . \qquad (12)$$

Similarly,

$$E_2 = \frac{I_o G}{M} \frac{\frac{k_{1a}}{k_{q1}} \frac{k_{21}}{k_{q2}} \left[1 - \left(\frac{\omega}{M} \right)^2 \left(\frac{1}{k_{q1}} \frac{1}{k_{q2}} \right) - \frac{i\omega}{M} \left(\frac{1}{k_{q1}} + \frac{1}{k_{q2}} \right) \right]}{\left[1 + \left(\frac{\omega}{k_{q1} M} \right)^2 \right] \left[1 + \left(\frac{\omega}{k_{q2} M} \right)^2 \right]} \qquad (13)$$

and

$$E_3 = \frac{I_o G}{M} \frac{k_{1a}}{k_{q1}} \frac{k_{21}}{k_{q2}} \frac{k_{32}}{k_{q3}}$$

$$\times \left\{ \frac{1 - \left(\frac{\omega}{M} \right)^2 \left(\frac{1}{k_{q1} k_{q2}} + \frac{1}{k_{q1} k_{q3}} + \frac{1}{k_{q2} k_{q3}} \right)}{\left[1 + \left(\frac{\omega}{k_{q1} M} \right)^2 \right] \left[1 + \left(\frac{\omega}{k_{q2} M} \right)^2 \right] \left[1 + \left(\frac{\omega}{k_{q3} M} \right)^2 \right]} \right.$$

$$\left. + \frac{i\omega}{M} \frac{\frac{1}{k_{q1}} + \frac{1}{k_{q2}} + \frac{1}{k_{q3}} - \left(\frac{\omega}{M} \right)^2 \left(\frac{1}{k_{q1}} \frac{1}{k_{q2}} \frac{1}{k_{q3}} \right)}{\left[1 + \left(\frac{\omega}{k_{q1} M} \right)^2 \right] \left[1 + \left(\frac{\omega}{k_{q2} M} \right)^2 \right] \left[1 + \left(\frac{\omega}{k_{q3} M} \right)^2 \right]} \right\} \qquad (14)$$

and so on for subsequent generations.

At this point we could follow the dc argument by constructing an arbitrary state as a sum over processes populating that state. For brevity we shall not repeat this; the generality of the discussion that immediately follows is in no way affected by this. The argument is again made that at sufficiently high pressure terms of the order of M^{-2} and lower may be neglected. This assumption is equivalent to the small angle assumption; i.e., that tangents of small angles may be added rather than the angles themselves. Under this assumption

$$E_1 = \frac{I_o G}{M} \frac{k_{1a}}{k_{q1}} \left[1 - \frac{i\omega}{M} \left(\frac{1}{k_{q1}} \right) \right]$$

$$E_2 = \frac{I_o G}{M} \frac{k_{1a}}{k_{q1}} \frac{k_{21}}{k_{q2}} \left[1 - \frac{i\omega}{M} \left(\frac{1}{k_{q1}} + \frac{1}{k_{q2}} \right) \right] \qquad (15)$$

$$E_3 = \frac{I_o G}{M} \frac{k_{1a}}{k_{q1}} \frac{k_{21}}{k_{q2}} \frac{k_{32}}{k_{q3}} \left[1 - \frac{i\omega}{M} \left(\frac{1}{k_{q1}} + \frac{1}{k_{q2}} + \frac{1}{k_{q3}} \right) \right]$$

and so on. For an arbitrary state E_k the population at high pressure will be given by

$$E_k = \frac{I_o G}{k_{qk} M} \left\{ \langle k_a \rangle_k - \frac{i\omega}{M} \left\langle \frac{k_a}{k_q} \right\rangle_k \right\} \qquad (16)$$

where

$$\langle k_a / k_q \rangle_k \equiv k_{ka}/k_{qk} + \sum_i k_{ia} \frac{k_{ki}}{k_{qi}} \left(\frac{1}{k_{qi}} + \frac{1}{k_{qk}} \right)$$

$$+ \sum_{ji} k_{ja} \frac{k_{ij}}{k_{qj}} \frac{k_{ki}}{k_{qi}} \left(\frac{1}{k_{qj}} + \frac{1}{k_{qi}} + \frac{1}{k_{qk}} \right)$$

$$+ \ldots .$$

For any state, at sufficiently high pressure where the assumptions made in the derivation are valid, the in-phase component of the population will have an inverse first power dependence on the total pressure and the out-of-phase component will have an inverse second power dependence. Thus, by the arguments given previously the in-phase and out-of-phase spectra will each have a high pressure limit. Further the ratio of the in-phase and out-of-phase components of the population of any quantum state will have a first order dependence on the total pressure:

$$E_k^{0°}/E_k^{-90°} = \omega^{-1} \frac{\langle k_a \rangle_k}{\langle k_a/k_q \rangle_k} M \equiv \omega^{-1} k^*_{qk} M \quad . \tag{17}$$

This expression is analogous to the limiting Stern-Volmer expression at high pressures:

$$E_1^{0°}/E_1^{-90°} = \omega^{-1} k_q M \quad .$$

However the value of the apparent quenching rate constant will differ from state to state. Nevertheless the spectrum of the ratio $E_k^{0°}/E_k^{-90°}$ will vary uniformly as M. The apparent lifetimes of different states will be in constant ratios one to another and will vary as the inverse first power of the total pressure.

The quantity k^*_{qk} is directly accessible experimentally in an ac experiment in which quantum states are spectrally resolved as the limiting slope (at high pressures) of a graph of $S_{0°}/S_{-90°}$. If the spectroscopy is not resolved, then an observed signal will be an average of contributions from numerous quantum states, as given by Eq. (10).

Similarly to the dc case, we may consider the intercept/slope ratio of the ac quantity $E_{0°}/E_{-90°}$, again taking the limiting high

pressure slope. This ratio is given by

$$P^*_{ac} = k_{fk} \frac{\langle k_a/k_q \rangle_k}{\langle k_a \rangle_k} = k_{fk}/k^*_{qk} \quad . \tag{18}$$

This quantity is not required to be equal to the corresponding quantity for dc excitation (equation 9).

Thus far we have discussed Eq. (16) only in terms of the ratio of the in-phase and out-of-phase components of the population. A comparison of Eqs. (16) and (8a) shows that the in-phase intensity of the ac excited population has the same pressure dependence (at high pressures where the approximations of the derivations are valid) as the dc population. Therefore the conclusions given previously concerning the pressure dependence of the dc population will apply to the in-phase ac population. Further, since at sufficiently high pressures the out-of-phase term in Eq. (16) will be small with respect to the in-phase term, then this equivalence will be valid as well for the total ac intensity,

$$S_{ac} = (S^2_{0°} + S^2_{-90°})^{1/2}$$

and for the Stern-Volmer intensity,

$$S_{S-V} = (S^2_{0°} + S^2_{-90°})/S_{0°}$$

A measure of this equivalence may be ascertained by the approach of the quantity $1 + (S_{-90°}/S_{0°})^2$ to the high pressure limit of unity.

Appendix D:

Migration of Excited Molecules

Because of the long lifetime of the excited NO_2 molecule the distance travelled under conditions of collision free motion by thermal molecules in their lifetime is the order of centimeters. If excited molecules are removed by wall collisions or leave the region of observation the measured values of intensity and lifetime at very low pressures will be reduced from their true values. In order to consider this effect quantitatively a model calculation was made of the magnitude of the error to be expected as a function of the size of the observed fluorescence region.

The conditions upon which the calculation was based are as follows:

1) The excitation takes place along an infinitely narrow line. Such a model is a good approximation for laser excited fluorescence. For conventional excitation where the beam of exciting radiation has a cross section of finite dimensions, the infinitely narrow model can be used as a Green's function source over the excitation region.

2) The observation geometry is cylindrical about the line of excitation. The intensity $I(\rho)$ is the intensity of all fluorescence at radius ρ; i.e., the integration over 2π for the angular distribution has been made. The integral of $I(\rho)$ from radius ρ to ∞ is also computed; this integral corresponds to the relative error in the observed fluorescence intensity resulting from observation only of the region from 0 to ρ. The analogous error quantity for the lifetime is also computed.

3) The Maxwell-Boltzmann velocity distribution is obeyed. The calculation was made in terms of the most probable velocity

$v_p = (2\ k\ T/\ m)^{1/2}$. Implicit here is the assumption that the exciting radiation does not select a non-Boltzmann sample of the ground state molecules. This assumption is good for excitation from a continuum source, but would be suspect for line source excitation. In the latter case a mis-match of the excitation and absorption lines would result in selective excitation of faster molecules on the tail of the Maxwell-Boltzmann distribution.

4) The fluorescence is exponential with a single time constant τ.

5) The mean free path of the molecules is large compared to the dimensions of observation and to the product $v_p\tau$.

Under these conditions the intensity distribution $I(\rho)$ can be obtained from the distribution $I(v,\rho)$ by integration over the radial velocity distribution in cylindrical coordinates $f(v_\rho)$. This distribution function may be obtained simply from the general Maxwell-Boltzmann distribution function by change of coordinates and integration over the coordinates ϕ and z.

$$f(v_\rho) = f(v) = \frac{2v}{v_p^2}\ e^{-v^2/v_p^2}$$

which satisfies the normalization:

$$\int_0^\infty f(v)\ dv = 1 \quad .$$

For a given radial velocity v we consider fluorescent intensity as a function of ρ, which will be equal to the decrease in particle flux per unit distance:

$$I(\rho) = -\frac{dN}{d\rho} \quad .$$

From the assumption of exponential decay,

$$dN = -\frac{N}{\tau}\, dt \quad .$$

Substituting $d\rho/v$ for dt,

$$\frac{dN}{d\rho} = -\frac{N}{v\tau} \ ,$$

yielding

$$N(\rho) = N(0)e^{-\rho/v\tau} \quad .$$

Hence

$$I(\rho,v) = \frac{1}{v\tau}\, N(0)\, e^{-\rho/v\tau} \quad .$$

This quantity must be integrated over the velocity distribution to yield the desired distribution function for the fluorescent intensity:

$$I(\rho) = \langle I(\rho,v)\rangle_v = \frac{2N(0)}{\tau\, v_p^2} \int_0^\infty e^{-(\rho/v\tau + v^2/v_p^2)}\, dv \quad .$$

In addition to this function we are also interested in the integral quantity

$$F(\rho) = \int_{\rho_1}^{\infty} I(\rho)\, d\rho \Big/ \int_0^\infty I(\rho)\, d\rho$$

that is, the fraction of the intensity that is emitted beyond a given radius ρ_1. This quantity may be obtained by integration of $I(\rho)$ before the average over $f(v)$ is taken.

$$\int_{\rho_1}^{\rho_2} I(\rho)\, d\rho = N(0)\left[e^{-\rho_1/v\tau} - e^{-\rho_2/v\tau}\right]$$

As required by normalization, for $\rho_1 = 0$ and $\rho_2 = \infty$ this integral takes

the values N(0). For the limits ρ_1 and ∞ the value is

$$N(0)\, e^{-\rho_1/v\tau}$$

so that

$$F(\rho) = \frac{2}{\tau v_p^2} \int_0^\infty v\, e^{-(\rho_1/v\tau + v^2/v_p^2)}\, dv \quad .$$

This integral is formally identical to that obtained by Landau and Teller[104] in their consideration of energy transfer probabilities for diatomic gas molecules upon collisions. Values for both I and F may be obtained with good accuracy by use of their approximation technique; i.e., expansion of the exponent about its maximum. However, since simple techniques for computer integration of such expressions are available, an exact calculation was made.

For the purpose of this calculation the dimensionless variables V and R were defined:

$$V = v/v_p$$

$$R = \rho/\tau v_p$$

whence

$$I(R) = 2\, N_0 \int_0^\infty e^{-(R/V + V^2)}\, dV$$

and

$$F(R) = 2 \int_0^\infty V\, e^{-(R/V + V^2)}\, dV \quad .$$

Finally, since we are interested only in the relative intensity distribution as a function of R, we may re-define I(R) by dividing by $I(0) = \pi^{1/2} N_0$ so that now

$$I(R) = 2/\sqrt{\pi} \int_0^\infty e^{-(R/V + V^2)}\, dV \quad .$$

These integrations were performed by the Romberg technique[105] with a required relative convergence limit of 10^{-6}. The results are given in Fig. C-1.

The preceding derivation has been developed for steady state or time independent excitation and observation. The extension, in general, to the time-dependent case would be involved; however, for the case of a flash-decay experiment this extension may readily be carried out, and the conclusions will probably be quite close to those obtained for sinusoidal excitation and observation.

For a flash at time $t = 0$, populating excited molecules as previously at $\rho = 0$, the time when an excited molecule of velocity v is located at radius ρ is given by

$$T(\rho,v) = \rho/v \quad .$$

This time T may be averaged over the observed intensity distribution to give an average observed fluorescence time lag:

$$\langle T \rangle \equiv \frac{\langle IT \rangle}{\langle I \rangle} = \frac{\int_\rho \int_v I(\rho,v)\ T(\rho,v)\ f(v)\ dv d\rho}{\int_\rho \int_v I(\rho,v)\ f(v)\ dv\ d\rho} \quad .$$

By substitution

$$\langle IT \rangle = \frac{2N(0)}{v_p^2 \tau} \int_{\rho_1}^{\rho_2} \int_0^\infty \frac{\rho}{v}\ e^{-(\rho/v\tau + v^2/v_p^2)}\ dv\ d\rho \quad .$$

By carrying out the integration over ρ

$$\langle IT \rangle_{\rho_1}^{\rho_2} = \frac{2N(0)}{v_p^2} \int_0^\infty (v\rho_1 + v^2)\ e^{-(\rho_1/vt + v^2/v_\rho^2)}\ dv$$

$$- \text{the same integral for } \rho_2 \quad .$$

Figure C1.

Radial distribution of fluorescence intensity and lifetime in cylindrical geometry. R is a dimensionless radius equal to the radius of observation (measured from an infinitely narrow excitation line source) divided by the product of the lifetime times the most probable velocity. Curve I gives the distribution of fluorescence intensity. The integration over 2π azimuthal distribution of molecular velocities has been included in the evaluation of I. Curve F gives the error in measured quantum yield if measurements are made only of fluorescence originating in the cylindrical volume extending to R. Curve E gives the analogous error in the measured lifetime.

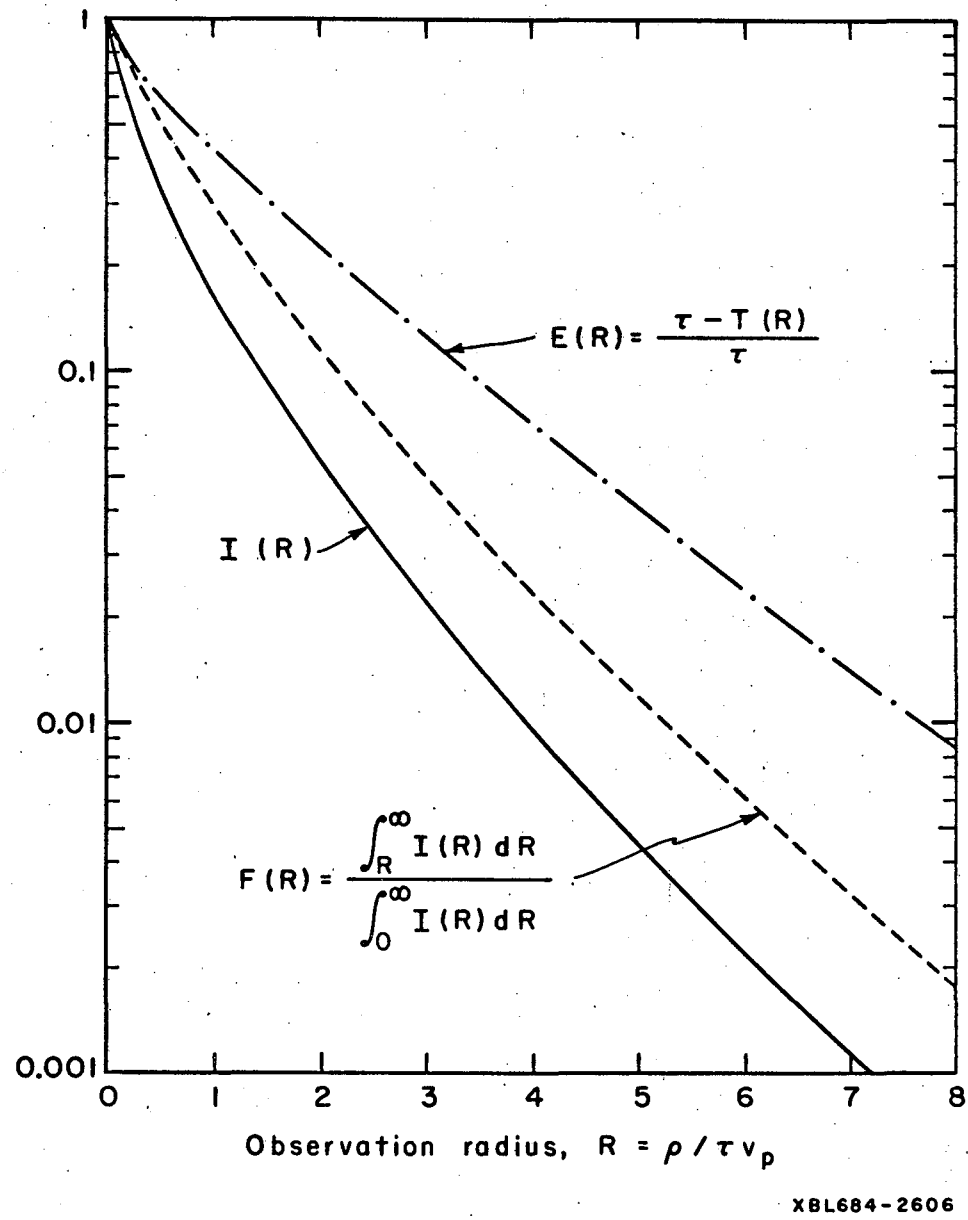
1
0.1
0.01
0.001
0
1
2
3
4
5
6
7
8
E(R) = (τ − T(R)) / τ
I(R)
F(R) = ∫_R^∞ I(R) dR / ∫_0^∞ I(R) dR
Observation radius, R = ρ / τ v_p
XBL684-2606

Figure C1

At this point we let $\rho_2 = \infty$, so that the second integral vanishes. By substitution of the dimensionless variables V and R

$$\langle IT \rangle_R^\infty = N(0)\tau \{2R \int_0^\infty e^{-(R/V + V^2)}\, dV + 2 \int_0^\infty Ve^{-(R/V + V^2)}\, dV\}$$

$$= N(0)\tau \{\sqrt{\pi}\, R\, I(R) + F(R)\}$$

where I and F are the integrals which have previously been evaluated. By way of a check we observe that $\langle IT \rangle_0^\infty = N(0)\tau$ as required. From manipulation of the limits of integration

$$\langle IT \rangle_0^R \equiv \langle IT \rangle_0^\infty - \langle IT \rangle_R^\infty$$

$$= N(0)t \{1 - \sqrt{\pi}\, RI(R) - F(R)\} .$$

Similarly,

$$\langle I \rangle_0^R = N(0)\, (1-F(R)) .$$

Hence,

$$\langle T \rangle_0^R = \tau \left\{ 1 - \frac{\sqrt{\pi}\, R\, I\,(R)}{1 - F(R)} \right\}$$

or

$$E(R) \equiv \frac{\tau - \langle T \rangle_0^R}{\tau} = \frac{\sqrt{\pi}\, RI(R)}{1 - F(R)} .$$

This quantity was computed from the values of I and F obtained previously and is also given in Fig. C-1 . The lifetime error is greater than the intensity error as expected because the fluorescence at large R is weighted to the long lived molecules.

The curves E and F may be used directly to estimate the expected

error in measured lifetime or quantum yield due to the finiteness of the region of observation. Thus for R = 5 the intensity measured will be decreased by 1.2% from the true intensity and the measured lifetime will be 4% too short. At R = 1 the values are 30% and 43%, respectively.

In conclusion it is felt that the results of this calculation demonstrate the necessity of detecting the fluorescence at distances of several $v_p \tau$ beyond the excitation region for precise measurements of fluorescence lifetimes and quantum yields.

Appendix D. Data Analysis

The purpose of this appendix is to present a discussion of the methods of handling the data from the measurements of fluorescence lifetimes and intensities as a function of pressure, and to present the original data and the results of the analysis. It was desired to present the original data in their entirety to allow for possible re-analysis.

The techniques of handling the data (least squares fitting and significance tests) were for the most part conventional and consequently are only summarized here. The least squares subroutines were standard programs available from the Lawrence Radiation Laboratory Berkeley Computer Center program library. The computations were performed on the Control Data Corporation 6600 computer.

Each set of data (data points at all pressures for a given excitation wavelength and observation filter) was fitted to four functions. The functions chosen were as follows:

1) A linear fit with two parameters: $F_1(P) = A + BP$.

2) A second degree polynomial fit, allowing for curvature in the data; three parameters: $F_2(P) = A + BP + CP^2$. The parameters were not constrained to be equal to those in the linear case.

3) A three parameter function allowing for curvature but having a first order dependence on P at high pressures: $F_3(P) = A/(1+C^2P) + BP$.

4) A four parameter function allowing for curvature and having a first order dependence on P at high pressures: $F_4(P) = (A^2 + B^2P + C^2P^2)/(1 + D^2P)$. The indicated parameters in functions 3 and 4 were squared to restrict the coefficients to positive values.

The functions 1 and 2 were capable of exact solution in the usual way. This was done by means of the subroutine package LSQPOL (Least Squares Polynomial Fit).[106] The functions 3 and 4 were fit by an approximate iterative technique. The program used was a modification of the LSQVMT program, which uses the VARMIT method of variable metric minimization.[107] In all cases the weighted error sum $S = \sum_i w_i[Y_i(P_i) - F(P_i)]^2$ was minimized with respect to the parameters. The statistical weights w_i were inversely proportional to the estimated variance, which was obtained from the propagated variance in $S_{0°}$ and $S_{-90°}$ added to the estimated variance from other sources. In the case of measurements of R this additional variance was computed from an estimated fractional error due to uncertainty in setting the phase of $0.01\times(R + 1/R)$. For intensity measurements the additional uncertainty was taken as 5%.

In addition to finding the parameters the program was also designed to compute the variance-covariance matrix $\underset{\sim}{V}$ which, in turn, allowed for the evaluation of the standard deviations in the parameters (and in any function of the parameters). For the polynomial expressions this matrix is obtained directly from the LSQPOL subroutine. For arbitrary functions such as F_3 and F_4 this matrix must be evaluated approximately. The function is expanded in a Taylor's series in the parameters about the function evaluated at their best value, and only the linear terms are retained. The $\underset{\sim}{V}$ matrix is then evaluated in the usual way.

The methods for obtaining the variance-covariance matrix $\underset{\sim}{V}$ have been discussed by Guest[108] and Wolberg,[109] and will be summarized here. In the case of the fit to a polynomial in the independent variable T we define the matrix $\underset{\sim}{\phi}$,

$$\phi_{jk} = \sum_{i=1}^{N} w_i T^{j+k} \qquad \begin{matrix} j = 0 \ldots\ldots p \\ k = 0 \ldots\ldots p \end{matrix}$$

where p is the degree of the polynomial, and N is the number of data points. The $\underset{\sim}{V}$ matrix is then given by

$$\underset{\sim}{V} = s^2 \underset{\sim}{\phi}^{-1}$$

where s^2 is the estimated variance, $s^2 = S/(N-p-1)$. In the case of an arbitrary fitting function $\underset{\sim}{\phi}$ is given by

$$\phi_{jk} = \sum_{i=1}^{N} w_i G_{j,i} G_{k,i} \qquad \begin{matrix} j = 1 \ldots\ldots N_p \\ k = 1 \ldots\ldots N_p \end{matrix}$$

where

$$G_{ji} = \left(\frac{\partial F(X_1, X_2, \ldots, X_j, \ldots, X_{N_p}; T_i)}{\partial X_j} \right)_{\underset{\sim}{X} = \underset{\sim}{X}^*} .$$

Here N_p is the number of fitting parameters, $\underset{\sim}{X}$ is the vector of the parameters, and $\underset{\sim}{X}^*$ is the vector of the values of the parameters for the least squares fit. $\underset{\sim}{V}$ is computed as above, with $s^2 = S/(N-N_p)$.

The usual F, or variance ratio, test was employed to determine whether the fit to the data was significantly improved by an increase in the number of parameters N_p. For any increase in N_p the error sum S will be somewhat decreased; the question that this test seeks to answer is whether this decrease is statistically significant. The use of this test is discussed by Guest.[108] For two different fitting functions having respectively N_{p1} and N_{p2} parameters ($N_{p2} > N_{p1}$) then

$$F(N_{p2} - N_{p1};\ N-N_{p2}) = \left(\frac{S_1}{S_2} - 1\right) \times \frac{N-N_{p2}}{N_{p2}-N_{p1}} \quad .$$

To test the significance of the improvement, tables of F (for example Table V of Fisher and Yates,[110]) are employed.

The choice of which of several fitted functions in the "best" fit to a set of data is inevitably a subjective one; the subjectivity may be in the determination of a required confidence level in application of the F test, or may enter into each individual decision. In the present work the latter course was chosen, although considerable reliance was placed upon the results of the F test. The criteria upon which the selections were based were:

1) Confidence level for improvement of F_2 and F_3 over $F_1 \gtrsim 0.90$ required to reject F_1.

2) Confidence level of F_4 over $F_3 \gtrsim 0.90$ required to select F_4 in preference to F_3.

3) Conventional and inverse Stern-Volmer plots were required to exhibit no irregularity in extrapolation to the zero intercept. Fits to Function F_2 were thereby excluded since the limit F_2/P is infinite at infinite pressure ($1/P = 0$). In no case was there any indication of such behavior in the data.

The data are presented in Table D-I. The entries in this table are as follows:

Pressure: The total NO_2 pressure in millitorr.

$S_{0°}$ and $S_{-90°}$: The measured in-phase and out-of-phase intensities, normalized as discussed in Chapter II, Sec. B-3.

I^{-1} and R^{-1}: The two Stern-Volmer quantities, inverse intensity and inverse intensity ratio, as defined in Chapter I, Sec. C. The intensities are given in arbitrary units proportional to quanta per cm^{-1} sec; thus intensities obtained with different filters (for the same excitation wavelength) may be directly compared. For convenience I^{-1} has been given as $10^8/I$.

Lifetime: The lifetime calculated directly from the measurement under the assumption of a single excited state; Eq. (I-B-5).

$E_{0°}$, $E_{-90°}$, E_I, and E_R: The fractional sample standard deviations associated with the measurements of the indicated quantities as determined from the variance of the raw, unaveraged readings from the counter (not presented). E_R is also the fractional error associated with the lifetime.

From the fitted functions for the quantities R^{-1} and I^{-1} the following data were included in the table, as well as the associated errors (fractional standard deviations) where applicable:

Function Type: F_1, F_3, or F_4.

Coefficients: The parameters (or parameters squared, as appropriate to the fitting function) in order A (or A^2), B (or B^2), C^2, D^2. The coefficients are given for R^{-1} and I^{-1} expressed as a function of the pressure in millitorr. The exponential format is used. Thus, for example, "E-01" signifies "$\times 10^{-1}$".

Intercept: The zero pressure intercept of F; for the lifetime data the zero pressure lifetime $\tau(0) = \omega^{-1}/R^{-1}(0)$ was also computed.

Slope: The infinite pressure limit of the slope of F, in units $mtorr^{-1}$; for the lifetime data this was expressed also as a rate

constant in units cm^3/molecule sec, by use of the conversion factor ω/M_o. Here M_o is the particle density at 1 mtorr and 296.4°K computed under the assumption of the ideal gas law, 3.257×10^{13} molecules/cm^3.

Quenching ratio: The ratio of the two previous quantities in units of $mtorr^{-1}$. The quenching pressure is the inverse of this quantity in units of mtorr.

Variance ratio: The variance ratio of the "best" fit referred to the linear fit, where applicable; the degrees of freedom are given in the conventional notation.[110]

Table D-I

Data of pressure dependent studies of NO_2 fluorescence kinetics. Explanations of column headings are given in the text.

EXCITATION WAVELENGTH 4000 A OBSERVATION FILTER NO. 1 (23200 CM-1) 13 DATA POINTS

PRESSURE M TORR	S(0)	S(-90)	E(0)	E(-90)	1/R	1/I	LIFETIME MICROSEC	E(R)	E(I)
1.05	10844	11585	.020	.012	.936	4307	47.23	.023	.013
1.54	11828	10168	.011	.021	1.163	4862	38.01	.024	.018
1.59	11238	9262	.011	.019	1.213	5299	36.44	.022	.016
3.27	10319	5848	.007	.006	1.765	7335	25.05	.009	.005
4.78	8135	3888	.004	.006	2.092	10007	21.13	.007	.003
10.20	4961	1442	.009	.023	3.440	18587	12.85	.025	.008
10.20	5082	1422	.005	.017	3.574	18249	12.37	.018	.005
15.06	4176	872	.009	.018	4.789	22946	9.23	.020	.008
15.06	4009	874	.010	.021	4.587	23812	9.64	.023	.009
30.30	2121	233	.006	.034	9.103	46585	4.86	.035	.006
30.30	2442	289	.004	.058	8.450	40384	5.23	.058	.004
48.10	1378	124	.004	.055	11.113	71986	3.98	.055	.004
48.10	1432	93	.002	.081	15.398	69539	2.87	.081	.002

LEAST SQUARES FIT FOR 1/R DATA FUNCTION TYPE F(1)

COEFFICIENTS FOR FITTING FUNCTION 7.311E-01 2.765E-01
FRACTIONAL ERRORS IN COEFFICIENTS 4.955E-02 4.086E-02

INTERCEPT .731 FRACTIONAL ERROR .050 ZERO P. LIFETIME 60.47 MICRO SEC
H.P. SLOPE .276 MTORR-1 FRACTIONAL ERROR .041 H.P. Q CONSTANT 19.20 E-11 CC/MOLEC SEC
Q RATIO .378 MTORR-1 FRACTIONAL ERROR .084 QUENCH PRESSURE 2.64 MTORR

LEAST SQUARES FIT FOR 1/I DATA FUNCTION TYPE F(1)

COEFFICIENTS FOR FITTING FUNCTION 2.913E+03 1.394E+03
FRACTIONAL ERRORS IN COEFFICIENTS 5.518E-02 2.317E-02

INTERCEPT 2913 FRACTIONAL ERROR .055
H.P. SLOPE 1394 MTORR-1 FRACTIONAL ERROR .023
Q RATIO .478 MTORR-1 FRACTIONAL ERROR .071 QUENCH PRESSURE 2.09 MTORR

XBL 688-5750

EXCITATION WAVELENGTH 4000 A OBSERVATION FILTER NO. 2 (22170 CM-1) 14 DATA POINTS

PRESSURE M TORR	S(0)	S(-90)	E(0)	E(-90)	1/R	1/I	LIFETIME MICROSEC	E(R)	E(I)
1.01	10263	11260	.020	.009	.911	4421	48.50	.022	.010
1.09	10150	11892	.022	.012	.854	4152	51.80	.025	.014
1.52	9534	9838	.017	.012	.969	5080	45.62	.021	.012
1.54	9165	9686	.028	.009	.946	5154	46.72	.029	.010
3.16	9107	7117	.006	.012	1.280	6817	34.55	.013	.009
4.77	8955	5562	.005	.009	1.610	8058	27.46	.010	.005
4.77	8377	5107	.008	.004	1.640	8703	26.95	.009	.004
4.78	9023	5546	.007	.007	1.627	8044	27.17	.010	.005
9.60	6965	2867	.002	.004	2.429	12277	18.20	.004	.002
10.20	6140	2380	.005	.009	2.580	14159	17.14	.010	.004
16.20	4971	1397	.002	.007	3.558	18644	12.42	.007	.002
30.30	3086	485	.005	.018	6.363	31623	6.95	.019	.005
45.60	2065	238	.007	.026	8.676	47791	5.10	.027	.007
48.10	1811	184	.003	.030	9.842	54654	4.49	.030	.003

LEAST SQUARES FIT FOR 1/R DATA FUNCTION TYPE F(1)

COEFFICIENTS FOR FITTING FUNCTION 6.927E-01 1.867E-01
FRACTIONAL ERRORS IN COEFFICIENTS 2.231E-02 2.166E-02

INTERCEPT .693 FRACTIONAL ERROR .022 ZERO P. LIFETIME 63.83 MICRO SEC
H.P. SLOPE .187 MTORR-1 FRACTIONAL ERROR .022 H.P. Q CONSTANT 12.96 E-11 CC/MOLEC SEC
Q RATIO .269 MTORR-1 FRACTIONAL ERROR .041 QUENCH PRESSURE 3.71 MTORR

LEAST SQUARES FIT FOR 1/I DATA FUNCTION TYPE F(1)

COEFFICIENTS FOR FITTING FUNCTION 3.436E+03 9.850E+02
FRACTIONAL ERRORS IN COEFFICIENTS 3.494E-02 2.532E-02

INTERCEPT 3436 FRACTIONAL ERROR .035
H.P. SLOPE 985 MTORR-1 FRACTIONAL ERROR .025
Q RATIO .287 MTORR-1 FRACTIONAL ERROR .054 QUENCH PRESSURE 3.49 MTORR

XBL 688-5751

EXCITATION WAVELENGTH 4000 A OBSERVATION FILTER NO. 3 (21460 CM-1) 12 DATA POINTS

PRESSURE M TORR	S(0)	S(-90)	E(0)	E(-90)	1/R	1/I	LIFETIME MICROSEC	E(R)	E(I)
1.05	15909	17288	.011	.014	.920	2882	48.04	.018	.015
1.09	18818	20024	.017	.003	.940	2492	47.04	.017	.003
1.54	18601	18812	.011	.005	.989	2658	44.71	.012	.005
1.59	17195	17358	.007	.005	.991	2880	44.63	.009	.005
3.27	16517	12365	.003	.006	1.336	3880	33.10	.007	.004
4.78	15476	9718	.002	.006	1.592	4635	27.77	.006	.004
4.78	15041	9769	.004	.004	1.540	4676	28.71	.006	.003
10.20	11913	4914	.001	.004	2.424	7174	18.24	.004	.001
15.06	9126	2788	.003	.009	3.271	10028	13.51	.009	.003
30.30	5699	965	.003	.013	5.906	17058	7.49	.013	.003
48.10	3212	385	.004	.018	8.343	30692	5.30	.018	.004
48.10	3222	377	.003	.021	8.546	30617	5.17	.021	.003

LEAST SQUARES FIT FOR 1/R DATA FUNCTION TYPE F(1)

COEFFICIENTS FOR FITTING FUNCTION 7.445E-01 1.686E-01
FRACTIONAL ERRORS IN COEFFICIENTS 1.467E-02 1.950E-02

INTERCEPT .744 FRACTIONAL ERROR .015 ZERO P. LIFETIME 59.39 MICRO SEC
H.P. SLOPE .169 MTORR-1 FRACTIONAL ERROR .020 H.P. Q CONSTANT 11.71 E-11 CC/MOLEC SEC
Q RATIO .226 MTORR-1 FRACTIONAL ERROR .032 QUENCH PRESSURE 4.42 MTORR

LEAST SQUARES FIT FOR 1/I DATA FUNCTION TYPE F(1)

COEFFICIENTS FOR FITTING FUNCTION 1.988E+03 5.476E+02
FRACTIONAL ERRORS IN COEFFICIENTS 4.557E-02 3.510E-02

INTERCEPT 1988 FRACTIONAL ERROR .046
H.P. SLOPE 548 MTORR-1 FRACTIONAL ERROR .035
Q RATIO .275 MTORR-1 FRACTIONAL ERROR .071 QUENCH PRESSURE 3.63 MTORR

XBL 688-5752

EXCITATION WAVELENGTH 4000 A OBSERVATION FILTER NO. 4 (20790 CM-1) 12 DATA POINTS

PRESSURE M TORR	S(0)	S(-90)	E(0)	E(-90)	1/R	1/I	LIFETIME MICROSEC	E(R)	E(I)
1.01	18087	21240	.008	.004	.852	2324	51.92	.009	.005
1.09	17139	20016	.007	.005	.856	2468	51.63	.009	.006
1.52	17015	18168	.005	.001	.937	2746	47.21	.005	.001
1.59	16371	17223	.004	.008	.951	2899	46.51	.009	.008
3.16	14866	12774	.003	.004	1.164	3870	37.99	.005	.003
4.77	14032	10606	.003	.002	1.323	4535	33.42	.004	.002
4.78	15885	11437	.005	.005	1.389	4146	31.83	.007	.004
9.60	12539	6120	.001	.004	2.049	6441	21.58	.004	.002
16.20	9225	3259	.003	.006	2.831	9637	15.62	.007	.003
30.30	6750	1370	.005	.007	4.927	14229	8.97	.009	.005
45.60	4252	591	.002	.016	7.195	23073	6.14	.016	.002
48.10	3940	544	.003	.016	7.243	24906	6.10	.016	.003

LEAST SQUARES FIT FOR 1/R DATA FUNCTION TYPE F(1)

COEFFICIENTS FOR FITTING FUNCTION 7.214E-01 1.353E-01
FRACTIONAL ERRORS IN COEFFICIENTS 1.225E-02 1.890E-02

INTERCEPT .721 FRACTIONAL ERROR .012 ZERO P. LIFETIME 61.29 MICRO SEC
H.P. SLOPE .135 MTORR-1 FRACTIONAL ERROR .019 H.P. Q CONSTANT 9.39 E-11 CC/MOLEC SEC
Q RATIO .188 MTORR-1 FRACTIONAL ERROR .029 QUENCH PRESSURE 5.33 MTORR

LEAST SQUARES FIT FOR 1/I DATA FUNCTION TYPE F(1)

COEFFICIENTS FOR FITTING FUNCTION 2.051E+03 4.553E+02
FRACTIONAL ERRORS IN COEFFICIENTS 3.969E-02 3.493E-02

INTERCEPT 2051 FRACTIONAL ERROR .040
H.P. SLOPE 455 MTORR-1 FRACTIONAL ERROR .035
Q RATIO .222 MTORR-1 FRACTIONAL ERROR .065 QUENCH PRESSURE 4.50 MTORR

XBL 688-5753

EXCITATION WAVELENGTH 4000 A OBSERVATION FILTER NO. 5 (20370 CM-1) 10 DATA POINTS

PRESSURE M TORR	S(0)	S(-90)	E(0)	E(-90)	1/R	1/I	LIFETIME MICROSEC	E(R)	E(I)
1.05	17629	20779	.009	.018	.848	2374	52.11	.020	.021
1.54	18408	19134	.008	.004	.962	2611	45.95	.009	.004
1.59	18334	19297	.009	.004	.950	2588	46.53	.010	.004
3.27	17974	15234	.004	.003	1.180	3238	37.47	.005	.003
4.78	16130	11801	.003	.005	1.367	4038	32.34	.006	.004
10.20	12222	6148	.001	.006	1.988	6530	22.24	.006	.002
15.06	11055	4267	.001	.016	2.591	7873	17.06	.016	.004
30.30	6713	1465	.001	.022	4.582	14219	9.65	.022	.002
48.10	4199	605	.002	.016	6.940	23331	6.37	.016	.002
48.10	4242	647	.002	.005	6.556	23038	6.74	.005	.002

LEAST SQUARES FIT FOR 1/R DATA FUNCTION TYPE F(1)

COEFFICIENTS FOR FITTING FUNCTION 7.549E-01 1.243E-01
FRACTIONAL ERRORS IN COEFFICIENTS 1.432E-02 2.105E-02

INTERCEPT .755 FRACTIONAL ERROR .014 ZERO P. LIFETIME 58.56 MICRO SEC
H.P. SLOPE .124 MTORR-1 FRACTIONAL ERROR .021 H.P. Q CONSTANT 8.63 E-11 CC/MOLEC SEC
Q RATIO .165 MTORR-1 FRACTIONAL ERROR .032 QUENCH PRESSURE 6.07 MTORR

LEAST SQUARES FIT FOR 1/I DATA FUNCTION TYPE F(1)

COEFFICIENTS FOR FITTING FUNCTION 1.921E+03 4.261E+02
FRACTIONAL ERRORS IN COEFFICIENTS 2.743E-02 2.100E-02

INTERCEPT 1921 FRACTIONAL ERROR .027
H.P. SLOPE 426 MTORR-1 FRACTIONAL ERROR .021
Q RATIO .222 MTORR-1 FRACTIONAL ERROR .042 QUENCH PRESSURE 4.51 MTORR

XBL 688-5754

EXCITATION WAVELENGTH 4000 A OBSERVATION FILTER NO. 6 (19960 CM-1) 14 DATA POINTS

PRESSURE M TORR	S(0)	S(-90)	E(0)	E(-90)	1/R	1/I	LIFETIME MICROSEC	E(R)	E(I)
1.05	16706	20389	.012	.004	.819	2404	53.96	.013	.005
1.52	16622	18451	.014	.007	.901	2695	49.07	.016	.008
1.59	16835	18574	.013	.005	.906	2679	48.78	.014	.006
3.16	16083	15157	.007	.007	1.061	3293	41.66	.010	.007
4.77	16677	13114	.006	.005	1.272	3705	34.76	.008	.004
4.78	17823	13823	.004	.004	1.289	3503	34.29	.006	.003
9.60	14252	8090	.005	.004	1.762	5307	25.10	.006	.003
10.20	13409	6983	.001	.004	1.920	5867	23.02	.004	.002
16.20	11626	4414	.003	.009	2.634	7518	16.78	.009	.003
30.30	7517	1720	.004	.009	4.370	12641	10.12	.010	.004
30.30	8000	1801	.001	.009	4.442	11897	9.95	.009	.001
30.30	8024	1892	.003	.009	4.241	11806	10.42	.009	.003
45.60	5328	871	.001	.016	6.117	18280	7.23	.016	.001
48.10	4908	725	.004	.014	6.770	19940	6.53	.015	.004

LEAST SQUARES FIT FOR 1/R DATA FUNCTION TYPE F(1)

COEFFICIENTS FOR FITTING FUNCTION 7.054E-01 1.181E-01
FRACTIONAL ERRORS IN COEFFICIENTS 1.33PE-02 1.568E-02

INTERCEPT .705 FRACTIONAL ERROR .013 ZERO P. LIFETIME 62.67 MICRO SEC
H.P. SLOPE .118 MTORR-1 FRACTIONAL ERROR .016 H.P. Q CONSTANT 8.20 E-11 CC/MOLEC SEC
Q RATIO .167 MTORR-1 FRACTIONAL ERROR .027 QUENCH PRESSURE 5.97 MTORR

LEAST SQUARES FIT FOR 1/I DATA FUNCTION TYPE F(1)

COEFFICIENTS FOR FITTING FUNCTION 2.094E+03 3.421E+02
FRACTIONAL ERRORS IN COEFFICIENTS 2.708E-02 2.157E-02

INTERCEPT 2094 FRACTIONAL ERROR .027
H.P. SLOPE 342 MTORR-1 FRACTIONAL ERROR .022
Q RATIO .163 MTORR-1 FRACTIONAL ERROR .043 QUENCH PRESSURE 6.12 MTORR

XBL 688-5755

EXCITATION WAVELENGTH 4000 A OBSERVATION FILTER NO. 7 (19350 CM-1) 12 DATA POINTS

PRESSURE M TORR	S(0)	S(-90)	E(0)	E(-90)	1/R	1/I	LIFETIME MICROSEC	E(R)	E(I)
1.01	20571	25483	.009	.003	.807	1918	54.77	.009	.004
1.09	20468	24989	.006	.009	.819	1962	53.97	.011	.011
1.52	20051	22046	.009	.004	.910	2258	48.61	.010	.004
1.59	20663	21744	.007	.006	.950	2296	46.52	.009	.006
3.16	18340	17213	.004	.007	1.065	2899	41.49	.008	.007
4.77	18363	15216	.003	.005	1.207	3229	36.63	.006	.004
4.78	19826	16223	.003	.006	1.222	3021	36.19	.007	.005
9.60	16014	9692	.002	.002	1.652	4570	26.76	.003	.001
16.20	12533	5385	.002	.004	2.327	6735	19.00	.004	.002
30.30	9466	2385	.002	.002	3.969	9934	11.14	.003	.002
45.60	6333	1117	.001	.005	5.670	15314	7.80	.005	.001
48.10	5871	975	.002	.007	6.022	16576	7.34	.007	.002

LEAST SQUARES FIT FOR 1/R DATA FUNCTION TYPE F(3)

COEFFICIENTS FOR FITTING FUNCTION 7.449E-01 1.145E-01 2.659E-02
FRACTIONAL ERRORS IN COEFFICIENTS 2.757E-02 6.970E-02 8.070E-01

INTERCEPT .745 FRACTIONAL ERROR .028 ZERO P. LIFETIME 59.35 MICRO SEC
H.P. SLOPE .115 MTORR-1 FRACTIONAL ERROR .070 H.P. Q CONSTANT 7.95 E-11 CC/MOLEC SEC
Q RATIO .154 MTORR-1 FRACTIONAL ERROR .061 QUENCH PRESSURE 6.51 MTORR

VARIANCE RATIO COMPARED TO LINEAR FIT, 1.1 FOR (1, 9) DEGREES FREEDOM

LEAST SQUARES FIT FOR 1/I DATA FUNCTION TYPE F(1)

COEFFICIENTS FOR FITTING FUNCTION 1.730E+03 2.965E+02
FRACTIONAL ERRORS IN COEFFICIENTS 2.984E-02 3.000E-02

INTERCEPT 1730 FRACTIONAL ERROR .030
H.P. SLOPE 296 MTORR-1 FRACTIONAL ERROR .030
Q RATIO .171 MTORR-1 FRACTIONAL ERROR .052 QUENCH PRESSURE 5.84 MTORR

XBL 688-5756

EXCITATION WAVELENGTH 4000 A OBSERVATION FILTER NO. 9 (17880 CM-1) 13 DATA POINTS

PRESSURE M TORR	S(0)	S(-90)	E(0)	E(-90)	1/R	1/I	LIFETIME MICROSEC	E(R)	E(I)
1.01	20687	24725	.012	.006	.837	1991	52.84	.013	.007
1.09	20886	27118	.010	.011	.770	1783	57.40	.015	.014
1.52	19289	22895	.014	.006	.842	2152	52.47	.015	.007
1.59	19068	23289	.004	.007	.819	2105	54.00	.008	.008
3.16	17686	18467	.008	.008	.958	2705	46.16	.011	.008
4.77	19336	18828	.002	.004	1.027	2655	43.05	.004	.004
4.77	17975	17164	.008	.002	1.047	2910	42.22	.008	.002
4.78	19568	18155	.012	.001	1.078	2746	41.02	.012	.001
9.60	17345	12972	.004	.006	1.337	3697	33.06	.007	.004
16.20	15132	7946	.004	.007	1.904	5180	23.22	.008	.004
30.30	11914	3619	.002	.009	3.292	7684	13.43	.009	.002
45.60	8257	1866	.001	.002	4.425	11522	9.99	.002	.001
48.10	7707	1661	.002	.009	4.640	12399	9.53	.009	.002

LEAST SQUARES FIT FOR 1/R DATA FUNCTION TYPE F(3)

COEFFICIENTS FOR FITTING FUNCTION 7.490E-01 9.349E-02 5.529E-02
FRACTIONAL ERRORS IN COEFFICIENTS 2.885E-02 4.093E-02 3.067E-01

INTERCEPT .749 FRACTIONAL ERROR .029 ZERO P. LIFETIME 59.03 MICRO SEC
H.P. SLOPE .093 MTORR-1 FRACTIONAL ERROR .041 H.P. Q CONSTANT 6.49 E-11 CC/MOLEC SEC
Q RATIO .125 MTORR-1 FRACTIONAL ERROR .038 QUENCH PRESSURE 8.01 MTORR

VARIANCE RATIO COMPARED TO LINEAR FIT, 9.9 FOR (1,10) DEGREES FREEDOM

LEAST SQUARES FIT FOR 1/I DATA FUNCTION TYPE F(1)

COEFFICIENTS FOR FITTING FUNCTION 1.750E+03 2.115E+02
FRACTIONAL ERRORS IN COEFFICIENTS 2.964E-02 3.634E-02

INTERCEPT 1750 FRACTIONAL ERROR .030
H.P. SLOPE 211 MTORR-1 FRACTIONAL ERROR .036
Q RATIO .121 MTORR-1 FRACTIONAL ERROR .058 QUENCH PRESSURE 8.27 MTORR

XBL 688-5757

EXCITATION WAVELENGTH 4000 A OBSERVATION FILTER NO. 10 (16960 CM-1) 12 DATA POINTS

PRESSURE M TORR	S(0)	S(-90)	E(0)	E(-90)	1/R	1/I	LIFETIME MICROSEC	E(R)	E(I)
1.01	23446	31763	.012	.009	.738	1504	59.90	.015	.012
1.52	23792	29520	.009	.007	.806	1655	54.85	.011	.009
1.54	23915	30060	.010	.008	.796	1621	55.57	.013	.010
3.27	23468	25451	.004	.003	.908	1925	48.70	.005	.003
4.77	19821	20638	.005	.004	.960	2421	46.03	.006	.004
4.78	21399	22004	.008	.005	.973	2271	45.46	.009	.005
9.60	19962	16273	.001	.004	1.227	3010	36.04	.004	.003
16.20	17288	10353	.001	.005	1.670	4258	26.48	.005	.003
30.30	13778	4993	.003	.004	2.759	6415	16.02	.005	.002
30.30	14839	5351	.001	.005	2.773	5964	15.94	.005	.001
45.60	10030	2502	0.	.002	4.009	9386	11.03	.002	.000
48.10	9380	2301	.003	.009	4.076	10056	10.85	.009	.003

LEAST SQUARES FIT FOR 1/R DATA FUNCTION TYPE F(3)

COEFFICIENTS FOR FITTING FUNCTION 7.260E-01 8.118E-02 5.520E-02
FRACTIONAL ERRORS IN COEFFICIENTS 2.309E-02 2.518E-02 2.116E-01

INTERCEPT .726 FRACTIONAL ERROR .023 ZERO P. LIFETIME 60.90 MICRO SEC
H.P. SLOPE .081 MTORR-1 FRACTIONAL ERROR .025 H.P. Q CONSTANT 5.64 E-11 CC/MOLEC SEC
Q RATIO .112 MTORR-1 FRACTIONAL ERROR .024 QUENCH PRESSURE 8.94 MTORR

VARIANCE RATIO COMPARED TO LINEAR FIT. 22.9 FOR (1. 9) DEGREES FREEDOM

LEAST SQUARES FIT FOR 1/I DATA FUNCTION TYPE F(1)

COEFFICIENTS FOR FITTING FUNCTION 1.391E+03 1.703E+02
FRACTIONAL ERRORS IN COEFFICIENTS 2.960E-02 2.980E-02

INTERCEPT 1391 FRACTIONAL ERROR .030
H.P. SLOPE 170 MTORR-1 FRACTIONAL ERROR .030
Q RATIO .122 MTORR-1 FRACTIONAL ERROR .052 QUENCH PRESSURE 8.17 MTORR

XBL 688-5758

EXCITATION WAVELENGTH 4000 A OBSERVATION FILTER NO. 11 (15850 CM-1) 12 DATA POINTS

PRESSURE M TORR	S(0)	S(-90)	E(0)	E(-90)	1/R	1/I	LIFETIME MICROSEC	E(R)	E(I)
1.05	16366	22611	.019	.008	.724	2101	61.08	.021	.012
1.52	16790	21973	.011	.007	.764	2196	57.86	.013	.009
1.59	16570	21625	.017	.010	.766	2233	57.70	.020	.013
3.16	15493	19049	.008	.006	.813	2570	54.36	.010	.007
4.77	16399	19286	.004	.004	.850	2559	51.99	.006	.005
4.78	18526	21498	.008	.004	.862	2300	51.30	.009	.005
9.60	17744	17457	.002	.004	1.016	2864	43.49	.004	.004
16.20	16258	11448	.002	.006	1.420	4112	31.13	.006	.004
30.30	14696	5980	.002	.008	2.457	5840	18.00	.008	.003
30.30	13983	5626	.003	.005	2.485	6155	17.79	.006	.003
45.60	10107	3037	.002	.005	3.328	9075	13.28	.005	.002
48.10	9674	2600	.005	.012	3.721	9641	11.88	.013	.005

LEAST SQUARES FIT FOR 1/R DATA FUNCTION TYPE F(3)

COEFFICIENTS FOR FITTING FUNCTION 7.622E-01 7.280E-02 1.138E-01
FRACTIONAL ERRORS IN COEFFICIENTS 4.139E-02 2.629E-02 1.925E-01

INTERCEPT .762 FRACTIONAL ERROR .041 ZERO P. LIFETIME 58.00 MICRO SEC
H.P. SLOPE .073 MTORR-1 FRACTIONAL ERROR .026 H.P. Q CONSTANT 5.06 E-11 CC/MOLEC SEC
Q RATIO .096 MTORR-1 FRACTIONAL ERROR .038 QUENCH PRESSURE 10.47 MTORR

VARIANCE RATIO COMPARED TO LINEAR FIT, 47.0 FOR (1, 9) DEGREES FREEDOM

LEAST SQUARES FIT FOR 1/I DATA FUNCTION TYPE F(3)

COEFFICIENTS FOR FITTING FUNCTION 2.159E+03 1.839E+02 7.857E-02
FRACTIONAL ERRORS IN COEFFICIENTS 5.779E-02 3.973E-02 3.509E-01

INTERCEPT 2159 FRACTIONAL ERROR .058
H.P. SLOPE 184 MTORR-1 FRACTIONAL ERROR .040
Q RATIO .085 MTORR-1 FRACTIONAL ERROR .053 QUENCH PRESSURE 11.75 MTORR

VARIANCE RATIO COMPARED TO LINEAR FIT, 11.8 FOR (1, 9) DEGREES FREEDOM

XBL 688-5759

EXCITATION WAVELENGTH 4000 A OBSERVATION FILTER NO. 12 (15130 CM-1) 12 DATA POINTS

PRESSURE M TORR	S(0)	S(-90)	E(0)	E(-90)	1/R	1/I	LIFETIME MICROSEC	E(R)	E(I)
1.01	14531	21355	.022	.011	.680	2178	64.97	.025	.017
1.05	14220	20414	.024	.022	.697	2297	63.47	.033	.031
1.52	14068	19756	.013	.009	.712	2392	62.08	.016	.013
1.54	15659	20903	.009	.011	.749	2296	59.01	.014	.014
3.16	15517	19228	.009	.003	.807	2542	54.78	.009	.004
4.77	15135	18442	.006	.004	.821	2659	53.87	.007	.005
4.78	15834	19439	.004	.003	.815	2519	54.28	.005	.004
9.60	15145	16017	.001	.001	.946	3117	46.76	.001	.001
16.20	14603	11268	.002	.001	1.296	4292	34.11	.002	.001
30.30	13459	6088	.004	.008	2.211	6168	20.00	.009	.004
45.60	9866	3183	.001	.002	3.100	9180	14.26	.002	.001
48.10	9304	2790	.001	.008	3.335	9861	13.26	.008	.002

LEAST SQUARES FIT FOR 1/R DATA FUNCTION TYPE F(3)

COEFFICIENTS FOR FITTING FUNCTION 7.206E-01 6.417E-02 9.418E-02
FRACTIONAL ERRORS IN COEFFICIENTS 4.467E-02 3.789E-02 2.460E-01

INTERCEPT .721 FRACTIONAL ERROR .045 ZERO P. LIFETIME 61.35 MICRO SEC
H.P. SLOPE .064 MTORR-1 FRACTIONAL ERROR .038 H.P. Q CONSTANT 4.46 E-11 CC/MOLEC SEC
Q RATIO .089 MTORR-1 FRACTIONAL ERROR .044 QUENCH PRESSURE 11.23 MTORR

VARIANCE RATIO COMPARED TO LINEAR FIT, 27.7 FOR (1, 9) DEGREES FREEDOM

LEAST SQUARES FIT FOR 1/I DATA FUNCTION TYPE F(3)

COEFFICIENTS FOR FITTING FUNCTION 2.216E+03 1.877E+02 6.202E-02
FRACTIONAL ERRORS IN COEFFICIENTS 3.041E-02 2.873E-02 2.369E-01

INTERCEPT 2216 FRACTIONAL ERROR .030
H.P. SLOPE 188 MTORR-1 FRACTIONAL ERROR .029
Q RATIO .085 MTORR-1 FRACTIONAL ERROR .031 QUENCH PRESSURE 11.80 MTORR

VARIANCE RATIO COMPARED TO LINEAR FIT, 20.7 FOR (1, 9) DEGREES FREEDOM

XBL 688-5760

EXCITATION WAVELENGTH 4000 A OBSERVATION FILTER NO. 13 (14270 CM-1) 12 DATA POINTS

PRESSURE M TORR	S(0)	S(-90)	E(0)	E(-90)	1/R	1/I	LIFETIME MICROSEC	E(R)	E(I)
1.01	16955	23038	.016	.012	.736	2072	60.07	.020	.016
1.09	15962	23298	.021	.009	.685	2001	64.53	.023	.014
1.52	15732	21320	.019	.014	.738	2241	59.91	.024	.019
1.59	15326	20745	.015	.008	.738	2304	59.86	.017	.011
3.16	14255	17706	.012	.003	.805	2759	54.91	.012	.004
4.77	15395	19090	.003	.006	.806	2560	54.82	.007	.007
4.78	15737	19802	.004	.003	.795	2460	55.63	.005	.004
9.60	15364	17144	.002	.006	.896	2899	49.33	.006	.007
16.20	15545	12736	.002	.002	1.221	3849	36.22	.003	.002
30.30	14311	7105	.003	.006	2.014	5606	21.95	.007	.003
45.60	10883	3741	.003	.007	2.909	8218	15.20	.008	.003
48.10	9934	3225	.003	.005	3.080	9107	14.35	.006	.003

LEAST SQUARES FIT FOR 1/R DATA FUNCTION TYPE F(3)

COEFFICIENTS FOR FITTING FUNCTION 7.470E-01 5.937E-02 1.021E-01
FRACTIONAL ERRORS IN COEFFICIENTS 4.325E-02 3.517E-02 2.179E-01

INTERCEPT .747 FRACTIONAL ERROR .043 ZERO P. LIFETIME 59.18 MICRO SEC
H.P. SLOPE .059 MTORR-1 FRACTIONAL ERROR .035 H.P. Q CONSTANT 4.12 E-11 CC/MOLEC SEC
Q RATIO .079 MTORR-1 FRACTIONAL ERROR .042 QUENCH PRESSURE 12.58 MTORR

VARIANCE RATIO COMPARED TO LINEAR FIT, 36.9 FOR (1, 9) DEGREES FREEDOM

LEAST SQUARES FIT FOR 1/I DATA FUNCTION TYPE F(3)

COEFFICIENTS FOR FITTING FUNCTION 2.084E+03 1.646E+02 4.420E-02
FRACTIONAL ERRORS IN COEFFICIENTS 5.300E-02 6.719E-02 5.557E-01

INTERCEPT 2084 FRACTIONAL ERROR .053
H.P. SLOPE 165 MTORR-1 FRACTIONAL ERROR .067
Q RATIO .079 MTORR-1 FRACTIONAL ERROR .063 QUENCH PRESSURE 12.66 MTORR

VARIANCE RATIO COMPARED TO LINEAR FIT, 3.7 FOR (1, 9) DEGREES FREEDOM

XBL 688-5761

EXCITATION WAVELENGTH 4000 A OBSERVATION FILTER NO. 14 (13320 CM-1) 11 DATA POINTS

PRESSURE M TORR	S(0)	S(-90)	E(0)	E(-90)	1/R	1/I	LIFETIME MICROSEC	E(R)	E(I)
1.09	20668	34976	.029	.030	.591	1252	74.82	.042	.047
1.54	17864	26984	.067	.042	.662	1706	66.78	.079	.064
1.59	21659	26296	.034	.032	.824	1866	53.67	.047	.039
3.27	20996	26896	.017	.016	.781	1803	56.63	.023	.020
4.78	18365	23717	.019	.015	.774	2041	57.09	.024	.019
10.20	16028	19179	.012	.004	.836	2566	52.90	.013	.005
10.20	16103	19520	.003	.012	.825	2515	53.59	.012	.014
15.06	17778	17640	.007	.011	1.008	2834	43.87	.013	.011
30.30	20459	10674	.005	.008	1.917	3842	23.07	.009	.004
48.10	13317	4637	.008	.016	2.872	6697	15.39	.018	.007
48.10	13958	4985	.005	.011	2.800	6354	15.79	.012	.005

LEAST SQUARES FIT FOR 1/R DATA FUNCTION TYPE F(3)

COEFFICIENTS FOR FITTING FUNCTION 7.570E-01 5.513E-02 1.488E-01
FRACTIONAL ERRORS IN COEFFICIENTS 1.449E-01 6.400E-02 4.665E-01

INTERCEPT .757 FRACTIONAL ERROR .145 ZERO P. LIFETIME 58.40 MICRO SEC
H.P. SLOPE .055 MTORR-1 FRACTIONAL ERROR .064 H.P. Q CONSTANT 3.83 E-11 CC/MOLEC SEC
Q RATIO .073 MTORR-1 FRACTIONAL ERROR .131 QUENCH PRESSURE 13.73 MTORR

VARIANCE RATIO COMPARED TO LINEAR FIT, 14.4 FOR (1, 8) DEGREES FREEDOM

LEAST SQUARES FIT FOR 1/I DATA FUNCTION TYPE F(1)

COEFFICIENTS FOR FITTING FUNCTION 1.444E+03 9.770E+01
FRACTIONAL ERRORS IN COEFFICIENTS 6.406E-02 7.916E-02

INTERCEPT 1444 FRACTIONAL ERROR .064
H.P. SLOPE 98 MTORR-1 FRACTIONAL ERROR .079
Q RATIO .068 MTORR-1 FRACTIONAL ERROR .128 QUENCH PRESSURE 14.78 MTORR

XBL 688-5762

EXCITATION WAVELENGTH 4000 A OBSERVATION FILTER NO. 15 (12480 CM-1) 12 DATA POINTS

PRESSURE M TORR	S(0)	S(-90)	E(0)	E(-90)	1/R	1/I	LIFETIME MICROSEC	E(R)	E(I)
1.05	23464	29897	.117	.098	.785	1624	56.33	.153	.124
1.54	16450	23668	.171	.112	.695	1980	63.61	.204	.162
1.59	12250	26299	.085	.110	.466	1455	94.91	.139	.189
3.27	15878	25413	.111	.047	.625	1768	70.76	.121	.083
4.78	18087	24224	.066	.042	.747	1979	59.21	.078	.057
10.20	15194	20246	.022	.031	.750	2371	58.91	.038	.040
10.20	16062	19732	.028	.015	.814	2481	54.31	.032	.019
15.06	16542	18572	.019	.010	.891	2674	49.64	.021	.011
30.30	18517	10926	.006	.017	1.695	4006	26.09	.018	.009
30.30	18213	10229	.010	.008	1.781	4174	24.83	.013	.006
48.10	13415	5004	.006	.016	2.681	6544	16.49	.017	.006
48.10	12830	4936	.010	.025	2.599	6789	17.01	.027	.010

LEAST SQUARES FIT FOR 1/R DATA FUNCTION TYPE F(3)

COEFFICIENTS FOR FITTING FUNCTION 7.176E-01 5.327E-02 2.225E-01
FRACTIONAL ERRORS IN COEFFICIENTS 2.767E-01 3.584E-02 5.790E-01

INTERCEPT .718 FRACTIONAL ERROR .277 ZERO P. LIFETIME 61.61 MICRO SEC
H.P. SLOPE .053 MTORR-1 FRACTIONAL ERROR .036 H.P. Q CONSTANT 3.70 E-11 CC/MOLEC SEC
Q RATIO .074 MTORR-1 FRACTIONAL ERROR .265 QUENCH PRESSURE 13.47 MTORR

VARIANCE RATIO COMPARED TO LINEAR FIT, 11.4 FOR (1, 9) DEGREES FREEDOM

LEAST SQUARES FIT FOR 1/I DATA FUNCTION TYPE F(3)

COEFFICIENTS FOR FITTING FUNCTION 1.667E+03 1.215E+02 5.246E-02
FRACTIONAL ERRORS IN COEFFICIENTS 1.040E-01 5.065E-02 5.186E-01

INTERCEPT 1667 FRACTIONAL ERROR .104
H.P. SLOPE 121 MTORR-1 FRACTIONAL ERROR .051
Q RATIO .073 MTORR-1 FRACTIONAL ERROR .090 QUENCH PRESSURE 13.72 MTORR

VARIANCE RATIO COMPARED TO LINEAR FIT, 5.6 FOR (1, 9) DEGREES FREEDOM

XBL 688-5763

EXCITATION WAVELENGTH 4300 A OBSERVATION FILTER NO. 2 (22170 CM-1) 17 DATA POINTS

PRESSURE M TORR	S(0)	S(-90)	E(0)	E(-90)	1/R	1/I	LIFETIME MICROSEC	E(R)	E(I)
.47	20532	36997	.100	.019	.555	1147	79.66	.102	.060
1.01	30431	38150	.014	.024	.798	1278	55.42	.028	.029
1.01	24379	35002	.045	.007	.697	1340	63.47	.046	.018
1.11	29288	33847	.030	.011	.865	1462	51.09	.032	.013
2.36	31355	29726	.014	.006	1.055	1680	41.91	.015	.006
2.36	29213	28322	.011	.001	1.031	1765	42.86	.011	.001
3.49	27145	22279	.007	.009	1.218	2201	36.28	.011	.007
5.26	25539	16880	.005	.005	1.513	2725	29.22	.007	.004
5.26	26180	16314	.005	.011	1.605	2751	27.55	.012	.007
10.20	20378	8071	.006	.017	2.525	4242	17.51	.018	.006
10.20	19695	8092	.006	.005	2.434	4344	18.16	.008	.005
16.80	15266	4235	.002	.014	3.605	6082	12.26	.014	.003
16.80	15380	4325	.001	.016	3.556	6025	12.43	.016	.002
29.00	8181	1412	.004	.037	5.794	11870	7.63	.037	.004
29.00	8090	1458	.013	.014	5.549	11972	7.97	.019	.012
41.30	5569	636	.001	.039	8.756	17725	5.05	.039	.001
41.30	5734	696	.007	.029	8.239	17187	5.37	.030	.007

LEAST SQUARES FIT FOR 1/R DATA FUNCTION TYPE F(1)

COEFFICIENTS FOR FITTING FUNCTION 5.998E-01 1.810E-01
FRACTIONAL ERRORS IN COEFFICIENTS 3.031E-02 2.518E-02

INTERCEPT .600 FRACTIONAL ERROR .030 ZERO P. LIFETIME 73.71 MICRO SEC
H.P. SLOPE .181 MTORR-1 FRACTIONAL ERROR .025 H.P. Q CONSTANT 12.57 E-11 CC/MOLEC SEC
Q RATIO .302 MTORR-1 FRACTIONAL ERROR .052 QUENCH PRESSURE 3.31 MTORR

LEAST SQUARES FIT FOR 1/I DATA FUNCTION TYPE F(3)

COEFFICIENTS FOR FITTING FUNCTION 1.079E+03 3.839E+02 1.287E-01
FRACTIONAL ERRORS IN COEFFICIENTS 9.183E-02 3.322E-02 6.073E-01

INTERCEPT 1079 FRACTIONAL ERROR .092
H.P. SLOPE 384 MTORR-1 FRACTIONAL ERROR .033
Q RATIO .356 MTORR-1 FRACTIONAL ERROR .083 QUENCH PRESSURE 2.81 MTORR

VARIANCE RATIO COMPARED TO LINEAR FIT, 6.1 FOR (1,14) DEGREES FREEDOM

XBL 688-5764

EXCITATION WAVELENGTH 4300 A OBSERVATION FILTER NO. 4 (20790 CM-1) 18 DATA POINTS

PRESSURE M TORR	S(0)	S(-90)	E(0)	E(-90)	1/R	1/I	LIFETIME MICROSEC	E(R)	E(I)
.45	49370	71316	.029	.002	.692	656	63.86	.029	.011
.47	39578	74461	.040	.010	.531	556	83.20	.041	.027
1.00	57585	77775	.016	.005	.740	615	59.71	.017	.008
1.01	57832	83301	.014	.010	.694	562	63.68	.017	.014
1.11	57684	79537	.016	.004	.725	598	60.96	.016	.007
2.36	63847	71360	.006	.002	.895	696	49.41	.006	.002
2.36	61996	65185	.005	.005	.951	766	46.48	.007	.005
3.49	61188	58095	.004	.003	1.053	860	41.97	.005	.003
3.49	60729	58675	.004	.003	1.035	852	42.71	.005	.003
5.26	59951	46795	.003	.005	1.281	1037	34.51	.006	.004
10.20	52633	26499	0.	.003	1.986	1516	22.26	.003	.001
10.20	52979	27388	.001	.003	1.934	1489	22.85	.003	.001
16.80	40287	14174	.002	.003	2.842	2209	15.55	.004	.002
16.80	40542	14163	0.	.006	2.863	2198	15.44	.006	.001
29.00	24999	5347	.003	.006	4.675	3825	9.46	.007	.003
29.00	25010	5427	.003	.009	4.608	3819	9.59	.009	.003
41.30	17510	2860	.002	.015	6.122	5563	7.22	.015	.002
41.30	17579	2810	.002	.013	6.256	5547	7.07	.013	.002

LEAST SQUARES FIT FOR 1/R DATA FUNCTION TYPE F(1)

COEFFICIENTS FOR FITTING FUNCTION 5.752E-01 1.366E-01
FRACTIONAL ERRORS IN COEFFICIENTS 2.263E-02 2.507E-02

INTERCEPT .575 FRACTIONAL ERROR .023 ZERO P. LIFETIME 76.86 MICRO SEC
H.P. SLOPE .137 MTORR-1 FRACTIONAL ERROR .025 H.P. Q CONSTANT 9.49 E-11 CC/MOLEC SEC
Q RATIO .238 MTORR-1 FRACTIONAL ERROR .044 QUENCH PRESSURE 4.21 MTORR

LEAST SQUARES FIT FOR 1/I DATA FUNCTION TYPE F(3)

COEFFICIENTS FOR FITTING FUNCTION 5.482E+02 1.270E+02 1.260E-01
FRACTIONAL ERRORS IN COEFFICIENTS 4.781E-02 2.687E-02 3.334E-01

INTERCEPT 548 FRACTIONAL ERROR .048
H.P. SLOPE 127 MTORR-1 FRACTIONAL ERROR .027
Q RATIO .232 MTORR-1 FRACTIONAL ERROR .045 QUENCH PRESSURE 4.32 MTORR

VARIANCE RATIO COMPARED TO LINEAR FIT. 14.0 FOR (1,15) DEGREES FREEDOM

XBL 688-5765

EXCITATION WAVELENGTH 4300 A OBSERVATION FILTER NO. 6 (19960 CM-1) 20 DATA POINTS

PRESSURE M TORR	S(0)	S(-90)	E(0)	E(-90)	1/R	1/I	LIFETIME MICROSEC	E(R)	E(I)
.45	90477	117722	.023	.010	.769	410	57.52	.025	.014
.47	84844	111266	.011	.006	.763	433	57.98	.013	.008
1.00	101639	127478	.002	.010	.797	382	55.45	.010	.012
1.00	87965	106564	.009	.005	.825	461	53.56	.010	.006
1.01	92847	112505	.005	.003	.825	436	53.57	.006	.004
1.11	103395	121805	.002	.006	.849	405	52.08	.006	.007
2.36	92243	94349	.003	.001	.978	530	45.22	.003	.001
2.36	100112	102099	.002	.003	.981	490	45.09	.004	.003
3.49	88494	80468	.004	.004	1.100	619	40.20	.006	.004
3.49	99276	89140	.003	.002	1.114	558	39.70	.004	.002
5.26	93918	72584	.002	.005	1.294	667	34.17	.005	.004
5.26	86368	64681	.003	.004	1.335	742	33.11	.005	.003
10.20	78315	40692	.002	.002	1.925	1005	22.97	.003	.001
10.20	77958	41672	.002	.006	1.871	998	23.63	.006	.003
16.80	60428	21937	.002	.003	2.755	1462	16.05	.004	.002
16.80	59486	21243	.001	.006	2.800	1491	15.79	.006	.002
29.00	36384	8365	.002	.003	4.350	2610	10.16	.004	.002
29.00	36766	8654	.001	.008	4.248	2577	10.41	.008	.001
41.30	26259	4481	.003	.008	5.860	3700	7.54	.009	.003
41.30	26524	4507	.002	.002	5.885	3664	7.51	.003	.002

LEAST SQUARES FIT FOR 1/R DATA FUNCTION TYPE F(3)

COEFFICIENTS FOR FITTING FUNCTION 7.111E-01 1.369E-01 3.735E-02
FRACTIONAL ERRORS IN COEFFICIENTS 8.839E-03 1.992E-02 2.201E-01

INTERCEPT .711 FRACTIONAL ERROR .009 ZERO P. LIFETIME 62.17 MICRO SEC
H.P. SLOPE .137 MTORR-1 FRACTIONAL ERROR .020 H.P. Q CONSTANT 9.51 E-11 CC/MOLEC SEC
Q RATIO .192 MTORR-1 FRACTIONAL ERROR .017 QUENCH PRESSURE 5.20 MTORR

VARIANCE RATIO COMPARED TO LINEAR FIT. 11.9 FOR (1,17) DEGREES FREEDOM

LEAST SQUARES FIT FOR 1/I DATA FUNCTION TYPE F(3)

COEFFICIENTS FOR FITTING FUNCTION 3.873E+02 8.468E+01 1.220E-01
FRACTIONAL ERRORS IN COEFFICIENTS 4.600E-02 2.947E-02 3.313E-01

INTERCEPT 387 FRACTIONAL ERROR .046
H.P. SLOPE 85 MTORR-1 FRACTIONAL ERROR .029
Q RATIO .219 MTORR-1 FRACTIONAL ERROR .044 QUENCH PRESSURE 4.57 MTORR

VARIANCE RATIO COMPARED TO LINEAR FIT. 14.2 FOR (1,17) DEGREES FREEDOM

XBL 688-5766

EXCITATION WAVELENGTH 4300 A OBSERVATION FILTER NO. 7 (19350 CM-1) 16 DATA POINTS

PRESSURE M TORR	S(0)	S(-90)	E(0)	E(-90)	1/R	1/I	LIFETIME MICROSEC	E(R)	E(I)
.45	85293	118901	.011	.006	.717	398	61.63	.013	.009
.47	85032	123744	.002	.003	.687	377	64.34	.004	.004
1.00	82432	109833	.009	.004	.751	437	58.91	.010	.006
1.11	84480	112988	.003	.003	.748	424	59.13	.004	.004
2.36	83994	101751	.005	.004	.825	482	53.56	.006	.005
2.36	85797	102557	.001	.004	.837	480	52.85	.004	.005
3.49	86961	91614	.004	.004	.949	545	46.58	.006	.004
5.26	88034	79316	.003	.006	1.110	627	39.83	.007	.005
10.20	85262	51506	.001	.004	1.655	859	26.71	.004	.002
10.20	81964	50356	.002	.004	1.628	886	27.16	.004	.002
16.80	66159	27291	.003	.004	2.424	1292	18.24	.005	.002
16.80	65045	28029	.002	.003	2.321	1297	19.05	.004	.002
29.00	42326	11275	0.	.003	3.754	2206	11.78	.003	.000
29.00	43994	11477	.002	.004	3.833	2128	11.53	.004	.002
41.30	31239	5961	.002	.009	5.241	3089	8.44	.009	.002
41.30	31319	5934	.001	.006	5.278	3082	8.38	.006	.001

LEAST SQUARES FIT FOR 1/R DATA FUNCTION TYPE F(3)

COEFFICIENTS FOR FITTING FUNCTION 6.701E-01 1.258E-01 9.495E-02
FRACTIONAL ERRORS IN COEFFICIENTS 1.298E-02 1.427E-02 1.216E-01

INTERCEPT .670 FRACTIONAL ERROR .013 ZERO P. LIFETIME 65.98 MICRO SEC
H.P. SLOPE .126 MTORR-1 FRACTIONAL ERROR .014 H.P. Q CONSTANT 8.74 E-11 CC/MOLEC SEC
Q RATIO .188 MTORR-1 FRACTIONAL ERROR .014 QUENCH PRESSURE 5.33 MTORR

VARIANCE RATIO COMPARED TO LINEAR FIT, 62.9 FOR (1,13) DEGREES FREEDOM

LEAST SQUARES FIT FOR 1/I DATA FUNCTION TYPE F(3)

COEFFICIENTS FOR FITTING FUNCTION 3.836E+02 7.063E+01 1.039E-01
FRACTIONAL ERRORS IN COEFFICIENTS 2.655E-02 1.850E-02 2.088E-01

INTERCEPT 384 FRACTIONAL ERROR .027
H.P. SLOPE 71 MTORR-1 FRACTIONAL ERROR .018
Q RATIO .184 MTORR-1 FRACTIONAL ERROR .026 QUENCH PRESSURE 5.43 MTORR

VARIANCE RATIO COMPARED TO LINEAR FIT, 36.9 FOR (1,13) DEGREES FREEDOM

XBL 688-5767

EXCITATION WAVELENGTH 4300 A OBSERVATION FILTER NO. 8 (18950 CM-1) 19 DATA POINTS

PRESSURE M TORR	S(0)	S(-90)	E(0)	E(-90)	1/R	1/I	LIFETIME MICROSEC	E(R)	E(I)
.45	66679	99986	.008	.006	.667	462	66.29	.010	.009
.47	75469	114762	.006	.005	.658	400	67.23	.008	.007
.47	71500	107819	.018	.005	.663	427	66.67	.019	.010
1.00	80332	118983	.005	.006	.675	390	65.48	.008	.008
1.11	79542	114953	.003	.002	.692	407	63.89	.004	.003
2.36	83991	107805	.004	.004	.779	450	56.74	.006	.005
2.36	82787	107943	.005	.006	.767	447	57.64	.008	.008
3.49	85969	98270	.003	.003	.875	504	50.54	.004	.003
3.49	90612	105005	.005	.003	.863	471	51.23	.006	.004
5.26	88493	86237	.002	.006	1.026	580	43.08	.006	.006
5.26	90269	86642	.001	.002	1.042	577	42.43	.002	.002
10.20	88482	58804	.001	.004	1.505	784	29.38	.004	.002
10.20	87248	58304	.002	.001	1.496	792	29.54	.002	.001
16.80	75074	34031	.002	0.	2.206	1105	20.04	.002	.001
16.80	71824	32413	.003	.003	2.216	1157	19.95	.004	.002
29.00	48446	13959	.001	.004	3.471	1906	12.74	.004	.001
29.00	49010	13836	.001	.004	3.542	1890	12.48	.004	.001
41.30	35176	7469	.001	.011	4.710	2720	9.39	.011	.001
41.30	35631	7525	.001	.007	4.735	2687	9.34	.007	.001

LEAST SQUARES FIT FOR 1/R DATA FUNCTION TYPE F(4)

COEFFICIENTS FOR FITTING FUNCTION 6.536E-01 2.585E-01 4.184E-02 3.959E-01
FRACTIONAL ERRORS IN COEFFICIENTS 1.564E-02 2.344E-01 2.986E-01 3.111E-01

INTERCEPT .654 FRACTIONAL ERROR .016 ZERO P. LIFETIME 67.64 MICRO SEC
H.P. SLOPE .106 MTORR-1 FRACTIONAL ERROR .016 H.P. Q CONSTANT 7.34 E-11 CC/MOLEC SEC
Q RATIO .162 MTORR-1 FRACTIONAL ERROR .028 QUENCH PRESSURE 6.18 MTORR

VARIANCE RATIO COMPARED TO LINEAR FIT, 144.5 FOR (2,15) DEGREES FREEDOM

LEAST SQUARES FIT FOR 1/I DATA FUNCTION TYPE F(3)

COEFFICIENTS FOR FITTING FUNCTION 4.144E+02 6.279E+01 1.610E-01
FRACTIONAL ERRORS IN COEFFICIENTS 3.166E-02 2.073E-02 1.703E-01

INTERCEPT 414 FRACTIONAL ERROR .032
H.P. SLOPE 63 MTORR-1 FRACTIONAL ERROR .021
Q RATIO .152 MTORR-1 FRACTIONAL ERROR .032 QUENCH PRESSURE 6.60 MTORR

VARIANCE RATIO COMPARED TO LINEAR FIT, 56.3 FOR (1,16) DEGREES FREEDOM

XBL 688-3768

EXCITATION WAVELENGTH 4300 A OBSERVATION FILTER NO. 9 (17880 CM-1) 18 DATA POINTS

PRESSURE M TORR	S(0)	S(-90)	E(0)	E(-90)	1/R	1/I	LIFETIME MICROSEC	E(R)	E(I)
.45	82081	126969	.015	.004	.646	359	68.39	.016	.008
.47	91125	138479	.011	.009	.658	332	67.18	.014	.013
1.00	91771	134675	.016	.011	.681	346	64.88	.019	.016
1.00	95823	136746	.012	.007	.701	344	63.09	.014	.010
1.11	98942	139434	.002	.004	.710	338	62.30	.004	.005
2.36	96425	126258	.003	.001	.764	382	57.89	.003	.001
2.36	96966	128364	.004	.004	.755	375	58.52	.006	.005
3.49	97556	117465	.003	.001	.831	418	53.23	.003	.001
3.49	95828	113258	.003	.002	.846	435	52.25	.004	.002
5.26	102478	110651	.002	.003	.926	451	47.74	.004	.003
10.20	105465	79029	.002	.001	1.335	607	33.13	.002	.001
10.20	106301	79838	.001	.002	1.331	601	33.20	.002	.001
16.80	88985	46489	.002	.002	1.914	883	23.10	.003	.001
16.80	89932	48129	.001	0.	1.869	864	23.66	.001	.001
29.00	62161	19719	.001	.002	3.152	1462	14.02	.002	.001
29.00	62701	20236	.001	.002	3.098	1444	14.27	.002	.001
41.30	45269	11086	.002	.008	4.083	2084	10.83	.008	.002
41.30	45562	10554	.001	.007	4.317	2083	10.24	.007	.001

LEAST SQUARES FIT FOR 1/R DATA FUNCTION TYPE F(3)

COEFFICIENTS FOR FITTING FUNCTION 6.469E-01 9.895E-02 9.716E-02
FRACTIONAL ERRORS IN COEFFICIENTS 1.376E-02 1.397E-02 1.074E-01

INTERCEPT .647 FRACTIONAL ERROR .014 ZERO P. LIFETIME 68.34 MICRO SEC
H.P. SLOPE .099 MTORR-1 FRACTIONAL ERROR .014 H.P. Q CONSTANT 6.87 E-11 CC/MOLEC SEC
Q RATIO .153 MTORR-1 FRACTIONAL ERROR .015 QUENCH PRESSURE 6.54 MTORR

VARIANCE RATIO COMPARED TO LINEAR FIT, 97.6 FOR (1,15) DEGREES FREEDOM

LEAST SQUARES FIT FOR 1/I DATA FUNCTION TYPE F(3)

COEFFICIENTS FOR FITTING FUNCTION 3.397E+02 4.710E+01 1.234E-01
FRACTIONAL ERRORS IN COEFFICIENTS 2.906E-02 2.098E-02 1.841E-01

INTERCEPT 340 FRACTIONAL ERROR .029
H.P. SLOPE 47 MTORR-1 FRACTIONAL ERROR .021
Q RATIO .139 MTORR-1 FRACTIONAL ERROR .028 QUENCH PRESSURE 7.21 MTORR

VARIANCE RATIO COMPARED TO LINEAR FIT, 51.5 FOR (1,15) DEGREES FREEDOM

XBL 688-5769

EXCITATION WAVELENGTH 4300 A OBSERVATION FILTER NO. 10 (16960 CM-1) 18 DATA POINTS

PRESSURE M TORR	S(0)	S(-90)	E(0)	E(-90)	1/R	1/I	LIFETIME MICROSEC	E(R)	E(I)
.47	98854	148408	.013	.005	.666	311	66.37	.014	.009
.47	99157	145280	.018	.008	.683	320	64.77	.020	.013
1.00	109605	151863	.004	.006	.722	312	61.25	.007	.008
1.01	125085	178205	.003	.001	.702	264	62.98	.003	.002
1.11	113132	163910	.004	.006	.690	285	64.05	.007	.008
2.36	112407	148898	.004	.001	.755	323	58.56	.004	.002
2.36	109139	146777	.002	.003	.744	326	59.46	.004	.004
3.49	114876	143365	.004	.001	.801	340	55.17	.004	.001
5.26	109251	126623	.001	.004	.863	391	51.24	.004	.005
10.20	123254	103094	.004	0.	1.196	477	36.98	.004	.001
10.20	119074	101010	.003	.002	1.179	488	37.50	.004	.002
16.80	107095	63173	.001	.003	1.695	693	26.08	.003	.002
16.80	106611	62965	.001	.003	1.693	695	26.11	.003	.002
29.00	79243	29289	.001	.002	2.706	1110	16.34	.002	.001
29.00	79854	29192	0.	.002	2.735	1105	16.16	.002	.000
29.00	82708	30087	.002	.003	2.749	1068	16.08	.004	.002
41.30	60299	16335	.002	.004	3.691	1545	11.98	.004	.002
41.30	61299	16524	.002	.003	3.710	1521	11.92	.004	.002

LEAST SQUARES FIT FOR 1/R DATA FUNCTION TYPE F(3)

COEFFICIENTS FOR FITTING FUNCTION 6.835E-01 8.730E-02 1.182E-01
FRACTIONAL ERRORS IN COEFFICIENTS 1.364E-02 1.199E-02 9.001E-02

INTERCEPT .683 FRACTIONAL ERROR .014 ZERO P. LIFETIME 64.68 MICRO SEC
H.P. SLOPE .087 MTORR-1 FRACTIONAL ERROR .012 H.P. Q CONSTANT 6.06 E-11 CC/MOLEC SEC
Q RATIO .128 MTORR-1 FRACTIONAL ERROR .013 QUENCH PRESSURE 7.83 MTORR

VARIANCE RATIO COMPARED TO LINEAR FIT, 179.1 FOR (1,15) DEGREES FREEDOM

LEAST SQUARES FIT FOR 1/I DATA FUNCTION TYPE F(3)

COEFFICIENTS FOR FITTING FUNCTION 2.955E+02 3.542E+01 1.155E-01
FRACTIONAL ERRORS IN COEFFICIENTS 3.737E-02 2.714E-02 2.462E-01

INTERCEPT 296 FRACTIONAL ERROR .037
H.P. SLOPE 35 MTORR-1 FRACTIONAL ERROR .027
Q RATIO .120 MTORR-1 FRACTIONAL ERROR .036 QUENCH PRESSURE 8.34 MTORR

VARIANCE RATIO COMPARED TO LINEAR FIT, 26.0 FOR (1,15) DEGREES FREEDOM

XBL 688-5770

EXCITATION WAVELENGTH 4300 A OBSERVATION FILTER NO. 11 (15850 CM-1) 17 DATA POINTS

PRESSURE M TORR	S(0)	S(-90)	E(0)	E(-90)	1/R	1/I	LIFETIME MICROSEC	E(R)	E(I)
.45	86798	135359	.018	.008	.641	336	68.94	.020	.014
.47	81804	130399	.012	.007	.627	345	70.47	.014	.011
1.00	88412	132590	.016	.009	.667	348	66.30	.018	.014
1.00	93396	145559	.008	.010	.642	312	68.90	.013	.015
1.11	94098	146305	.005	.003	.643	311	68.74	.006	.005
2.36	88950	134672	.005	.002	.660	341	66.93	.005	.003
2.36	88937	136925	.004	.004	.650	334	68.06	.006	.006
3.49	92082	135072	.006	.005	.682	345	64.85	.008	.007
5.26	100460	135428	.001	.005	.742	353	59.60	.005	.006
10.20	112027	109795	.002	.002	1.020	455	43.33	.003	.002
10.20	111263	109408	.004	.002	1.017	457	43.47	.004	.002
16.80	107166	71872	.001	.004	1.491	644	29.65	.004	.003
16.80	103521	70541	.002	.003	1.468	660	30.13	.004	.002
29.00	80110	34404	.001	.005	2.329	1054	18.99	.005	.002
29.00	82846	35139	.003	.006	2.357	1023	18.75	.007	.003
41.30	61977	19602	.002	.004	3.162	1467	13.98	.004	.002
41.30	61744	19808	.001	.004	3.117	1468	14.18	.004	.001

LEAST SQUARES FIT FOR 1/R DATA FUNCTION TYPE F(3)

COEFFICIENTS FOR FITTING FUNCTION 6.552E-01 7.615E-02 1.625E-01
FRACTIONAL ERRORS IN COEFFICIENTS 1.460E-02 1.027E-02 7.346E-02

INTERCEPT .655 FRACTIONAL ERROR .015 ZERO P. LIFETIME 67.48 MICRO SEC
H.P. SLOPE .076 MTORR-1 FRACTIONAL ERROR .010 H.P. Q CONSTANT 5.29 E-11 CC/MOLEC SEC
Q RATIO .116 MTORR-1 FRACTIONAL ERROR .014 QUENCH PRESSURE 8.60 MTORR

VARIANCE RATIO COMPARED TO LINEAR FIT, 315.4 FOR (1,14) DEGREES FREEDOM

LEAST SQUARES FIT FOR 1/I DATA FUNCTION TYPE F(3)

COEFFICIENTS FOR FITTING FUNCTION 3.483E+02 3.379E+01 1.764E-01
FRACTIONAL ERRORS IN COEFFICIENTS 2.678E-02 1.778E-02 1.285E-01

INTERCEPT 348 FRACTIONAL ERROR .027
H.P. SLOPE 34 MTORR-1 FRACTIONAL ERROR .018
Q RATIO .097 MTORR-1 FRACTIONAL ERROR .026 QUENCH PRESSURE 10.31 MTORR

VARIANCE RATIO COMPARED TO LINEAR FIT, 134.2 FOR (1,14) DEGREES FREEDOM

XBL 688-5771

EXCITATION WAVELENGTH 4300 A OBSERVATION FILTER NO. 12 (15130 CM-1) 16 DATA POINTS

PRESSURE M TORR	S(0)	S(-90)	E(0)	E(-90)	1/R	1/I	LIFETIME MICROSEC	E(R)	E(I)
.47	71934	117030	.010	.006	.615	381	71.93	.012	.010
.47	70414	118715	.012	.004	.593	370	74.54	.013	.008
1.00	79634	123873	.005	.013	.643	367	68.77	.014	.019
1.01	82915	133785	.008	.007	.620	335	71.33	.011	.011
2.36	78711	121839	.002	.002	.646	374	68.43	.003	.003
2.36	80628	127659	.007	.002	.632	354	70.00	.007	.004
3.49	84410	126920	.005	.002	.665	363	66.47	.005	.003
5.26	81322	114480	.004	.003	.710	412	62.24	.005	.004
10.20	104146	113873	.002	.002	.915	437	48.34	.003	.002
10.20	101698	111384	.003	.003	.913	447	48.42	.004	.003
16.80	93108	71766	.001	.001	1.297	674	34.08	.001	.001
16.80	95400	72304	.003	0.	1.319	666	33.51	.003	.001
29.00	81757	37689	.002	.006	2.169	1009	20.38	.006	.002
29.00	80229	37483	.002	.004	2.140	1023	20.65	.004	.002
41.30	61726	21092	.002	.006	2.926	1451	15.11	.006	.002
41.30	63004	21532	0.	.002	2.926	1421	15.11	.002	.000

LEAST SQUARES FIT FOR 1/R DATA FUNCTION TYPE F(3)

COEFFICIENTS FOR FITTING FUNCTION 6.320E-01 6.774E-02 1.493E-01
FRACTIONAL ERRORS IN COEFFICIENTS 2.222E-02 1.669E-02 1.149E-01

INTERCEPT .632 FRACTIONAL ERROR .022 ZERO P. LIFETIME 69.95 MICRO SEC
H.P. SLOPE .068 MTORR-1 FRACTIONAL ERROR .017 H.P. Q CONSTANT 4.70 E-11 CC/MOLEC SEC
Q RATIO .107 MTORR-1 FRACTIONAL ERROR .022 QUENCH PRESSURE 9.33 MTORR

VARIANCE RATIO COMPARED TO LINEAR FIT, 143.6 FOR (1,13) DEGREES FREEDOM

LEAST SQUARES FIT FOR 1/I DATA FUNCTION TYPE F(3)

COEFFICIENTS FOR FITTING FUNCTION 3.838E+02 3.283E+01 1.654E-01
FRACTIONAL ERRORS IN COEFFICIENTS 3.934E-02 2.739E-02 1.848E-01

INTERCEPT 384 FRACTIONAL ERROR .039
H.P. SLOPE 33 MTORR-1 FRACTIONAL ERROR .027
Q RATIO .086 MTORR-1 FRACTIONAL ERROR .038 QUENCH PRESSURE 11.69 MTORR

VARIANCE RATIO COMPARED TO LINEAR FIT, 65.1 FOR (1,13) DEGREES FREEDOM

XBL 688-5772

EXCITATION WAVELENGTH 4300 A OBSERVATION FILTER NO. 13 (14270 CM-1) 18 DATA POINTS

PRESSURE M TORR	S(0)	S(-90)	E(0)	E(-90)	1/R	1/I	LIFETIME MICROSEC	E(R)	E(I)
.45	67916	108603	.019	.018	.625	414	70.69	.026	.027
.47	81054	135498	.015	.014	.598	325	73.91	.021	.022
1.00	74040	126576	.014	.011	.585	344	75.58	.018	.018
1.11	89763	145879	.008	.002	.615	306	71.85	.008	.005
2.36	82026	128858	.008	.002	.637	352	69.45	.008	.004
2.36	83132	128211	.004	.002	.648	356	68.18	.004	.003
3.49	88393	136374	.005	.008	.648	335	68.21	.009	.011
3.49	91655	142150	.002	.003	.645	320	68.57	.004	.004
5.26	81717	114715	.009	.006	.712	412	62.06	.011	.008
5.26	81143	116702	.005	.005	.695	402	63.58	.007	.007
10.20	105131	123873	.003	.001	.849	398	52.09	.003	.001
10.20	103583	121028	.003	.005	.856	408	51.66	.006	.006
16.80	95846	78398	.001	.001	1.223	625	36.16	.001	.001
16.80	96823	79696	.003	.005	1.215	616	36.39	.006	.004
29.00	91506	45697	.002	.002	2.002	875	22.08	.003	.001
29.00	91386	45587	.003	.006	2.005	876	22.05	.007	.003
41.30	70755	26209	.002	.002	2.700	1243	16.38	.003	.002
41.30	70957	26278	.001	.002	2.700	1239	16.37	.002	.001

LEAST SQUARES FIT FOR 1/R DATA FUNCTION TYPE F(3)

COEFFICIENTS FOR FITTING FUNCTION 6.302E-01 6.209E-02 1.397E-01
FRACTIONAL ERRORS IN COEFFICIENTS 2.879E-02 1.975E-02 1.315E-01

INTERCEPT .630 FRACTIONAL ERROR .029 ZERO P. LIFETIME 70.16 MICRO SEC
H.P. SLOPE .062 MTORR-1 FRACTIONAL ERROR .020 H.P. Q CONSTANT 4.31 E-11 CC/MOLEC SEC
Q RATIO .099 MTORR-1 FRACTIONAL ERROR .027 QUENCH PRESSURE 10.15 MTORR

VARIANCE RATIO COMPARED TO LINEAR FIT, 104.4 FOR (1,15) DEGREES FREEDOM

LEAST SQUARES FIT FOR 1/I DATA FUNCTION TYPE F(3)

COEFFICIENTS FOR FITTING FUNCTION 3.519E+02 2.817E+01 1.251E-01
FRACTIONAL ERRORS IN COEFFICIENTS 6.096E-02 4.728E-02 2.969E-01

INTERCEPT 352 FRACTIONAL ERROR .061
H.P. SLOPE 28 MTORR-1 FRACTIONAL ERROR .047
Q RATIO .080 MTORR-1 FRACTIONAL ERROR .061 QUENCH PRESSURE 12.49 MTORR

VARIANCE RATIO COMPARED TO LINEAR FIT, 18.6 FOR (1,15) DEGREES FREEDOM

XBL 688-5773

EXCITATION WAVELENGTH 4800 A OBSERVATION FILTER NO. 6 (19960 CM-1) 18 DATA POINTS

PRESSURE M TORR	S(0)	S(-90)	E(0)	E(-90)	1/R	1/I	LIFETIME MICROSEC	E(R)	E(I)
.49	62842	74226	.014	.034	.847	664	52.22	.037	.040
.49	50468	72525	.034	.011	.696	646	63.53	.036	.019
1.12	60326	61978	.033	.012	.973	806	45.42	.035	.012
1.12	62886	57685	.007	.015	1.090	864	40.55	.017	.014
1.18	45604	49577	.050	.008	.920	1005	48.06	.051	.010
1.42	56566	52523	.021	.010	1.077	949	41.05	.023	.009
2.35	63255	48699	.009	.017	1.299	993	34.04	.019	.013
2.50	63496	47497	.010	.004	1.337	1010	33.07	.011	.004
5.05	53424	27931	.005	.007	1.913	1470	23.11	.009	.004
5.05	54278	29078	.007	.010	1.867	1432	23.68	.012	.006
10.94	35031	11034	.003	.020	3.175	2597	13.93	.020	.004
10.94	35134	10942	.004	.013	3.211	2595	13.77	.014	.004
17.60	24350	5037	.003	.021	4.834	3938	9.15	.021	.003
17.60	22714	4818	.002	.013	4.714	4213	9.38	.013	.002
30.90	12665	1738	.005	.019	7.287	7750	6.07	.020	.005
30.90	12799	1707	.008	.030	7.498	7677	5.90	.031	.008
47.40	7994	782	.004	.063	10.223	12391	4.32	.063	.004
47.40	8398	709	.003	.073	11.845	11823	3.73	.073	.003

LEAST SQUARES FIT FOR 1/R DATA FUNCTION TYPE F(1)

COEFFICIENTS FOR FITTING FUNCTION 7.261E-01 2.303E-01
FRACTIONAL ERRORS IN COEFFICIENTS 3.513E-02 3.735E-02

INTERCEPT .726 FRACTIONAL ERROR .035 ZERO P. LIFETIME 60.89 MICRO SEC
H.P. SLOPE .230 MTORR-1 FRACTIONAL ERROR .037 H.P. Q CONSTANT 15.99 E-11 CC/MOLEC SEC
Q RATIO .317 MTORR-1 FRACTIONAL ERROR .066 QUENCH PRESSURE 3.15 MTORR

LEAST SQUARES FIT FOR 1/I DATA FUNCTION TYPE F(3)

COEFFICIENTS FOR FITTING FUNCTION 6.609E+02 2.332E+02 1.872E-01
FRACTIONAL ERRORS IN COEFFICIENTS 9.843E-02 3.665E-02 5.764E-01

INTERCEPT 661 FRACTIONAL ERROR .098
H.P. SLOPE 233 MTORR-1 FRACTIONAL ERROR .037
Q RATIO .353 MTORR-1 FRACTIONAL ERROR .091 QUENCH PRESSURE 2.83 MTORR

VARIANCE RATIO COMPARED TO LINEAR FIT, 9.0 FOR (1,15) DEGREES FREEDOM

XBL 688-5774

EXCITATION WAVELENGTH 4800 A OBSERVATION FILTER NO. 7 (19350 CM-1) 14 DATA POINTS

PRESSURE M TORR	S(0)	S(-90)	E(0)	E(-90)	1/R	1/I	LIFETIME MICROSEC	E(R)	E(I)
1.18	61891	60770	.030	.011	1.018	823	43.41	.032	.011
1.42	61664	64854	.012	.007	.951	770	46.50	.014	.007
2.35	73890	65745	.011	.006	1.124	755	39.34	.013	.005
2.50	69779	62353	.010	.007	1.119	797	39.50	.012	.006
5.05	65058	42761	.005	.004	1.521	1073	29.06	.006	.003
5.05	65036	41778	.006	.003	1.557	1088	28.40	.007	.003
10.94	45971	18254	.005	.005	2.518	1879	17.55	.007	.004
10.94	47379	18326	.001	.006	2.585	1836	17.10	.006	.002
17.60	31790	8615	.007	.008	3.690	2930	11.98	.011	.006
17.60	30796	8359	.005	.003	3.684	3024	12.00	.006	.004
30.90	17384	2993	.003	.015	5.808	5587	7.61	.015	.003
30.90	18346	2829	.006	.012	6.485	5324	6.82	.013	.006
47.40	11672	1239	.004	.016	9.421	8472	4.69	.016	.004
47.40	10995	1263	.003	.030	8.705	8977	5.08	.030	.003

LEAST SQUARES FIT FOR 1/R DATA FUNCTION TYPE F(1)

COEFFICIENTS FOR FITTING FUNCTION 7.232E-01 1.666E-01
FRACTIONAL ERRORS IN COEFFICIENTS 2.378E-02 2.307E-02

INTERCEPT .723 FRACTIONAL ERROR .024 ZERO P. LIFETIME 61.13 MICRO SEC
H.P. SLOPE .167 MTORR-1 FRACTIONAL ERROR .023 H.P. Q CONSTANT 11.57 E-11 CC/MOLEC SEC
Q RATIO .230 MTORR-1 FRACTIONAL ERROR .044 QUENCH PRESSURE 4.34 MTORR

LEAST SQUARES FIT FOR 1/I DATA FUNCTION TYPE F(4)

COEFFICIENTS FOR FITTING FUNCTION 8.816E+02 4.442E+01 4.338E+01 2.264E-01
FRACTIONAL ERRORS IN COEFFICIENTS 1.243E-01 4.729E-01 4.518E-01 4.890E-01

INTERCEPT 882 FRACTIONAL ERROR .124
H.P. SLOPE 192 MTORR-1 FRACTIONAL ERROR .046
Q RATIO .217 MTORR-1 FRACTIONAL ERROR .157 QUENCH PRESSURE 4.60 MTORR

VARIANCE RATIO COMPARED TO LINEAR FIT, 55.8 FOR (2,10) DEGREES FREEDOM

XBL 688-5775

EXCITATION WAVELENGTH 4800 A OBSERVATION FILTER NO. 9 (17880 CM-1) 16 DATA POINTS

PRESSURE M TORR	S(0)	S(-90)	E(0)	E(-90)	1/R	1/I	LIFETIME MICROSEC	E(R)	E(I)
.49	70186	106991	.014	.006	.656	429	67.39	.015	.010
1.12	74960	103878	.009	.006	.722	457	61.26	.011	.008
1.12	86797	121926	.004	.004	.712	387	62.10	.006	.005
1.18	63298	88454	.007	.005	.716	535	61.78	.009	.007
1.42	73225	95325	.005	.004	.768	507	57.55	.006	.005
2.35	84719	100974	.002	.002	.839	488	52.69	.003	.002
5.05	95468	85873	.002	.001	1.112	579	39.77	.002	.001
5.05	94782	85831	.002	.002	1.104	580	40.03	.003	.002
10.94	81134	44092	.002	.002	1.840	952	24.03	.003	.001
10.94	79609	42807	.003	.003	1.860	974	23.77	.004	.002
17.60	61837	22647	.002	.002	2.730	1426	16.19	.003	.002
17.60	56390	21312	.001	.004	2.646	1552	16.71	.004	.001
30.90	35732	8344	.002	.008	4.282	2654	10.32	.008	.002
30.90	36508	8074	.001	.008	4.522	2611	9.78	.008	.001
47.40	23091	3337	.002	.008	6.920	4242	6.39	.008	.002
47.40	23152	3655	.001	.017	6.334	4214	6.98	.017	.001

LEAST SQUARES FIT FOR 1/R DATA FUNCTION TYPE F(3)

COEFFICIENTS FOR FITTING FUNCTION 6.220E-01 1.388E-01 9.445E-02
FRACTIONAL ERRORS IN COEFFICIENTS 1.683E-02 1.594E-02 1.613E-01

INTERCEPT .622 FRACTIONAL ERROR .017 ZERO P. LIFETIME 71.08 MICRO SEC
H.P. SLOPE .139 MTORR-1 FRACTIONAL ERROR .016 H.P. Q CONSTANT 9.64 E-11 CC/MOLEC SEC
Q RATIO .223 MTORR-1 FRACTIONAL ERROR .016 QUENCH PRESSURE 4.48 MTORR

VARIANCE RATIO COMPARED TO LINEAR FIT, 39.6 FOR (1,13) DEGREES FREEDOM

LEAST SQUARES FIT FOR 1/I DATA FUNCTION TYPE F(4)

COEFFICIENTS FOR FITTING FUNCTION 4.337E+02 3.632E+01 6.671E+00 6.447E-02
FRACTIONAL ERRORS IN COEFFICIENTS 7.262E-02 2.570E-01 7.629E-01 9.215E-01

INTERCEPT 434 FRACTIONAL ERROR .073
H.P. SLOPE 103 MTORR-1 FRACTIONAL ERROR .174
Q RATIO .239 MTORR-1 FRACTIONAL ERROR .223 QUENCH PRESSURE 4.19 MTORR

VARIANCE RATIO COMPARED TO LINEAR FIT, 17.2 FOR (2,12) DEGREES FREEDOM

XBL 688-5776

EXCITATION WAVELENGTH 4800 A OBSERVATION FILTER NO. 10 (16960 CM-1) 17 DATA POINTS

PRESSURE M TORR	S(0)	S(-90)	E(0)	E(-90)	1/R	1/I	LIFETIME MICROSEC	E(R)	E(I)
.49	76501	123478	.017	.007	.620	363	71.36	.018	.013
1.12	79967	124403	.008	.007	.643	366	68.78	.011	.010
1.12	90535	138360	.005	.001	.654	331	67.56	.005	.002
1.18	78723	121169	.010	.002	.650	377	68.05	.010	.005
2.35	97664	131988	.003	.001	.740	362	59.75	.003	.002
2.50	83219	111954	.004	.001	.743	428	59.48	.004	.002
2.50	96937	132840	.004	.001	.730	358	60.58	.004	.002
5.05	110186	119631	.001	.002	.921	417	48.00	.002	.002
5.05	111991	121796	.004	.001	.919	409	48.08	.004	.001
10.94	103312	68024	.001	.001	1.519	675	29.11	.001	.001
10.94	100447	66238	.001	.005	1.516	694	29.15	.005	.003
17.60	81086	36658	.003	.006	2.212	1024	19.99	.007	.003
17.60	78798	35217	.001	.003	2.237	1058	19.76	.003	.001
30.90	52108	14114	.001	.006	3.692	1788	11.97	.006	.001
30.90	53453	14306	.001	.006	3.736	1746	11.83	.006	.001
47.40	35035	6385	.002	.005	5.487	2763	8.06	.005	.002
47.40	34875	6152	.002	.001	5.669	2781	7.80	.002	.002

LEAST SQUARES FIT FOR 1/R DATA FUNCTION TYPE F(3)

COEFFICIENTS FOR FITTING FUNCTION 6.076E-01 1.168E-01 1.512E-01
FRACTIONAL ERRORS IN COEFFICIENTS 1.421E-02 8.746E-03 7.780E-02

INTERCEPT .608 FRACTIONAL ERROR .014 ZERO P. LIFETIME 72.76 MICRO SEC
H.P. SLOPE .117 MTORR-1 FRACTIONAL ERROR .009 H.P. Q CONSTANT 8.11 E-11 CC/MOLEC SEC
Q RATIO .192 MTORR-1 FRACTIONAL ERROR .013 QUENCH PRESSURE 5.20 MTORR

VARIANCE RATIO COMPARED TO LINEAR FIT, 236.0 FOR (1,14) DEGREES FREEDOM

LEAST SQUARES FIT FOR 1/I DATA FUNCTION TYPE F(3)

COEFFICIENTS FOR FITTING FUNCTION 3.979E+02 5.580E+01 3.146E-01
FRACTIONAL ERRORS IN COEFFICIENTS 7.142E-02 2.419E-02 2.309E-01

INTERCEPT 398 FRACTIONAL ERROR .071
H.P. SLOPE 56 MTORR-1 FRACTIONAL ERROR .024
Q RATIO .140 MTORR-1 FRACTIONAL ERROR .067 QUENCH PRESSURE 7.13 MTORR

VARIANCE RATIO COMPARED TO LINEAR FIT, 61.0 FOR (1,14) DEGREES FREEDOM

XBL 688-5777

EXCITATION WAVELENGTH 4800 A OBSERVATION FILTER NO. 11 (15850 CM-1) 17 DATA POINTS

PRESSURE M TORR	S(0)	S(-90)	E(0)	E(-90)	1/R	1/I	LIFETIME MICROSEC	E(R)	E(I)
.49	70091	126387	.061	.006	.555	336	79.72	.061	.034
1.12	71887	124885	.004	.005	.576	346	76.80	.006	.008
1.12	71290	123920	.005	.003	.575	349	76.85	.006	.005
1.18	89025	135440	.013	.003	.657	339	67.26	.013	.007
1.18	63485	108801	.011	.005	.583	400	75.77	.012	.009
1.42	73077	128334	.005	.003	.569	335	77.64	.006	.005
2.35	88297	138605	.004	.003	.637	327	69.40	.005	.005
5.05	115629	133234	.072	.004	.868	372	50.94	.072	.011
5.05	103037	121954	.004	.066	.845	404	52.33	.066	.077
10.94	107129	84052	.002	.001	1.275	578	34.69	.002	.001
10.94	110763	87160	.002	.002	1.271	558	34.79	.003	.002
17.60	94621	50120	.002	.003	1.888	825	23.42	.004	.002
17.60	88752	47436	.002	.003	1.871	876	23.63	.004	.002
30.90	59074	19362	.002	.006	3.051	1529	14.49	.006	.002
30.90	59319	19053	.003	.006	3.113	1528	14.20	.007	.003
47.40	40547	8770	.002	.013	4.623	2356	9.56	.013	.002
47.40	41534	9327	.001	.006	4.453	2292	9.93	.006	.001

LEAST SQUARES FIT FOR 1/R DATA FUNCTION TYPE F(3)

COEFFICIENTS FOR FITTING FUNCTION 5.471E-01 9.640E-02 1.340E-01
FRACTIONAL ERRORS IN COEFFICIENTS 4.818E-02 2.595E-02 3.290E-01

INTERCEPT .547 FRACTIONAL ERROR .048 ZERO P. LIFETIME 80.81 MICRO SEC
H.P. SLOPE .096 MTORR-1 FRACTIONAL ERROR .026 H.P. Q CONSTANT 6.69 E-11 CC/MOLEC SEC
Q RATIO .176 MTORR-1 FRACTIONAL ERROR .036 QUENCH PRESSURE 5.68 MTORR

VARIANCE RATIO COMPARED TO LINEAR FIT, 17.5 FOR (1,14) DEGREES FREEDOM

LEAST SQUARES FIT FOR 1/I DATA FUNCTION TYPE F(4)

COEFFICIENTS FOR FITTING FUNCTION 3.712E+02 1.500E+01 7.106E+00 1.319E-01
FRACTIONAL ERRORS IN COEFFICIENTS 5.741E-02 4.191E-01 4.142E-01 4.751E-01

INTERCEPT 371 FRACTIONAL ERROR .057
H.P. SLOPE 54 MTORR-1 FRACTIONAL ERROR .073
Q RATIO .145 MTORR-1 FRACTIONAL ERROR .116 QUENCH PRESSURE 6.89 MTORR

VARIANCE RATIO COMPARED TO LINEAR FIT, 54.8 FOR (2,13) DEGREES FREEDOM

XBL 688-5778

EXCITATION WAVELENGTH 4800 A OBSERVATION FILTER NO. 12 (15130 CM-1) 18 DATA POINTS

PRESSURE M TORR	S(0)	S(-90)	E(0)	E(-90)	1/R	1/I	LIFETIME MICROSEC	E(R)	E(I)
.49	70051	126726	.014	.003	.553	334	79.98	.014	.009
1.12	69010	124652	.005	.002	.554	340	79.86	.005	.004
1.12	70989	126594	.009	.002	.561	337	78.84	.009	.006
1.18	58347	105411	.005	.002	.554	402	79.87	.005	.004
1.18	62630	113257	.006	.007	.553	374	79.95	.009	.011
2.35	81443	135362	.005	.004	.602	326	73.48	.006	.006
2.50	83016	138206	.010	.002	.601	319	73.60	.010	.006
2.50	72085	116167	.006	.004	.621	386	71.25	.007	.006
5.05	97644	136554	.003	.002	.715	346	61.83	.004	.003
5.05	97671	140357	.004	.003	.696	334	63.53	.005	.004
10.94	106394	93468	.001	.001	1.138	530	38.84	.001	.001
10.94	112669	97615	.002	.001	1.154	507	38.30	.002	.001
17.60	95768	58001	.001	.002	1.651	764	26.78	.002	.001
17.60	89209	54310	.002	.002	1.643	818	26.91	.003	.001
30.90	65386	22972	.002	.002	2.846	1361	15.53	.003	.002
30.90	63786	23418	.001	.002	2.724	1382	16.23	.002	.001
47.40	43752	10414	0.	.003	4.201	2163	10.52	.003	.000
47.40	43614	10033	.001	.010	4.347	2178	10.17	.010	.001

LEAST SQUARES FIT FOR 1/R DATA FUNCTION TYPE F(3)

COEFFICIENTS FOR FITTING FUNCTION 5.606E-01 8.720E-02 1.940E-01
FRACTIONAL ERRORS IN COEFFICIENTS 2.242E-02 1.161E-02 1.012E-01

INTERCEPT .561 FRACTIONAL ERROR .022 ZERO P. LIFETIME 78.86 MICRO SEC
H.P. SLOPE .087 MTORR-1 FRACTIONAL ERROR .012 H.P. Q CONSTANT 6.06 E-11 CC/MOLEC SEC
Q RATIO .156 MTORR-1 FRACTIONAL ERROR .020 QUENCH PRESSURE 6.43 MTORR

VARIANCE RATIO COMPARED TO LINEAR FIT, 190.3 FOR (1,15) DEGREES FREEDOM

LEAST SQUARES FIT FOR 1/I DATA FUNCTION TYPE F(4)

COEFFICIENTS FOR FITTING FUNCTION 3.799E+02 5.737E+00 6.029E+00 1.159E-01
FRACTIONAL ERRORS IN COEFFICIENTS 6.222E-02 1.171E+00 4.161E-01 5.025E-01

INTERCEPT 380 FRACTIONAL ERROR .062
H.P. SLOPE 52 MTORR-1 FRACTIONAL ERROR .102
Q RATIO .137 MTORR-1 FRACTIONAL ERROR .145 QUENCH PRESSURE 7.30 MTORR

VARIANCE RATIO COMPARED TO LINEAR FIT, 43.5 FOR (2,14) DEGREES FREEDOM

XBL 688-5779

EXCITATION WAVELENGTH 4800 A OBSERVATION FILTER NO. 13 (14270 CM-1) 17 DATA POINTS

PRESSURE M TORR	S(0)	S(-90)	E(0)	E(-90)	1/R	1/I	LIFETIME MICROSEC	E(R)	E(I)
.49	60626	115704	.017	.006	.524	355	84.37	.018	.014
1.12	76192	146685	.018	.009	.519	279	85.11	.020	.018
1.12	65099	123480	.014	.008	.527	334	83.86	.016	.015
1.18	62078	115864	.009	.002	.536	359	82.51	.009	.006
1.42	68458	128558	.016	.006	.533	323	83.02	.017	.013
2.35	83629	150162	.003	.002	.557	283	79.38	.004	.003
2.50	81427	145664	.006	.003	.559	292	79.09	.007	.006
5.05	95556	151158	.004	.003	.632	299	69.93	.005	.005
5.05	95863	149312	.009	.001	.642	304	68.86	.009	.004
10.94	114013	110561	.002	.002	1.031	452	42.87	.003	.002
10.94	114934	112628	.002	.004	1.020	444	43.32	.004	.004
17.60	107868	71950	.001	.003	1.499	642	29.49	.003	.002
17.60	101659	69069	.002	.002	1.472	673	30.04	.003	.001
30.90	76303	30008	.002	.002	2.543	1135	17.39	.003	.002
30.90	74393	29606	.003	.003	2.513	1160	17.59	.004	.002
47.40	51944	13934	.002	.008	3.728	1796	11.86	.008	.002
47.40	53851	14023	.002	.008	3.840	1739	11.51	.008	.002

LEAST SQUARES FIT FOR 1/R DATA FUNCTION TYPE F(3)

COEFFICIENTS FOR FITTING FUNCTION 5.538E-01 7.871E-02 2.314E-01
FRACTIONAL ERRORS IN COEFFICIENTS 2.207E-02 9.164E-03 8.492E-02

INTERCEPT .554 FRACTIONAL ERROR .022 ZERO P. LIFETIME 79.82 MICRO SEC
H.P. SLOPE .079 MTORR-1 FRACTIONAL ERROR .009 H.P. Q CONSTANT 5.47 E-11 CC/MOLEC SEC
Q RATIO .142 MTORR-1 FRACTIONAL ERROR .020 QUENCH PRESSURE 7.04 MTORR

VARIANCE RATIO COMPARED TO LINEAR FIT, 329.2 FOR (1,14) DEGREES FREEDOM

LEAST SQUARES FIT FOR 1/I DATA FUNCTION TYPE F(4)

COEFFICIENTS FOR FITTING FUNCTION 3.927E+02 1.038E+01 1.036E+01 2.676E-01
FRACTIONAL ERRORS IN COEFFICIENTS 7.639E-02 1.029E+00 3.580E-01 4.046E-01

INTERCEPT 393 FRACTIONAL ERROR .076
H.P. SLOPE 39 MTORR-1 FRACTIONAL ERROR .062
Q RATIO .099 MTORR-1 FRACTIONAL ERROR .121 QUENCH PRESSURE 10.14 MTORR

VARIANCE RATIO COMPARED TO LINEAR FIT, 66.9 FOR (2,13) DEGREES FREEDOM

XBL 688-5780

Appendix E

Dynamic Range in Analog Photon Counters

In this appendix we wish to consider the requirements upon the dynamic range of analog circuits imposed by the single shot characteristics of the optical signal. With signals of a small number of counts per second it is necessary to amplify each pulse (either in voltage or duration) in order to obtain a high level average signal. If the pulse duration is kept short then the voltage must be amplified, and this necessitates a wide dynamic range.

We consider as typical a signal of 100 counts/sec of 10^{-6} sec duration. For an average filtered dc signal of 10 mV the peak response of the pulse amplifier must be 10 mV/(100×10^{-6}) or 100V; yet the stability of the amplifier must be of the order of 0.1 mV. The requirement on the dynamic range will of course be lessened if the pulse width is increased. However, increasing the pulse width at the output of the one-shot increases the coincidence loss due to shortly spaced pulses. Consequently analog means of increasing the pulse width are indicated. However, in ac work where the phase of the signal is important it is necessary that the broadened pulse still be much shorter than the period of the modulation (in the present case 277 μsec) so that perhaps only one order of magnitude can be gained.

The means of spreading the width of the single photoelectron pulses that was found most satisfactory was to utilize a sharply tuned amplifier such as is in the signal channel of the JB-5 lock-in amplifier ($Q \sim 25$). The response of such a circuit to a fast pulse (whose Fourier spectrum contains all frequencies) is to select frequencies about the

tuned frequency ω; i.e., to produce a ringing sinusoidal wave form (Fig. E-1), decaying with a time constant $\tau = 2Q/\omega$. The rectified wave form (Fig. E-2) will be considerably spread out in time, the effective pulse width now given by $T = \omega^{-1} \coth(\pi/4Q)$; for large Q, $T = 4Q/\pi\omega$. In the present case with $\omega^{-1} = 44.21$ μsec and $Q \sim 25$, $T = 1.4$ msec. Now the required dynamic range is approximately $3 \times (10\ \text{mV})/(100 \times 1.4 \times 10^{-3})$ on the order of 0.2 volt, where the additional factor of 3 has been allowed for adding closely spaced pulses. Since the method of spreading pulses is analog the response is linear to the arrival of multiple pulses within the ring time as shown by Fig. E-3. A newly arriving pulse adds its voltage to the residual voltage from previous pulses.

The final requirement that has been placed upon the circuit is that it retain the time information of the input photoelectron pulse. This information is retained in the phase of the decaying sinusoid compared to the rectification points of the lock-in as shown by comparison of Figs. E-2 and E-4. The wave form in Fig. E-2 is rectified in-phase; that in Fig. E-4 is rectified approximately 90° out of phase and makes no contribution to the dc signal. Pulses of intermediate phase make appropriate contributions to each channel.

The disadvantage in using sharply tuned filters in phase measurements is of course the severe sensitivity of the output phase to very slight changes of the frequency. Quantitatively,

$$d\phi = 2Q \frac{d\omega}{\omega}$$

or for $Q = 25$, a phase error of 1% is produced by a change in frequency of 0.02%.

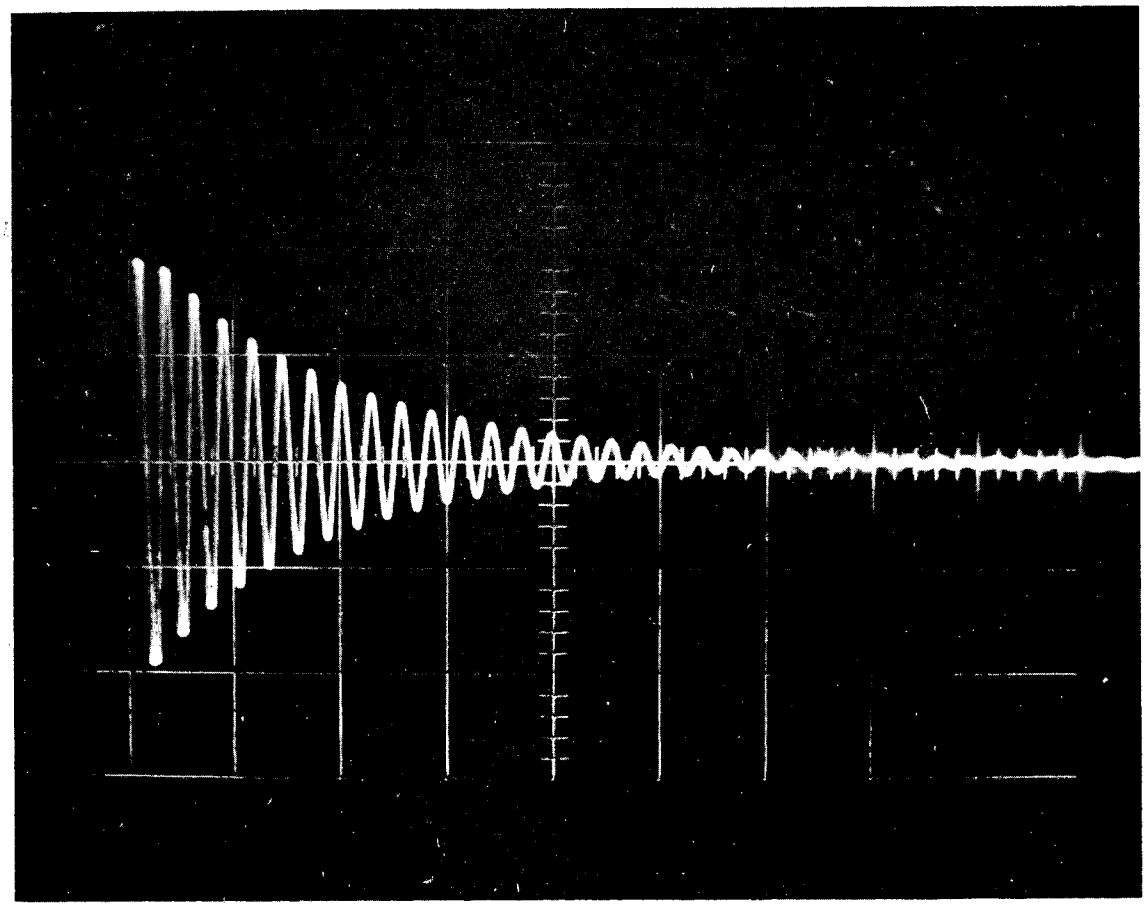

XBB 685-2754

Fig. E1 Response of tuned circuit to a single photon pulse. Horizontal scale: 1 m sec/major division.

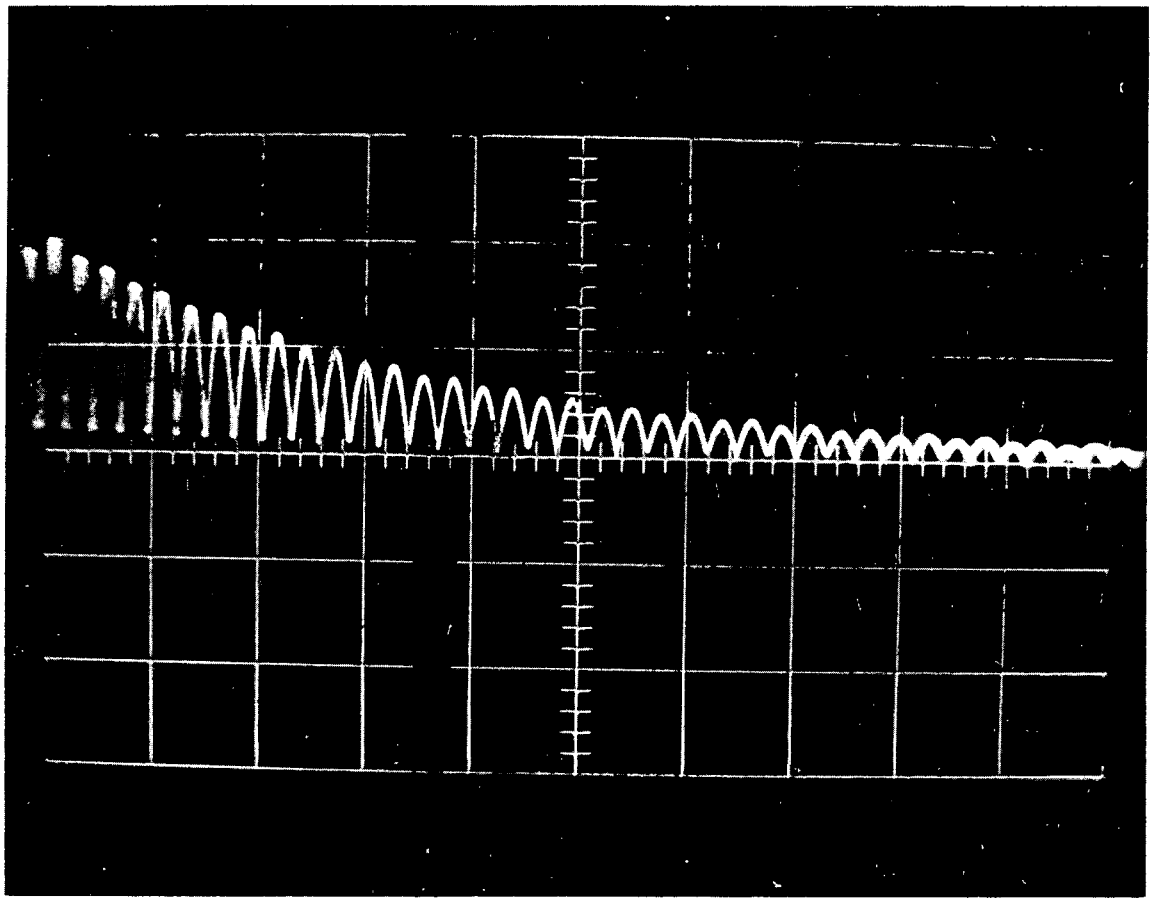

XBB 685-2757

Fig. E2 Lock-in rectified response to a single photon pulse (in-phase). Horizontal scale: 0.5 m sec/major division.

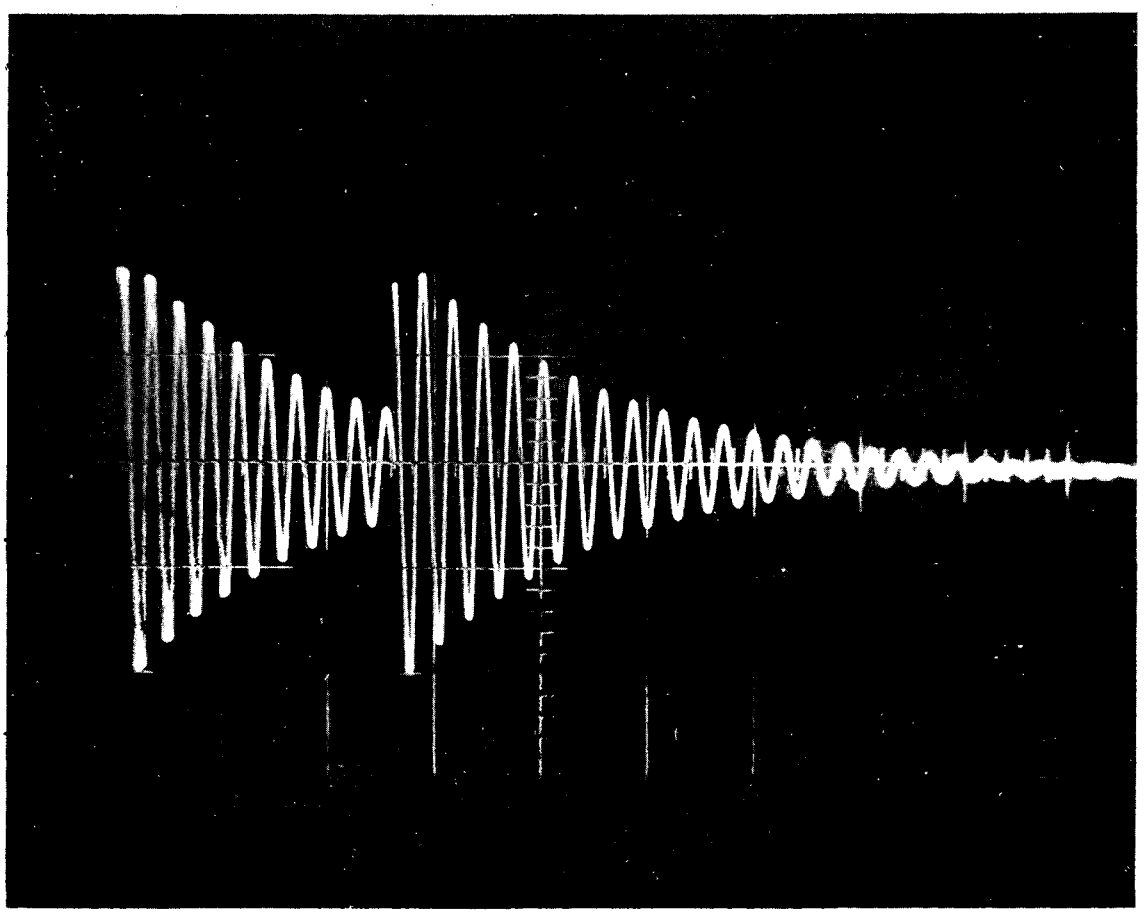

XBB 685-2755

Fig. E3 Additive response to two closely spaced pulses.
Horizontal scale: 1 m sec/major division.

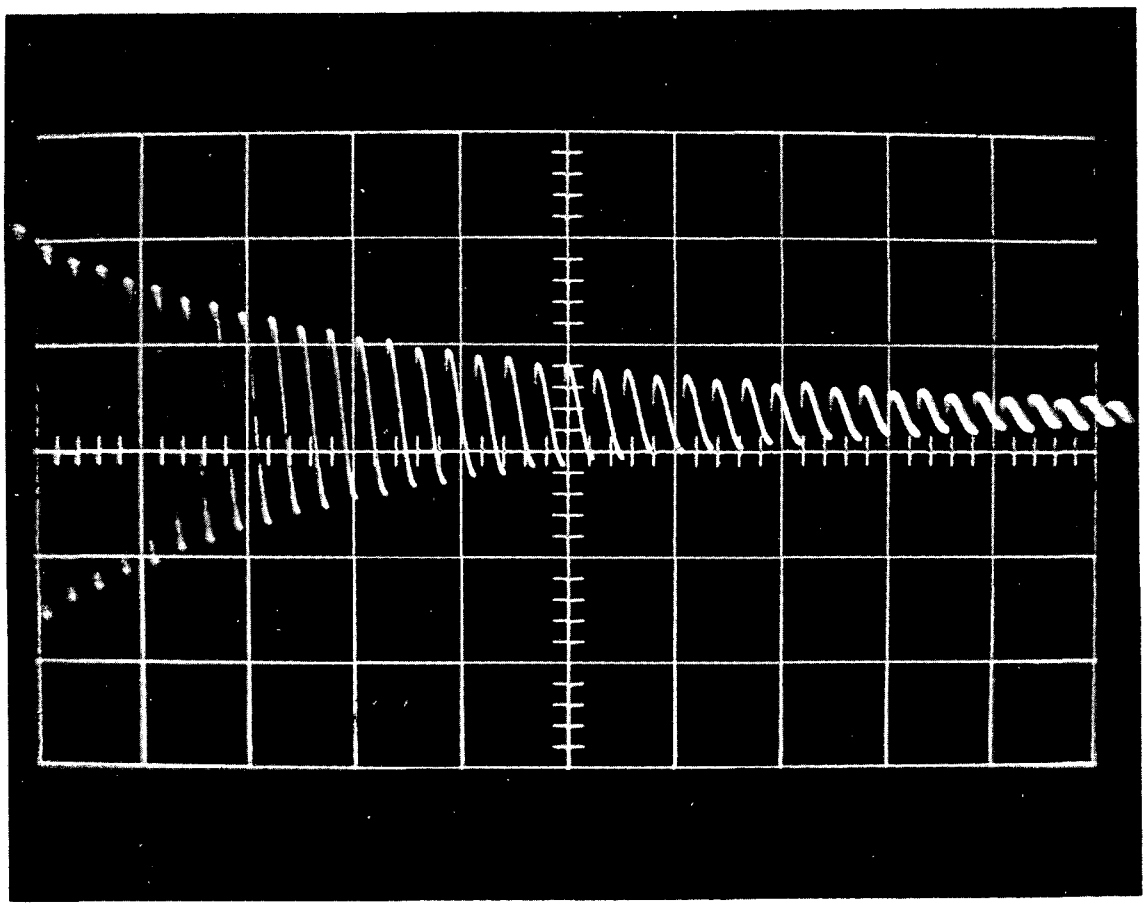

XBB 685-2756

Fig. E4 Lock-in rectified response to a single photon pulse (quadrature). Horizontal scale: 0.5 m sec/major division.

Appendix F

Circuit Diagrams

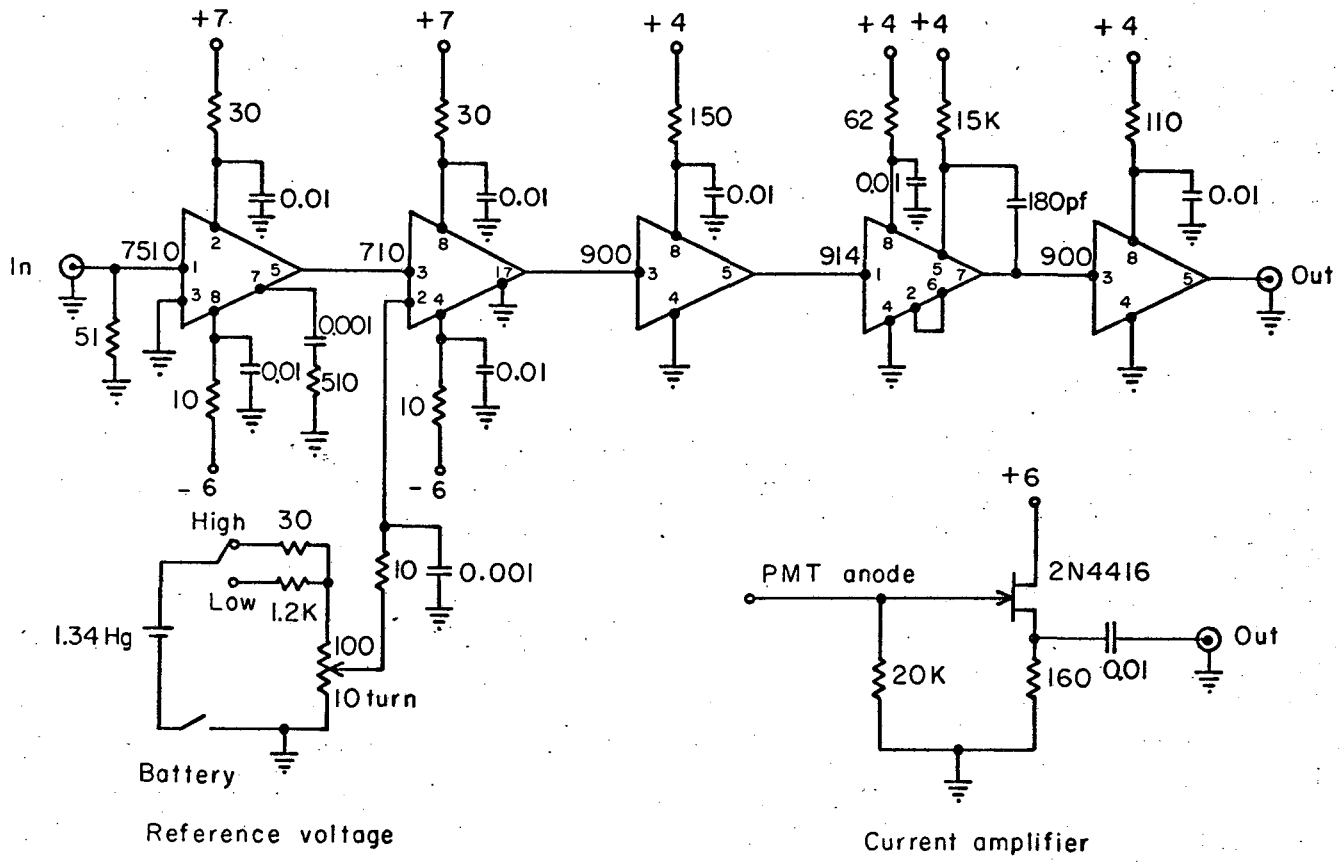

XBL688-3775

Fig. F1. Current amplifier and pulse shaping electronics for optical detection circuit. Current amplifier is located close to the base of the photomultiplier to reduce dissipative capacitance, which reduces voltage of single event pulses from the photomultiplier. The integrated circuits are used in the following functions: 7510 voltage amplifier; 710, Schmitt trigger; 914 monostable multivibrator (one-shot); 900 buffer amplifier.

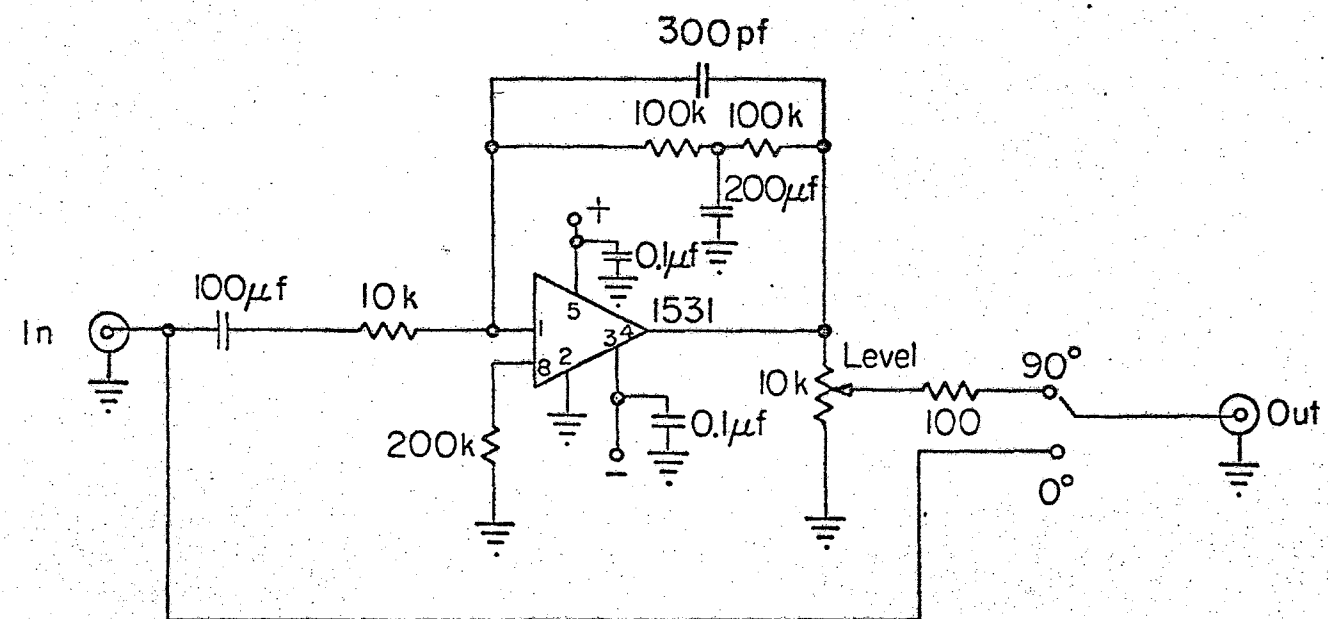

Fig. F2: Quadrature phase shifter for reference signal. Integrated circuit 1531 is used as an integrator.

ACKNOWLEDGEMENTS

I wish to express my appreciation to Professor Harold S. Johnston for his guidance of this research. The gentle manner in which he offered advice and suggestions has allowed me to discover for myself what he already knew. His knowledge and insight have stimulated my thinking and deeply influenced this work.

It has been a pleasure to conduct this research among colleagues and friends who have been very generous in their assistance and encouragement and who have helped to make my years at Berkeley an enjoyable and meaningful experience.

I wish to acknowledge extensive support from the personnel of the Department of Chemistry and of the Lawrence Radiation Laboratory, who have contributed substantially to the conduct of this research.

I am grateful to the National Science Foundation for a Graduate Fellowship. This work was conducted under the auspices of the United States Atomic Energy Commission.

REFERENCES

1. O. K. Rice, Some Problems in Energy Exchange Related to Chemical Kinetics, in Energy Transfer in Gases, R. Stoops, Ed. (Interscience, New York, 1962.).
2. V. N. Kondrat'ev, Chemical Kinetics of Gas Reactions, (Pergamon Press, Oxford, 1964) a. Chapter 6, b. Chapter 4.
3. D. R. Herschbach, Reactive Scattering in Molecular Beams, in Adv. Chem. Phys. 10, Molecular Beams, John Ross, Ed. (Interscience, New York, 1966) p. 319.
4. R. G. W. Norrish, Proc. Roy. Soc. (London) A301, 1 (1967).
5. B. A. Thrush, Chem. in Brit. 1966, 287.
6. P. Pringsheim, Fluorescence and Phosphorescence, (Interscience, New York, 1949.).
7. a) K. F. Herzfeld and T. A. Litovitz, Absorption and Dispersion of Ultrasonic Waves, (Academic Press, New York, 1959). b) R. N. Schwartz, Z. I. Slawsky, and K. F. Herzfeld, J. Chem. Phys. 20, 1591 (1952).
8. T. L. Cottrell and J. C. McCoubrey, Molecular Energy Transfer in Gases, (London, Butterworth, 1961).
9. D. C. Tardy and B. S. Rabinovitch, J. Chem. Phys. 45, 3720 (1966).
10. F. J. Fletcher, B. S. Rabinovitch, H. W. Watkins and D. J. Locker, J. Phys. Chem 70, 2823 (1966), and references cited to earlier work .
11. R. C. Millikan and D. R. White, J. Chem. Phys. 39, 3209 (1963).
12. K. G. Anlauf, P. J. Kurtz, D. H. Maylotte, P. D. Pacey, J. C. Polanyi, Disc. Faraday Soc. 44 (1968).

13. N. Basco and R. G. W. Norrish, Can. J. Chem. 38, 1769 (1960).

14. a) J. I. Steinfeld and W. Klemperer, J. Chem. Phys. 42, 3475 (1965);
b) J. I. Steinfeld, J. Chim. Phys. 64, 17 (1967).

15. J. T. Yardley and C. B. Moore, Jr., J. Chem. Phys. 45, 1066 (1967).

16. W. H. Flygare, Accts. Chem. Res. 1, 121 (1968).

17. B. Stevens, Collisional Activation in Gases, (Pergamon Press, Oxford, 1967).

18. D. Neuberger and A. B. F. Duncan, J. Chem. Phys. 22, 1693 (1954).

19. G. H. Myers, D. M. Silver, and F. Kaufman, J. Chem. Phys. 44, 718 (1966).

20. A. E. Douglas, J. Chem. Phys. 45, 1007 (1966).

21. P. N. Clough and B. A. Thrush, Chem. Comm. 1966, 783.

22. P. N. Clough and B. A. Thrush, Trans. Faraday Soc. 63, 915 (1967).

23. S. J. Strickler and R. A. Berg, J. Chem. Phys. 37, 814 (1962).

24. R. S. Mulliken, J. Chem. Phys. 7, 14 (1939).

25. G. W. Robinson, J. Chem. Phys. 47, 1967 (1967).

26. M. Bixon and J. Jortner, J. Chem. Phys. 48, 715 (1968).

27. J. Jortner and S. Berry, J. Chem. Phys. 48, 2757 (1968).

28. D. P. Chock, J. Jortner, and S. A. Rice, On the Theory of Radiationless Transitions in an Isolated Molecule, to be published. I wish to thank Professor Rice for making copies of this and the two preceding referencesavailable prior to publication.

29. H. P. Broida, H. I. Schiff, and T. M. Sugden, Trans. Faraday Soc. 57, 259 (1961).

30. G. Doherty and N. Jonathan, Disc. Faraday Soc. 37, 73 (1964).

31. A. Fontijn, C. B. Meyer, H. I. Schiff, J. Chem. Phys. 40, 64 (1964).

32. N. Jonathan and R. Petty, Trans. Faraday Soc. 64, 1240 (1968).

33. K. H. Becker, W. Groth, and F. Joo, Ber. Bunsenges. 72, 157 (1968).

34. R. R. Reeves, P. Harteck, and W. H. Chace, J. Chem.Phys. 41, 764 (1964).

35. D. Applebaum, P. Harteck, and R. R. Reeves, Photochem. and Photobiol. 4, 1003 (1965).

36. T. R. Rolfes, R. R. Reeves, and P. Harteck, J. Phys. Chem. 69, 849 (1965).

37. M. A. A. Clyne, B. A. Thrush, R. P. Wayne, Trans. Faraday Soc. 60, 359 (1964).

38. J. C. Greaves and D. Garvin, J. Chem. Phys. 30, 348 (1959); ASTIA Report AD201510 (1958).

39. M. Nicolet, J. Geophys. Res. 70, 691 (1965).

40. C. A. Barth, Nitrogen and Oxygen Atomic Reactions in the Chemosphere in Chemical Reactions in the Upper and Lower Atmospheres, (Interscience, New York, 1961).

41. A. D. Walsh, J. Chem. Soc. 1953, 2260.

42. A. E. Douglas and K. P. Huber, Can. J. Phys. 43, 74 (1965)

43. A. Einstein, Physik Z. 18, 121 (1917).

44. L. Brewer, Radiation Relations for a Single Line with Multiplet Structure, privately circulated, 1967.

45. L. Brewer and L. G. Hagan, to be published.

46. G. Herzberg, Molecular Spectra and Molecular Structure, Vol. III, Electronic Spectra and Electronic Structure of Polyatomic Molecules, (Van Nostrand, Princeton, 1966) a. Sec. II, 1; b. Sec. III, 2; c. Sec. I, 2; d. Sec. IV, 3.

47. H. E. Radford and H. P. Broida, J. Chem. Phys. 38, 644 (1963).

48. T. C. Hall, Jr. and F. E. Blacet, J. Chem. Phys. 20, 1745 (1952).

49. F. H. Verhoek and F. Daniels, J. Am. Chem. Soc. 53, 1250 (1931).

50. J. H. Dixon, J. Chem. Phys. 8, 157 (1940).

51. J. B. Birks and W. A. Little, Proc. Phys. Soc. London A66, 921 (1953).

52. L. Brewer, C. G. James, R. G. Brewer, F. E. Stafford, R. A. Berg, and G. A. Rosenblatt, Rev. Sci. Instr. 33, 1450 (1962).

53. A. Muller, R. Lumry, H. Kokubun, Rev. Sci. Instr. 36, 1214 (1965).

54. E. D. Morris, Jr. and H. S. Johnston, Rev. Sci. Instr. 39, 620 (1968).

55. H. S. Johnston, G. E. McGraw, T. T. Paukert, L. W. Richards and J. Van Den Bogaerde, Proc. Natl. Acad. Sci. U. S. 57, 5, 1146 (1967).

56. G. E. McGraw and H. S. Johnston, Molecular-Modulation Spectrometry: CH_3ONO Photolysis and Detection of Nitroxyl. To be published.

57. H. G. Kloss and G. Wendel, Z. Naturforsch. 16a, 61 (1961).

58. A. M. Bonch-Bruevich, Izv. Akad. Nauk. SSSR Ser. Fiz. 20, 591 (1956).

59. O. Stern and M. Volmer, Physik. Z. 20, 183 (1919).

60. A thorough discussion of Stern-Volmer kinetics is given in A. C. G. Mitchell and M. W. Zemansky, Resonance Radiation and Excited Atoms, (Cambridge Univ. Press, Cambridge, 1961).

61. R. G. W. Norrish, J. Chem. Soc. 1929, 1611.

62. W. P. Baxter, J. Am. Chem. Soc. 52, 3920 (1930).

63. O. Heil, Z. Physik. 77, 563 (1932).

64. D. L. Akins, S. E. Schwartz and C. B. Moore, Rev. Sci. Instr. 39, 715 (1968); and references therein.

65. S. D. Gabelnick, Ph.D. Thesis, University of Calif. to be submitted, 1968.

66. J. C. De Vos, Physica 20, 690 (1954); G. A. W. Rutgers and J. C. De Vos, Physica 20, 715 (1954).

67. P. R. Rony, Design, Construction and Operation of a Differential Micromanometer, Part II. Theory and Operational Characteristics, UCRL-11218 Pt. II.

68. K. F. Greenough and A. B. F. Duncan, J. Am. Chem. Soc. 83,555 (1961).

69. H. D. Mettee, Vibronic Relaxation in Gases, I. SO_2. To be published. I wish to thank Dr. Mettee for making a copy of his article available prior to publication.

70. R. W. Nicholls and A. L. Stewart, Allowed Transitions, in Atomic and Molecular Processes, D. R. Bates, Ed. (Academic Press, New York, 1962).

71. R. S. Mulliken, Can. J. Chem. 36, 10 (1958).

72. G. B. Kistiakowsky and C. S. Parmenter, J. Chem. Phys. 42, 2942 (1965).

73. See for example H. S. Johnston, Gas Phase Reaction Rate Theory (Ronald Press, New York, 1966).

74. B. H. Mahan, J. Phys. Chem. 62, 100 (1958).

75. L. Brewer, R. A. Berg, G. M. Rosenblatt, J. Chem. Phys. 38, 1381 (1963).

76. Y. Miyahara and E. G. Richardson, J. Accoust. Soc. Am. 28, 1016 (1956); see also Millikan and White (Ref. 11).

77. B. S. Neporent, Zhur. Fiz. Khim. 21, 1111 (1947); 1219 (1950).

78. M. Boudart and J. T. Dubois, J. Chem. Phys. 23, 223 (1955).

79. E. W. Schlag, H. Von Weyssenhoff, M. E. Starzak, Ber. Bunsenges, 72 ,153 (1968); H. Von Weyssenhoff, E. W. Schlag, M. E. Starzak, Ibid. 155.

80. E. W. Schlag, H. Von Weyssenhoff, M. E. Starzak, J. Chem. Phys. 47, 860 (1967).

81. M. Stockburger, a) Ber. Bunsenges. 72, 151 (1968); b) Z. Physik. Chem. N. F. 35, 179 (1962).

82. R. E. Harrington, B. S. Rabinovitch and M. R. Hoare, J. Chem. Phys. 33, 744 (1960).

83. R. A. Marcus, J. Chem. Phys. 20, 352,359 (1952); R. A. Marcus and O. K. Rice, J. Phys. . Chem. 55, 894 (1951).

84. J. W. Simons, B. S. Rabinovitch. and D. W. Setser, J. Chem. Phys. 41, 800 (1964).

85. T. Carrington and N. Davidson, J. Phys. Chem. 57, 418 (1953).

86. A. K. Barua, and T. K. Rai Dastidar, J. Chem. Phys. 43, 4140 (1965).

87. J. N. Pitts, Jr., J. H. Sharp, S. I. Chan, J. Chem. Phys. 42, 3655 (1964).

88. E. T. Arakawa and A. H. Nielson, J. Mol. Spectr. 2, 413 (1958).

89. H. W. Ford and S. Jaffe, J. Chem. Phys. 38, 2935 (1963).

90. P. Brix and G. Herzberg, Can. J. Phys. 32, 110 (1954).

91. W. F. Giauque and J. D. Kemp, J. Chem. Phys. 6, 40 (1938).

92. W. H. Eberhardt and H. Renner, J. Mol. Spectr. 6, 483 (1961).

93. B. P. Levitt, Trans. Faraday Soc. 59, 59 (1963).

94. B. P. Levitt, Trans. Faraday Soc. 58,1789 (1962).

95. M. A. A. Clyne and B. A. Thrush, Proc. Roy. Soc. (London). A269, 404 (1962).

96. F. Kaufman, Proc. Roy. Soc. (London). A 247, 123 (1958).

97. R. G. Gordon, J. Chem. Phys. 46, 4399 (1967).

98. See for example L. R. Ford, Differential Equations, second edition, (McGraw Hill, New York, 1955).

99. J. B. Birks, D. J. Dyson, I. H. Munro, Proc. Roy. Soc. (London) A275, 575 (1963); J. B. Birks and I. H. Munro, Fluorescence Lifetimes of Aromatic Molecules, in Progress in Reaction Kinetics, IV, G. Porter, Ed. (Pergamon Press, Oxford, 1967), p. 239.

100. G. M. Lawrence and B. D. Savage, Phys. Rev. 141, 67 (1966).

101. H. Dreeskamp, A. K. Ghosh, M. Burton, Rev. Sci. Instr. 32, 304 (1961).

102. E. Fink, Ber. Bunsenges. 72, 155 (1968).

103. D. R. Jenkins, Trans. Faraday Soc. 64, 36 (1968).

104. L. Landau and E. Teller, Phys. Z. Sowjetunion, 10, 34 (1936).

105. Subroutine RMERG, LRL Identification D1 BKY RMERG written by L. Vardas, (1966).

106. Subroutine package LSQPOL, LRL Identification E2 AN E206; a modification by W. Dempster of a program originally written by B. S. Garbow, Argonne National Laboratories, (1959).

107. Subroutine package LSQVMT LRL Identification E2 BKY LSQVMT, written by E. R. Beals, (1966). The method is due to W. C. Davidson, Argonne National Laboratories and is described in report ANL 5990 (Rev. 1959).

108. P. G. Guest, Numerical Methods of Curve Fitting, (Cambridge University Press, Cambridge, England, 1961).

109. J. R. Wolberg, Prediction Analysis, (Van Nostrand, Princeton, New Jersey, 1967).

110. R. A. Fisher and F. Yates, Statistical Tables for Biological, Agricultural and Medical Research, fifth edition, (Hafner Publishing Co., New York City, 1957).